

PDF hosted at the Radboud Repository of the Radboud University Nijmegen

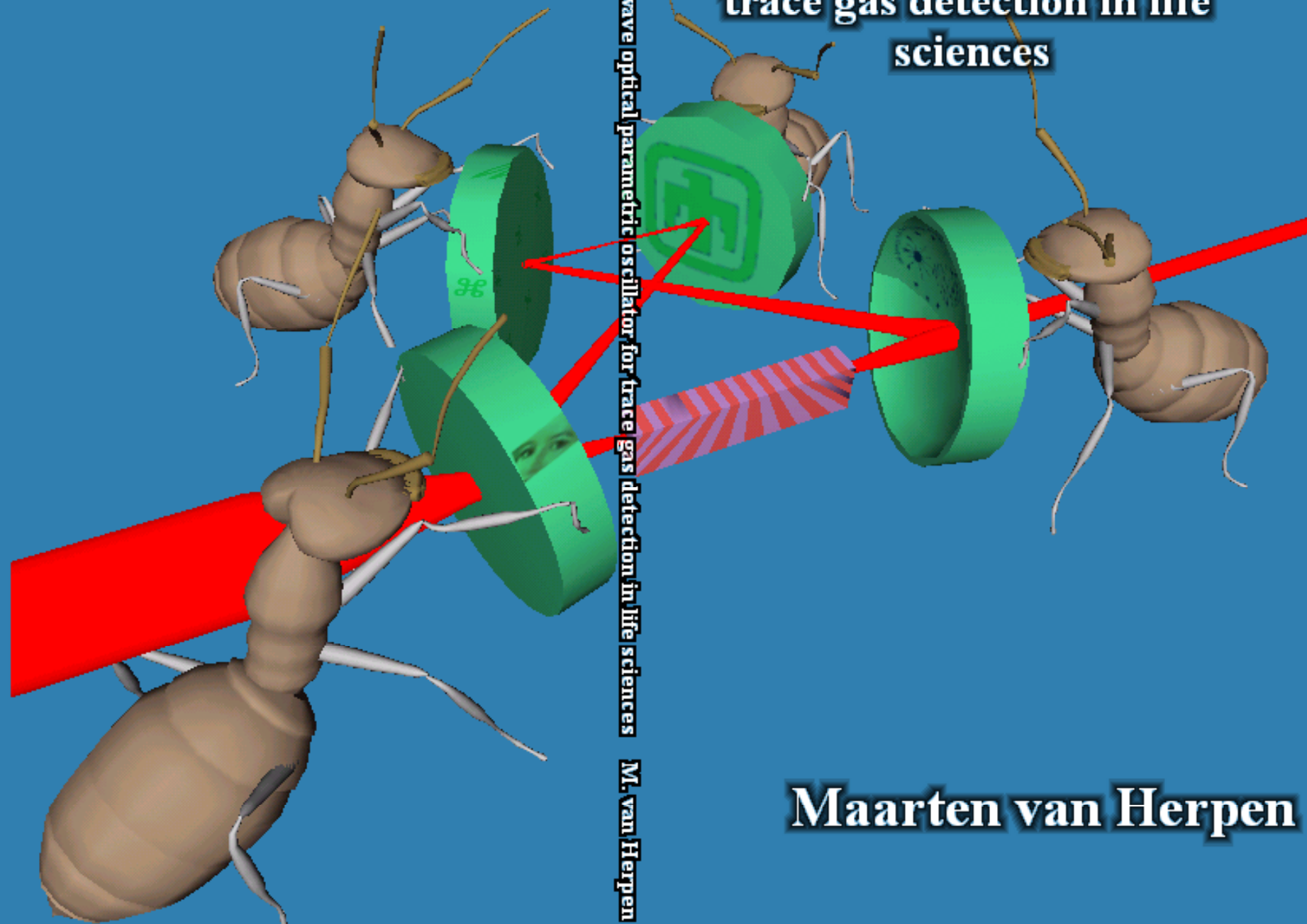
The following full text is a publisher's version.

For additional information about this publication click this link.

<http://hdl.handle.net/2066/60686>

Please be advised that this information was generated on 2018-07-08 and may be subject to change.

Continuous-wave optical parametric oscillator for trace gas detection in life sciences



Continuous-wave optical parametric oscillator for trace gas detection in life sciences M. van Herpen

Maarten van Herpen

Continuous-wave optical parametric
oscillator for trace gas detection in life
sciences

Maarten van Herpen

Continuous-wave optical parametric oscillator for trace gas detection in life sciences
M.M.J.W. van Herpen
Thesis Katholieke Universiteit Nijmegen – Illustrated
With references – With summary in Dutch
ISBN: 90-9017723-X
NUR: 926

Cover: 3D digital artist impression of an optical parametric oscillator by M. v. Herpen
with ants holding the cavity mirrors.

Continuous-wave optical parametric oscillator for trace gas detection in life sciences

Een wetenschappelijke proeve op het gebied van de
Natuurwetenschappen, Wiskunde en Informatica

Proefschrift

Ter verkrijging van de graad van doctor
aan de Katholieke Universiteit Nijmegen,
volgens besluit van het College van Decanen
in het openbaar te verdedigen op woensdag 4 februari 2004
Des namiddags om 13.30 uur

door

Maarten Marinus Johannus Wilhelmus van Herpen

Geboren op 12 december 1976
te Oss

Promotor: Prof. Dr. D.H. Parker

Co-promotors: Dr. F.J.M. Harren

Dr. S.E. Bisson
Sandia National Laboratories, Livermore, CA, USA

Manuscriptcommisie: Prof. Dr. K.J. Boller
University of Twente, Enschede

Prof. Dr. W.J. van der Zande

Dr. J. Oomens
FOM-institute for Plasma Physics, Rijnhuizen

*“De meest fundamentele ideeën van de wetenschap
zijn in wezen eenvoudig en kunnen in de regel worden
uitgedrukt in een taal die voor iedereen begrijpelijk is.”*

Albert Einstein

Voorwoord

Volgens mij zijn deze twee bladzijden van het voorwoord de meest gelezen bladzijden van dit proefschrift. Een proefschrift waar ik vier jaar met veel plezier en inzet aan gewerkt heb. In het eerste jaar moest ik wachten op de onderdelen die ik nodig had voor de bouw van de OPO laser en dus heb ik gewerkt met een andere laser, namelijk de color center laser. Wat leeftijd betreft kun je zeggen dat dit een antieke laser is, maar in principe is hij nog steeds goed bruikbaar. Toch was ik blij toen ik kon beginnen met de opbouw van mijn eigen OPO laser. Daarna is het onderzoek zeer snel verlopen en zijn er vele artikelen gepubliceerd. De resultaten van dit werk zijn te vinden in dit proefschrift, waarvan je nu het voorwoord aan het lezen bent.

Ik vind het voorwoord één van de belangrijkste delen van dit proefschrift. Op deze twee bladzijden kan ik namelijk de mensen bedanken die tijdens mij promotie belangrijk voor me zijn geweest. Hoewel ik niet genoeg bladzijden heb om iedereen uitgebreid te bedanken wil ik toch een aantal mensen speciaal noemen.

De eerste en meest belangrijke persoon die ik wil bedanken is Frans. Bij mijn publicaties zou ik hem het liefst altijd als tweede auteur genoemd hebben, maar hij stond er altijd op om als laatste genoemd te worden. Nu kan ik hem dan eindelijk als eerste noemen. Frans was tijdens mijn promotie mijn directe begeleider en hij heeft deze taak voortreffelijk volbracht. Wat ik vooral fijn vond is dat Frans af en toe een hele dag bij me in het laboratorium kwam helpen. Ik vond zulke dagen erg gezellig en we kregen ook ontzettend veel werk gedaan. Frans was ook erg goed in het sturen van mijn onderzoek. Hij liet me in principe mijn eigen pad kiezen, maar gaf wel af en toe een duwtje in de juiste richting.

The second very important person to thank is the person who has been my mentor: Scott Bisson. I spend about 1 month with him at Sandia National Laboratories in Livermore (California) to learn everything about OPOs. When I returned I had enough knowledge and experience to build a similar OPO in Nijmegen. Throughout my PhD he also kept a close eye on my progress and gave me a lot of advice and tips (sometimes on a daily basis)! Without the help from Scott I would not have been able to achieve this much during my PhD. But this is not the only thing I want to thank Scott for. Next to teaching me many things about lasers, Scott also took me out on trips across his country. I am still very grateful for the great time I had during my stay in the USA.

Vervolgens bedank ik Dave Parker voor de interesse en het enthousiasme dat hij als mijn promotor getoond heeft voor mijn onderzoek. Verder bedank ik de leden van de manuscript commissie (Klaus Boller, Jos Oomes en Wim v/d Zande), voor het lezen en becommentarieren

van dit proefschrift. Jos Oomes is daarnaast degene die het projectvoorstel van mijn onderzoek geschreven heeft. Ook bedankt daarvoor, want zonder die inspanningen zou dit onderzoek nooit plaats hebben gevonden!

Verder zijn tijdens mij promotie nog veel meer mensen erg belangrijk geweest. Ik wil met name Sacco, Li en Cor hier noemen. Sacco heeft me continu met raad en daad bijgestaan en ik heb veel van hem kunnen leren. Aan het begin van mijn project heeft Sacco mij ook begeleid als post-doc. Li is een promovendus uit China. Hij heeft voor ongeveer 2 jaar met mij samengewerkt. Het lijkt me leuk om hem in zijn eigen taal een woord van dank te kunnen zeggen, dus:

李，很高兴能与您一起工作，我在此要感谢您的合作使我们一起完成了很多工作。

Naast Leander, Chris en Peter bedank ik Cor voor zijn technische ondersteuning. Maar voornamelijk bedank ik Cor voor zijn morele steun wanneer het even tegen zat. Bij Cor heb ik een luisterend oor gevonden voor alle soorten problemen. Hij begrijpt me goed en geeft altijd goede raad. Naast Cor heeft ook Magda voor mij een belangrijke rol gespeeld voor morele ondersteuning op de werkvloer. Ook Magda bedankt hiervoor.

Verder heb ik tijdens mijn promotie met veel andere mensen samengewerkt. Vooral in de eerste twee jaar van mijn promotie heb ik vaak de hulp nodig gehad van Nico in verband met de color center laser. Ik ben blij dat hij me hiermee wilde helpen. Vervolgens heeft er een student uit Italië bij me gewerkt in mijn eerste jaar als AIO. Dit was Gianmarco Billanco. Daarna heeft Michiel Alsters, een student informatica, me geholpen met de software voor de aansturing van de OPO laser. In mijn vierde jaar heb ik Chen Limin begeleid bij het doen van cavity enhanced absorption spectroscopy experimenten en daarna is Anthony begonnen. Anthony is als AIO gestart op een vervolgproject van mijn onderzoek. In mijn laatste half jaar als AIO heeft hij met mij samengewerkt. Bedankt allemaal hiervoor.

Ik bedank Johannes Hackstein voor zijn hulp bij de metingen van de Drosophila vliegjes. Het was heel fijn dat ik altijd bij Johannes terecht kon om een paar vliegjes op te halen en dus nooit hoefde te wachten. Ik bedankt Ernst Woltering voor zijn hulp bij de CO₂ metingen aan de tomaten cellen.

Natuurlijk bedank ik ook al de andere collega's voor de gezelligheid op de afdeling. Zo bedank ik bijvoorbeeld Ine (ook vanwege haar secretariële ondersteuning). Bas, Marco, Simona, Iulia, Luc-Jan en Hans bedank ik voor de gezellige lunches en interessante gesprekken. Verder noem ik ook Jeroen, Robert, Iris, Rik, Edi, Tim, Stefan, Ivan, Reijer, Kjeld, Karen, Erna, Thijs en Kasper.

Ten slotte bedank ik natuurlijk mijn familie en mijn vrienden voor de steun die ze mij in de afgelopen vier jaar hebben gegeven. Met name noem ik hier mijn ouders maar in het bijzonder bedank natuurlijk Melina voor de liefde en steun waar ik altijd op kan rekenen.

Contents

Voorwoord		vii
Contents		ix
<i>Chapter 1</i>		
Introduction		1
1.1	Trace gas detection	1
1.2	Optical Parametric Oscillator	1
<i>Chapter 2</i>		
Theoretical introduction		5
2.1	Introduction	6
2.2	Birefringent phase matching	7
2.3	Quasi phase-Matching	12
2.4	Manley-Rowe relation	13
2.5	Periodically Poled Lithium Niobate	14
2.6	Introduction to tuning methods	16
2.7	Tuning with poling period and temperature	17
2.8	Tuning with intra-cavity elements	19
2.9	Pump tuning	23
2.10	OPO cavity design	24
2.11	Oscillation threshold for a singly resonant OPO	26
2.12	Photo-acoustic spectroscopy	27
<i>Chapter 3</i>		
Calculation of cavity dimensions		31
3.1	Introduction	31
3.2	Basic Theory of Gaussian beam transformation matrices	32
3.3	Calculation of Q for OPO cavity	33
3.4	Discussion	39

<i>Chapter 4</i>		
Continuous 34 GHz tuning of a singly resonant optical parametric oscillator using a skewed bowtie ring cavity		43
4.1	Introduction	44
4.2	Experiment	45
4.3	Results	46
4.4	Conclusion	48
<i>Chapter 5</i>		
Wide single mode tuning of a 3.0-3.8 micron, 700 mW, continuous wave Nd:YAG-pumped optical parametric oscillator based on periodically poled lithium niobate		51
5.1	Introduction	52
5.2	Experiment	52
5.3	Results	55
5.4	Conclusion	57
<i>Chapter 6</i>		
Tuning and stability of a continuous-wave mid infrared high power single resonant optical parametric oscillator		59
6.1	Introduction	60
6.2	Experimental setup	61
6.3	Air-spaced etalon	64
6.4	Solid Etalon	66
6.5	Trace gas detection	66
6.6	OPO wavelength stability	68
6.7	Conclusion	69
<i>Chapter 7</i>		
Photoacoustic trace gas detection of ethane using a continuously tunable, continuous-wave optical parametric oscillator based on periodically poled lithium niobate		71
7.1	Introduction	72
7.2	Experiment	72
7.3	Results	73
7.4	Conclusion	77

Chapter 8

Continuous-wave operation of single frequency optical parametric oscillator between 4-5 μm based on periodically poled LiNbO₃ **79**

8.1	Introduction	80
8.2	Experiment	80
8.3	Results	82
8.4	Conclusion	85

Chapter 9

Wide pump tuning and high power of a continuous-wave single resonant optical parametric oscillator **87**

9.1	Introduction	88
9.2	Experimental setup	89
9.3	Output power	91
9.4	Tunability	92
9.5	Frequency stability	95
9.6	OPO operation between 4 and 5 μm	97
9.7	Conclusion	98

Chapter 10

Real-time monitoring of the respiration of small insects and single cells with laser based CO₂ detection **103**

10.1	Introduction	104
10.2	Experiment	105
10.3	Detection limit of CO ₂	105
10.4	Monitoring insect breath	107
10.5	Improving the sensitivity	110
10.6	Single cell respiration	110
10.7	Conclusion	110

Summary **113**

Populair wetenschappelijke samenvatting **115**

Publications **117**

Curriculum Vitae **119**

1

Introduction

1.1 Trace gas detection

The term *trace gas detection* is used for measurements of minute concentrations of gasses, which are then related to biological, medical or atmospheric processes. A good example of trace gas detection put into practice is the breath-test that the police uses to determine the concentration of alcohol in your breath, which is then related to the concentration of alcohol in your blood. Without such a breath-test it would be very difficult to prove that a driver is drunk, because the only alternative method to test this would be taking a blood sample and analyzing it in a laboratory. I am pretty sure that most people would prefer a breath test over a blood test!

You could say that in the previous example ‘being drunk’ is a medical condition and alcohol is the trace gas used to test for this condition. The possibilities stretch a lot further than this though, because plants, animals and humans exhale and emit hundreds of different types of gasses. Trace gas detection of these gasses can be used to learn more about processes inside a living being. For example the storage lifetime of some fruit types has been greatly improved by studying the effect of different storage parameters on the release of trace gasses related to fermentation of the fruits. Next to research on plants, trace gas detection is also used frequently in research on insects. For example chapter 10 of this thesis describes the detection of the CO₂ respiration of one single ant and of one single fruit fly.

Very important developments are also being made in the application of trace gas detection in research on humans. In future the doctors can probably use breath analyzers to aid them in diagnosing a patient. The first steps towards this goal have been made already. For instance it is now possible to measure the damage done to human skin during sunbathing by monitoring the level of ethylene in the breath. When the skin is damaged, lipid peroxidation causes ethylene to be emitted as one of the by-products. Via the blood the ethylene is transported to the lungs and is eventually exhaled by the patient.

1.2 Optical Parametric Oscillator

Figure 1c shows the transmission spectrum of an atmospheric sample from earth over 300 meter pathlength. It shows that certain light frequencies are absorbed, where others are being transmitted. This is because every molecule absorbs light at a different set of frequencies (fig. 1b). A laser is able to produce just one single frequency of light and that means it is often able to select the absorption of just one type of molecule within a mixture of many kinds of gasses. That is why lasers are very powerful tools to use for trace gas detection.

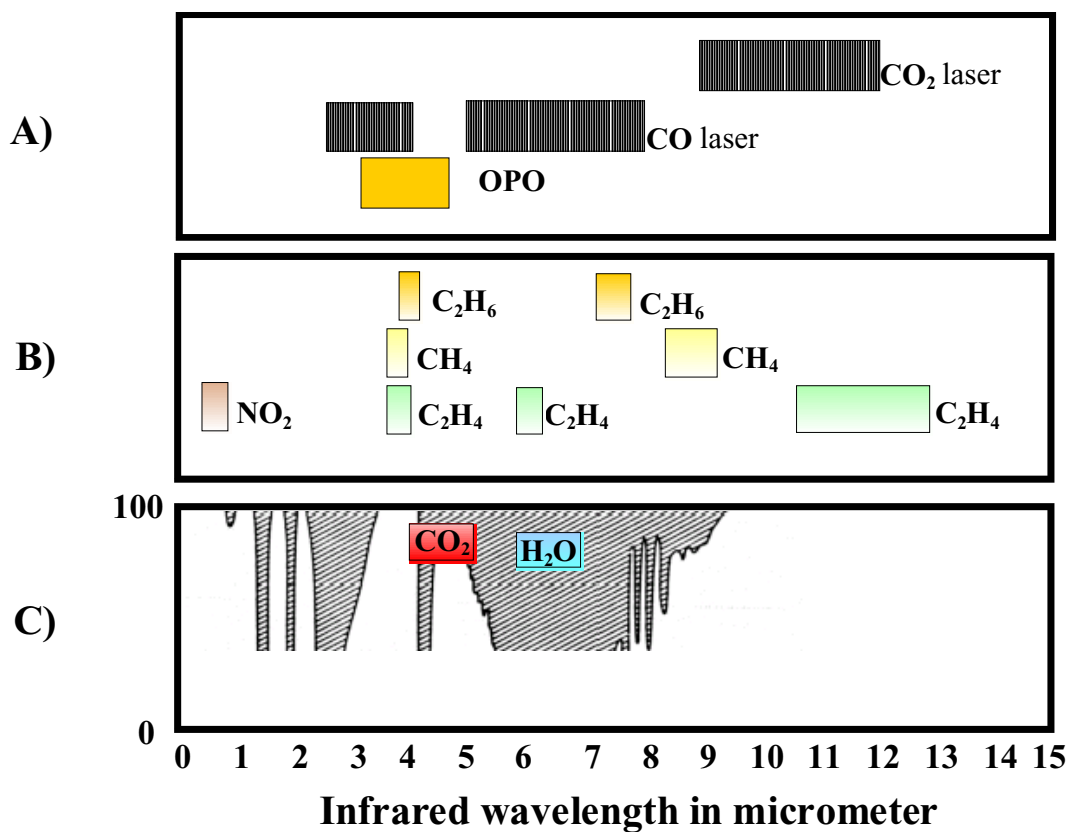


Fig. 1. The use of an OPO system compared to the CO and CO₂ laser that are currently used often. Panel A) shows the wavelength range in which the OPO works and this is compared to the CO and CO₂ lasers. Panel B) shows the ranges with the strongest absorptions for some important trace gasses. Panel C) shows the transmission spectrum of ambient air. Strong absorptions from CO₂ and H₂O are indicated. Important is that between 3 and 4 micrometer there is almost 100% transmission of the air. This means that it is easy to operate an OPO in this range.

A popular technique for detecting gasses with lasers is photo acoustic spectroscopy. In the next chapter this technique will be explained, but for now it is important to know that the performance of photo-acoustic spectroscopy depends on the total power of the laser emission. Typically high-power lasers such as CO and CO₂ lasers (figure 1a) are used and some very good results have been achieved with them. However, these lasers are line-tunable, which means that they can only produce certain frequencies within their operating range. Such lasers are only able to measure certain kinds of molecules, because they rely on a coincidental overlap between the laser frequency and the absorption of the molecule.

To solve this, we have developed a new Optical Parametric Oscillator (OPO). An OPO can convert one laser beam into two new laser beams with different frequencies. In such a way any laser frequency can be generated within the operation range of the OPO. Next to that, very high output powers can be achieved by using a very high-power pump source. This makes the OPO an ideal source for trace gas detection. However, the OPO developed here has many other features, which are not needed for photo acoustic spectroscopy. Most importantly, it has a very narrow linewidth and good stability. Combined with continuous tunability this makes the OPO very suited for high-resolution spectroscopy. It might seem strange that we choose to build an OPO, because it is better than is required for photo-acoustic spectroscopy. This is because there are no other laser sources available that combine high-power and wide continuous tunability in the wavelength range between 3 and 5 μm .

Figure 1b shows some molecules and the wavelength ranges for their strongest absorptions. There are many gasses that absorb between 3 and 4 μm , mainly due to the absorption of the C-H stretch, which lies in this region and is present in many molecules. This makes this wavelength range a 'fingerprint' area, which contains sets absorptions of many kinds of gasses. Since every molecule normally has a different set of absorptions, every gas has its own unique 'fingerprint'.

Chapters 4,5 and 6 of this thesis will present the development of two OPO systems operating in the wavelength range from 3.0 to 3.7 μm . The focus has been to be able to continuously tune these OPO systems, in order to make them easy to use for trace gas detection. The performance of the systems is studied and improved, leading to a combination of high output power and wide continuous tunability which is not matched by any other continuous-wave single-frequency OPO system in the world. In chapter 7 the use for trace gas detection will be demonstrated by setting a new state of the art record in sensitivity for Ethane.

Chapter 8 reports an OPO in the wavelength range of 3.9 to 4.8 μm . It is the first time that a single-frequency OPO operates in this range, because the OPO crystal absorbs the generated light. By using a high-power pump source we were able to overcome this problem. Chapter 9 shows the development of a new OPO system that uses a very high-power pump source and is very easy to use. Due to the high pump-power this system was also be operated up to 4.7 μm wavelength.

In chapter 10 this thesis concludes with a demonstration of the use of an OPO system for trace gas detection in life science research. The use is demonstrated by monitoring the CO₂ release of one single ant and of one single fruit fly. Hypothetically, the system should even be able to monitor the CO₂ release of single plant cells.

2

Theoretical introduction

Abstract

This chapter gives a short overview of the most important terms and theory related to this thesis. Because there are too many subjects to discuss, a selection has been made that should give enough background information to understand the contents of this thesis. This chapter starts with a discussion of birefringent phase matching, which is used as a basis to explain quasi phase matching. Next to this, the various tuning methods of an OPO and OPO cavity design are discussed. The chapter concludes with a short paragraph regarding photo acoustic spectroscopy.

2.1 Introduction

In simple terms it can be said that in an Optical Parametric Oscillator (OPO) the photons from a pump beam are split in two parts, forming two new photons with different energies. This process normally occurs inside a nonlinear crystal. The generated photon with the highest energy is termed the signal, and the other photon is termed the idler. The generated photons cannot be of any frequency due to energy conservation. In addition to that destructive interference between the photons needs to be prevented. This gives rise to a second restriction, called *phase matching*. Equation (1) shows these two restrictions for a birefringent phase-matched OPO:

$$\left\{ \begin{array}{l} \text{Energy conservation: } \omega_{pump} = \omega_{signal} + \omega_{idler} \\ \text{Phase matching: } n_{pump} \omega_{pump} = n_{signal} \omega_{signal} + n_{idler} \omega_{idler} \end{array} \right\} \quad (1)$$

In these equations ω is the energy of the photons and n is the index of refraction for the wavelength involved. Since this is a set of two equations with two unknowns it can be solved to calculate the signal and idler frequencies. Changing the signal and idler frequencies is difficult, but is possible if the values of n_i , n_s and n_p are changed, for instance by rotating or heating the crystal. With quasi phase matching a special crystal is used, which has a certain *poling period* Λ in the optical axis. This gives rise to an extra term in the phase-matching condition, and the resulting set of equations looks like this:

$$\left\{ \begin{array}{l} \text{Energy conservation: } \omega_{pump} = \omega_{signal} + \omega_{idler} \\ \text{Phase matching: } n_{pump} \omega_{pump} = n_{signal} \omega_{signal} + n_{idler} \omega_{idler} + 2\pi/\Lambda \end{array} \right\} \quad (2)$$

Again, this can be solved to get the signal and idler frequencies, but in this case the generated signal and idler frequencies can be changed by altering the value of Λ , for instance by translating the crystal if it has multiple poling periods. By poling the crystal with the right value for Λ , the phase-matching condition can always be met for any combination of pump and signal photons.

In the next two paragraphs, the theory of birefringent and quasi phase-matching will be discussed into more detail. After that, the Periodically Poled Lithium Niobate (PPLN) crystals, some theory related to OPO cavity design and OPO tuning will be discussed. This chapter concludes with a paragraph regarding photo acoustic spectroscopy, which is a detection technique often used with the OPOs reported in this thesis.

2.2 Birefringent phase matching

When a medium with nonlinear susceptibility χ is subject to an electric field E , generated for instance by a laser beam, a dielectric polarization P is generated. This can be written as an expansion in powers of the applied field:

$$P = \epsilon_0 (\chi^{(1)} E + \chi^{(2)} E^2 + \chi^{(3)} E^3 + \dots) \quad (1)$$

where $\chi^{(k)}$ is the k^{th} -order susceptibility tensor of rank k . Notice that $\chi^{(2)}$ is a tensor with components χ_{ijk} depending on the symmetry properties of the nonlinear crystal. Often these components are written in the *reduced Voigt notation* as d_{lm} . Suppose an EM wave composed out of two different frequencies ω_1 and ω_2 is incident on the nonlinear medium:

$$E = E_1 \cos(\omega_1 t - k_1 z) + E_2 \cos(\omega_2 t - k_2 z) \quad (2)$$

The induced polarization at a fixed position (say $z=0$) in the crystal is generated by the combined action of both frequencies. The first component of equation (1) with $\chi^{(1)} E$ gives the linear polarization. The first nonlinear part is given by the quadratic term $\chi^{(2)} E^2$ and gives these contributions (at $z=0$):

$$P^{(2)} = \epsilon_0 \chi^{(2)} E^2 = \quad (3a)$$

$$= \epsilon_0 \chi^{(2)} (E_1^2 \cos^2(\omega_1 t) + E_2^2 \cos^2(\omega_2 t) + 2E_1 E_2 \cos(\omega_1 t) \cos(\omega_2 t)) \quad (3b)$$

$$= \epsilon_0 \chi^{(2)} \left\{ \begin{array}{l} \frac{1}{2}(E_1^2 + E_2^2) + \frac{1}{2}E_1^2 \cos(2\omega_1 t) + \frac{1}{2}E_2^2 \cos(2\omega_2 t) \\ + E_1 E_2 [\cos((\omega_1 + \omega_2)t) + \cos((\omega_1 - \omega_2)t)] \end{array} \right\} \quad (3c)$$

There is a DC polarization with AC components at the second harmonic frequencies $2\omega_1$ and $2\omega_2$, and at the sum or difference frequencies $\omega_1 \pm \omega_2$. An OPO uses the difference frequency component, where the pump wave $\omega_p = \omega_1$ and a signal wave $\omega_s = \omega_2$ are mixed to generate a traveling polarization wave at the difference frequency $\omega_i = \omega_p - \omega_s$, called the idler frequency:

$$P(\omega_i, z) = \epsilon_0 \chi^{(2)} E_p E_s \cos((\omega_p - \omega_s)t) \quad (4)$$

Since the generated polarization field is driven by ω_p and ω_s , it travels with the same velocity, determined by n_p and n_s . The polarization wave radiates an idler wave, which travels at a velocity determined by n_i . Generally $n_p > n_s > n_i$, because of normal dispersion in the material, which means that the signal, pump and idler waves travel at different phase velocities, leading to an oscillation in the relative phase difference between the waves. This causes the direction of the power flow from one wave to the other to alternate as well, resulting in constructive and destructive interference. The distance over

which the relative phase of the waves changes by π is the *coherence length* L_C . This is shown schematically in figure 1:

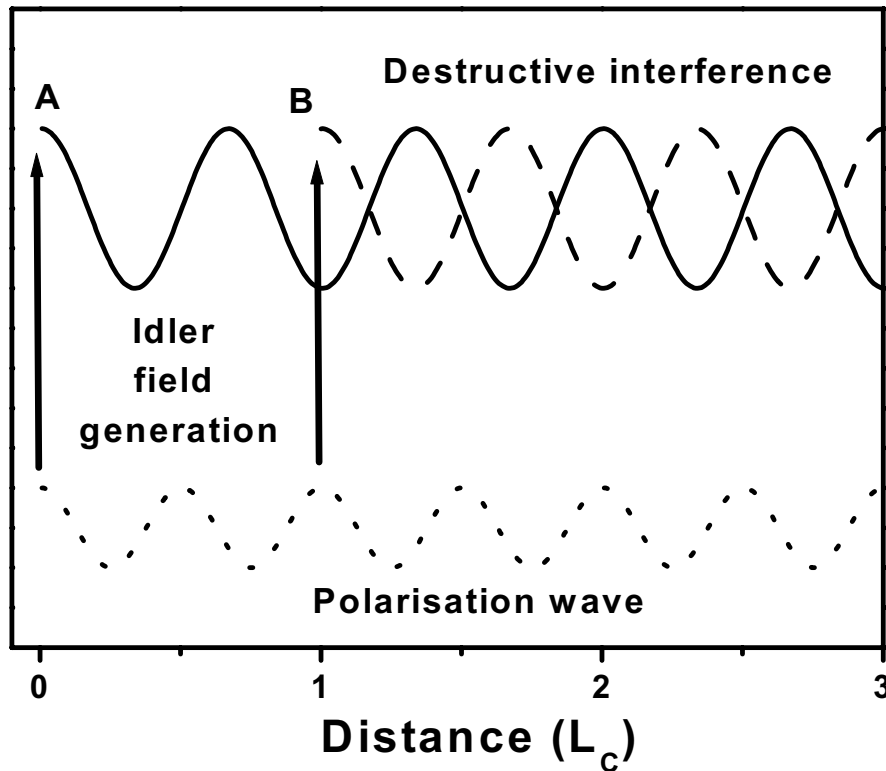


Fig. 1. The polarization wave (dotted line) radiates idler waves at all positions inside the crystal. At distance 0 a certain wave A is generated, indicated with the solid line. Exactly one coherence length L_C later, a wave B is emitted that is exactly out of phase with wave A, causing destructive interference between the two generated waves. Without phase matching any wave that is generated will be cancelled one coherence length L_C later, by a wave that is exactly out of phase.

Crystalline materials may have different indices of refraction associated with different crystallographic directions. A common situation with mineral crystals is that there are two distinct indices of refraction, and they are called birefringent materials (this is also known as double refraction). If the y- and z- directions are equivalent in terms of the crystalline forces, then the x-axis is unique and is called the optic axis of the material. The propagation of light along the optic axis would be independent of its polarization, because its electric field is everywhere perpendicular to the optic axis. This is called the ordinary- or o-wave. The light wave with E-field parallel to the optic axis is called the extraordinary- or e-wave.

By adjusting the birefringence of the crystal (for instance by rotating the crystal to change the angle between the pump beam and the crystal axis), the generated polarization wave

can be made to travel at the same velocity as the freely propagating idler wave, giving a cumulative growth. This is called the phase-matching condition and can be written as:

$$\mathbf{k}_p = \mathbf{k}_i + \mathbf{k}_s \quad (5)$$

which can be interpreted as *conservation of momentum of the three photons participating in the mixing process*.

The generated idler wave also mixes with the pump wave to generate a polarization wave at the signal frequency, resulting into a growth of the signal field. While this process continues both the signal and the idler fields will grow, while the pump field will decay as a function of the traveling distance in the crystal. The equations describing this process are given by [1-3]:

$$\frac{dE_s}{dz} = i\omega_s \frac{d_{eff}}{n_s c} E_p E_i^* \exp(-i\Delta kz) \quad (6a)$$

$$\frac{dE_i}{dz} = i\omega_i \frac{d_{eff}}{n_i c} E_p E_s^* \exp(-i\Delta kz) \quad (6b)$$

$$\frac{dE_p}{dz} = i\omega_p \frac{d_{eff}}{n_p c} E_s E_i \exp(i\Delta kz) \quad (6c)$$

where the quantities E_s , E_i and E_p are the amplitudes of the plane waves, n_s , n_i and n_p are the plane wave impedances (index of refraction) of the three waves and d_{eff} is the effective nonlinear coefficient. The value of d_{eff} follows from the d_{lm} values in the $\chi^{(2)}$ tensor and depends on the propagation direction relative to the crystal axis and on the polarization of the waves.

A small k vector mismatch is allowed and is given by Δk :

$$\Delta k = k_p - k_s - k_i \quad (7)$$

In this case, we are interested in generating idler power, so equation 6b is the most important. By integrating equation 6b the resulting idler output field can be calculated. Doing so can be difficult, due to the contributions of E_p and E_s , which are also depending on z (given by equation 6a and 6c). However, if just low idler power is generated the depletion or growth of E_p and E_s can be neglected. In the case of phase-matching $\Delta k=0$ and integrating equation 6b with constant E_p and E_s becomes trivial. The result is:

$$E_I(L) = i\omega_I \frac{d_{eff}}{n_I c} E_P E_S^* L \quad (8)$$

giving an idler intensity of:

$$\begin{aligned} I_I(L) &= \left(\frac{2}{n_I c \epsilon_0} \right) E_I(L) E_I(L)^* \\ &= \left(\frac{2}{n_I c \epsilon_0} \right) i\omega_I \frac{d_{eff}}{n_I c} E_P E_S^* L^* \left(-i\omega_I \frac{d_{eff}}{n_I c} E_P E_S^* L \right) \\ &= 2\omega_I^2 \frac{d_{eff}^2 L^2}{n_I^3 c^3 \epsilon_0} I_P I_S \end{aligned} \quad (9)$$

When Δk is not zero the integral of 6b can be written as [4]:

$$E_I(L) = i\omega_I \frac{d_{eff}}{n_I c} E_P E_S^* \frac{\sin(\Delta k L)}{\Delta k} \quad (10)$$

Notice that for $\Delta k=0$, equation 10 becomes the same as equation 8. The intensity can now be calculated to be:

$$I_I(L) = \left(\frac{2}{n_I c \epsilon_0} \right) E_I(L) E_I(L)^* = 2\omega_I^2 \frac{d_{eff}^2 L^2}{n_I^3 c^3} I_P I_S \left(\frac{\sin^2(\Delta k L)}{(\Delta k L)^2} \right) \quad (11)$$

The comparison between the generated idler E-field in the phase-matched and non phase-matched situation (eq. 8 and 10) is shown graphically in figure 2. With phase-matching the idler field increases linearly with the distance, but the non-phase-matched idler field keeps varying around zero due to the repetition of constructive and destructive interference.

Because constructive and destructive interference are periodically repeating it is possible to generate some idler radiation without phase-matching. However, only a small length of the crystal is really useful in producing idler radiation, because the destructive interference cancels out any positive effects of additional constructive interference. This is shown schematically in figure 3, which displays the intensity of the idler radiation as a function of the distance inside the crystal. The maximum length of the crystal that is useful in producing idler radiation is called the *coherence length*. This is the maximum possible length over which there is constructive interference and it is given by:

$$L_c = \pi/\Delta k \quad (12)$$

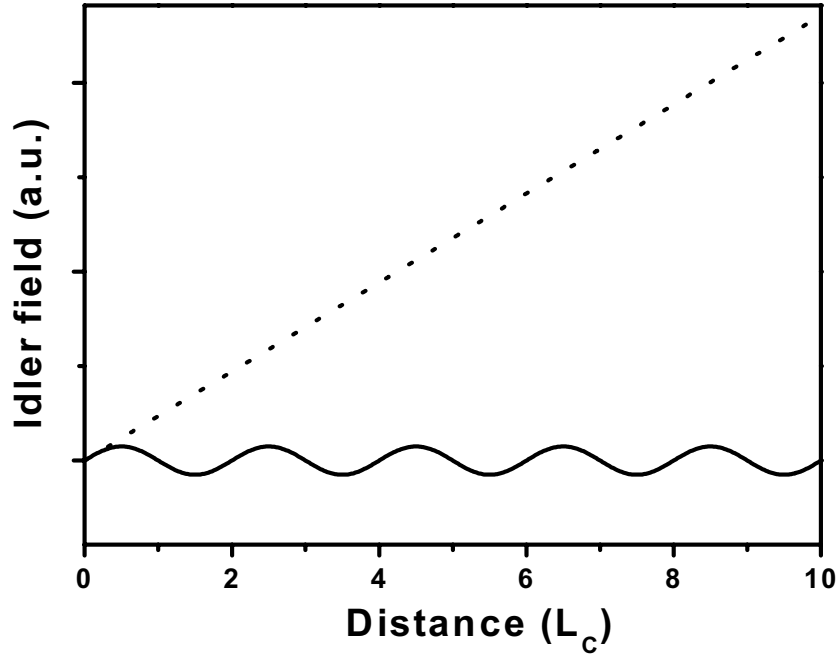


Fig. 2. The generated electric field for the idler frequency as a function of the distance inside the nonlinear crystal is shown for the phase-matched (dotted curve) and non phase-matched (solid curve) conditions. The distance is given in numbers of coherence lengths L_C . The non phase-matched curve oscillates around zero with a period of 2 times L_C . Since the intensity is the square of the electrical field, the intensity of the non phase-matched idler radiation will have a period of one L_C .

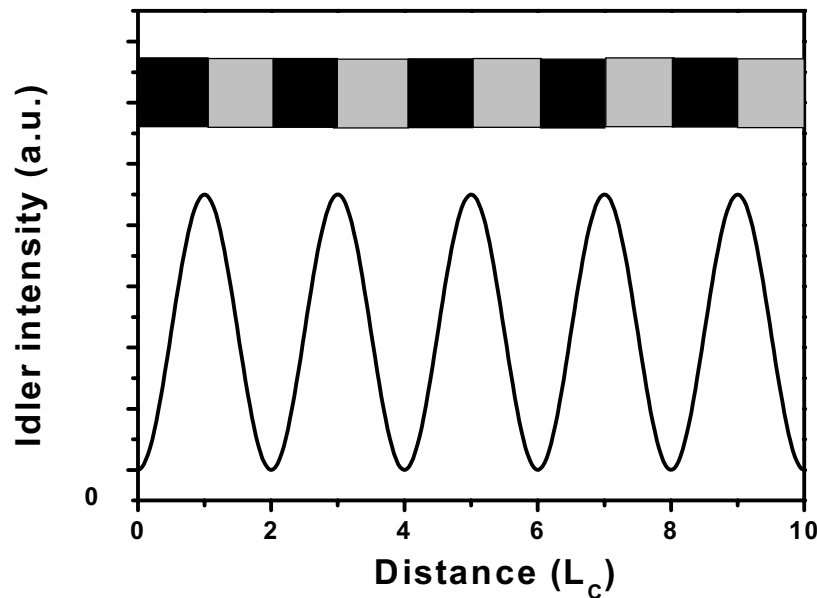


Fig. 3. The intensity of the idler radiation is shown relative to the length inside the nonlinear crystal. Periodically, constructive interference (indicated with a black bar) over a crystal length L_C is followed by destructive interference (light-gray bar) over the same length. If any idler radiation is generated, the maximum crystal length that has been useful is L_C .

2.3 Quasi phase-Matching

Quasi phase matching was devised independently by Armstrong *et al.* [5] in 1962 and by Franken *et al.* [6] in 1963. The invention removes the effect of the destructive interference by resetting the phase difference between the idler wave and the generated polarization wave after an odd number of coherence lengths. This can be achieved by periodically inverting the generated polarization wave, which is done by changing the sign of the nonlinear coefficient.

A way to do this is by forming a stack of thin wafers of the nonlinear crystal, rotating subsequent wafers by 180 degrees. In the past researchers had constructed alternating stacks of thin plates of CdTe [7], GaAs [8,9], quartz [10] and LiNbO₃ [10] for QPM second harmonic generation. A more practical approach involves forming regions of periodically reversed spontaneous polarization domains (with length Λ) in ferroelectric crystals like LiNbO₃, which is a technique commonly used these days.

The greatest conversion efficiency can be reached when the sign of the polarization is flipped every coherence length. This is called *first order QPM*. In figure 4 the idler field generated with QPM is compared to birefringent phase-matching and no phase-matching.

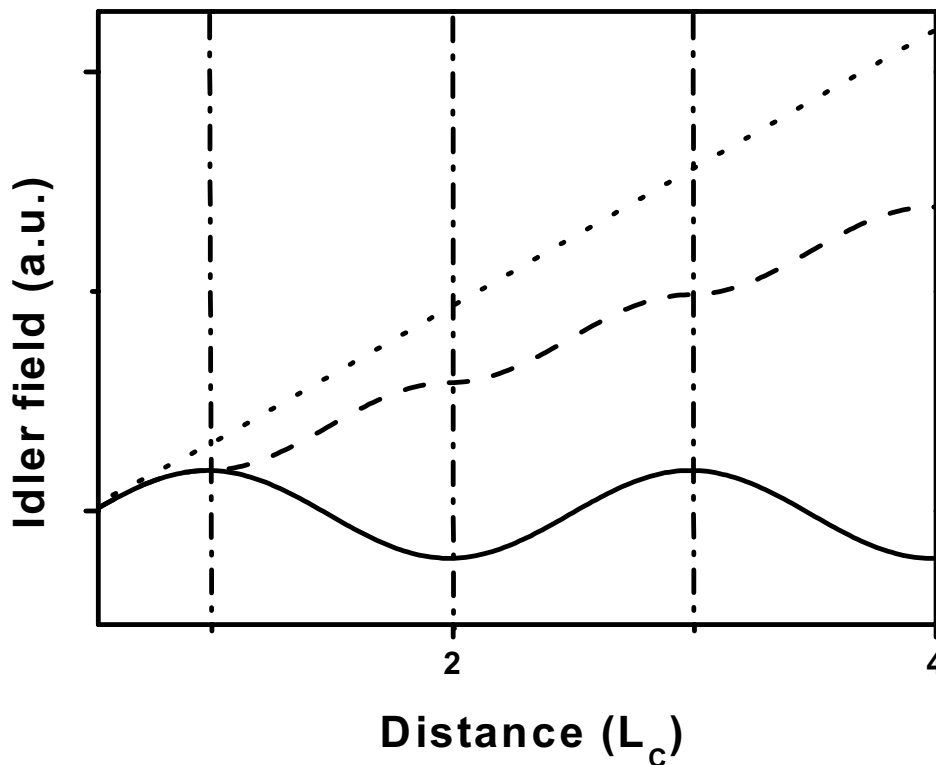


Fig. 4. The generated idler field is shown for no phase-matching (solid line), birefringent phase-matching (dotted line) and quasi phase-matching (dashed line). In quasi phase-matching the polarization-wave is inverted at the point where the solid curve starts to decrease (indicated by a vertical slash-dot line).

Figure 4 also shows that QPM is less efficient than birefringent phase matching. However, this does not mean that QPM will have a lower conversion efficiency. In contrast, it generally has a much higher efficiency, due to several additional advantages of QPM.

The first advantage of using QPM is that the idler, signal and pump waves can propagate collinearly. With birefringent phase-matching the crystal is rotated to adjust the birefringence of the crystal. This often means that the three waves will have different paths inside the crystal, limiting the range in which the beams overlap. With QPM the waves can have normal incidence on the nonlinear crystal, giving collinear propagation. This gives the maximum overlap between the waves. In addition, this means that with QPM very long crystals can be used, since the full length can be used as effective interaction zone.

A second advantage of QPM is that very high nonlinear coefficients can be used. With birefringent phase-matching the propagation direction through the crystal is determined by the angle required for phase-matching. Generally this means that the crystal direction with the highest nonlinear coefficient cannot be used. With QPM this problem doesn't exist, resulting in the use of much higher nonlinear coefficients. Next to that, with QPM it is also possible to use nonlinear crystals that are not birefringent, but have a very high nonlinear coefficient, such as for example GaAs and ZnSe.

With QPM there is no real phase matching, but on average the proper phase relationship is maintained for growth of the idler field. The effect of QPM is a (partial) compensation of the k-vector mismatch, which is now [3]:

$$\Delta k = k_p - k_s - k_i - \frac{2\pi}{\Lambda} \quad (13)$$

In which the length of the poling period of the crystal is given by Λ (for this thesis a typical number for this is $30 \mu\text{m}$). Thanks to this effect, the k-vector mismatch can always be zero by choosing the right value for Λ for a given combination of pump, signal and idler frequencies. This means that the phase-matching condition can always be reached, so the only remaining restriction is energy conservation.

2.4 Manley-Rowe relation

The energy of a photon depends on the frequency ($E = \hbar\omega$). If every converted pump photon results into one signal and one idler photon, it can be expected that the ratio between the powers of the generated signal and idler beams equals the ratio of their frequencies. This relation is called the Manley-Rowe relation, and it can be derived from the coupled amplitude equations (6) [1]. It is expressed in terms of intensity variations ΔI of the plane waves:

$$-\frac{\Delta I_{pump}}{\omega_{pump}} = \frac{\Delta I_{signal}}{\omega_{signal}} = \frac{\Delta I_{idler}}{\omega_{idler}} \quad (14)$$

2.5 Periodically Poled Lithium Niobate

In 1965 the first large boules of Lithium Niobate were grown at Bell Laboratories using the so-called Czochralski technique [11] and in that same year the first birefringent phase-matched OPO was reported using a 5-mm long Lithium Niobate crystal [12]. Even though the principle of QPM was already known at this time [5,6], it was almost 30 years after this, before Bosenberg *et al.* built the first quasi phase matched OPO in 1996 [13,14], using a Periodically Poled Lithium Niobate (PPLN) crystal with a single poling period (see figure 5).

PPLN is a good material to use for quasi phase matching due to its high nonlinear coefficient d_{lm} (which is a component of the $\chi^{(2)}$ tensor), combined with a wide transparency range (see table 1). Recently, periodically poled GaAs has also gained a lot of interest [15], but the growth this material is not very well developed yet. However, the poled structure of PPLN can be engineered with a photolithographic mask, which makes it easy to produce. These days there are many companies that specialize in growing PPLN, which makes the material cheap and easy to get.

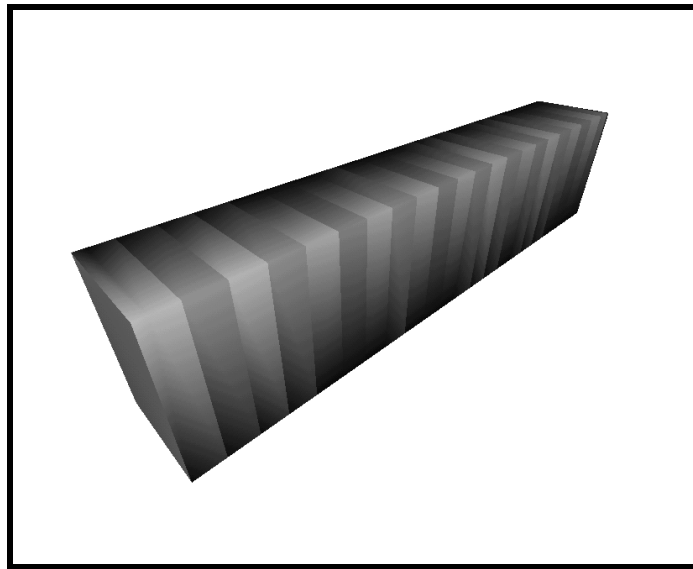


Fig. 5. PPLN crystal with a single poling period. In this picture the poling period is strongly exaggerated. A typical crystal is 5 cm long with a poling period around 30 μm .

Because the poled regions can be controlled through photolithography a single crystal can be engineered to have several instead of just one poling period. Currently crystals with as many as eight different poling regions are available (fig. 6). When such crystals are used in an OPO, the operation range can be increased significantly by selecting the poling period of the crystal with translation of the PPLN through the laser beam.

Table 1: Approximate values of nonlinear coefficients and transparency range of several types of periodically poled crystals

Type	Nonlinear Coefficient d_{lm} (pm/V)	Transparency range (μm)
PPLN	$d_{33}=27$	0.33-4.5
PPKTP	$d_{33}=10.7$	0.35-4.5
PPRTA	$d_{33}=12.1$	0.35-5.8
PPGaAs[15]	$d_{14}= 90-150$	0.9-12.5
PPLT	$d_{33}=13.8$	0.28-7

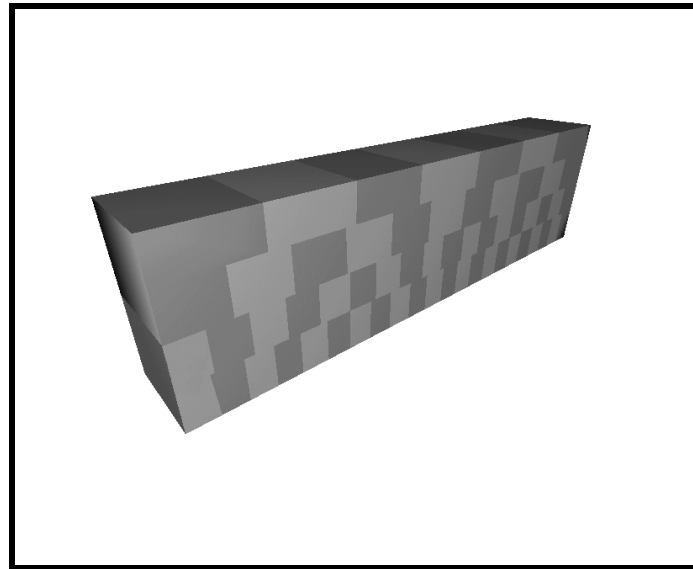


Fig. 6. Periodically Poled Lithium Niobate crystal with a step grating design that has four different poling periods. Typically a PPLN crystal has eight periods.

To take full advantage of this novel way to engineer PPLN crystals, one could use a fan-out grating design (fig. 7), as was demonstrated in 1998 at Sandia National Laboratories by Powers *et al.* [16]. Such a design gives access to any poling period within its minimum and maximum poling periods by translating the crystal through the OPO cavity. In this thesis both step grating and fan-out grating PPLN crystals are used.

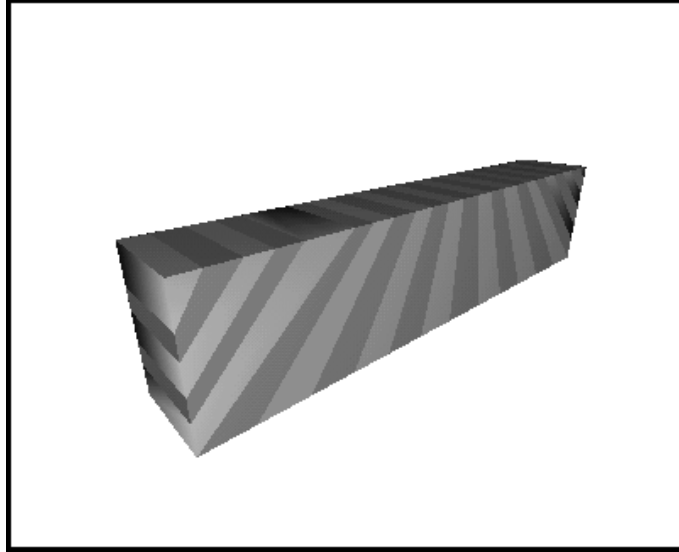


Fig. 7. Periodically Poled Lithium Niobate crystal with a fan-out grating design. The poling period is strongly exaggerated in this picture.

Even though PPLN has many advantages, it is not without problems. It has a relatively low damage threshold compared to other common nonlinear materials, and it suffers from photo-refractive damage. Heating the PPLN crystal has been found to prevent this damage. This is a commonly used solution, but it can affect the performance of the OPO system, because the temperature affects the point at which phase matching occurs. In chapter 6 it will be shown that temperature fluctuations in the PPLN crystal can lead to instabilities of the idler frequency. An alternative way to prevent photo-refractive damage is by doping the crystal with another material, such as MgO. For this thesis, only crystal heating was used to avoid photo-refractive damage, because the available doped crystals were not of the same high quality as the normal PPLN crystals.

2.6 Introduction to tuning methods

One of the main advantages of OPOs compared to other laser systems is their wide wavelength tunability, which means that they can cover a wide range of molecular absorptions. In this thesis tuning is categorized into two groups, namely *total tuning range* and *continuous tuning range*.

The *total tuning range* is the total range of available wavelengths that the OPO can generate. However, if the total tuning range of a laser system is said to be for instance from 3.0 to 3.5 μm , this does not necessarily mean that it is able to generate any wavelength within this range. Good examples of this are the line-tunable CO laser (total tuning range is roughly 2.5 to 4 μm and 5 to 8 μm) and CO₂ laser (9-12 μm), which can only generate specific wavelengths within their operation range. For the OPOs reported in this thesis, the total tuning range is achieved by tuning the poling periods and temperature of the crystal. However, also pump tuning can be used for this depending on the pump source that is used.

The wavelength range between which the OPO is able to generate any wavelength, without making a hop in between, is called the *continuous tuning range*. This range is important, because for high resolution spectroscopy a continuous tuning range over at least one, but preferably multiple ro-vibrational lines is necessary. Here, this will mainly be achieved using pump tuning, but also tuning of the intra-cavity elements is a possibility that is explored in chapter 4.

Normally, standard temperature and pressure (STP) are used with trace-gas detection. Typically this means that absorption lines will have a broadness of about 7.5 GHz. In order to accurately measure such an absorption line it is not necessary to be able to continuously tune the OPO, but it is sufficient if the OPO can tune in steps that are small enough to achieve a good resolution of the scan. This can be achieved with mode-hop tuning [17], which is an alternative way to tune the OPO with intra-cavity elements.

In the next three paragraphs these different tuning methods will be discussed separately.

2.7 Tuning with poling period and temperature

In paragraph 3 it has been shown that the generated signal and idler frequencies depend on the poling period of the PPLN crystal. For a particular PPLN grating period and temperature, the idler wavelength can be calculated using the Sellmeier equations as was done by Jundt [18] in 1997. Figure 8 shows the calculated signal and idler frequencies as a function of the poling period at a temperature of 180 °C, pumped by a 1064 nm laser source. The use of this figure is not only to determine the generated wavelengths for a given poling period, but it can also be used to decide which poling period to use for the OPO if the desired wavelength is known. For example, in chapter 7 idler radiation at 3333 nm is used in order to measure a strong absorption of ethane. Using a pump source of 1064 nm, a poling period of 29.5 μm at a temperature of 180 °C can be used to achieve this.

In figure 8 the solid line indicates the calculated idler and signal wavelengths, but in practice a PPLN crystal has just one, or several (typically up to 8) different periods. Since this limits the wavelengths that the OPO can generate, additional tuning methods need to be used in order to cover the full wavelength range. If a fan-out grating design is used, then the total wavelength range could be covered without using additional methods of tuning [17] (see paragraph 5).

Tuning with the grating period means that the PPLN crystal needs to be translated through the OPO cavity, which is usually slow. Translation needs to be done very carefully to prevent the PPLN crystal from breaking when the pump beam hits a potentially damaged spot. An additional problem with this tuning method is that the OPO cavity may need re-alignment. Due to this, it is also difficult to automate translation with a stepper motor.

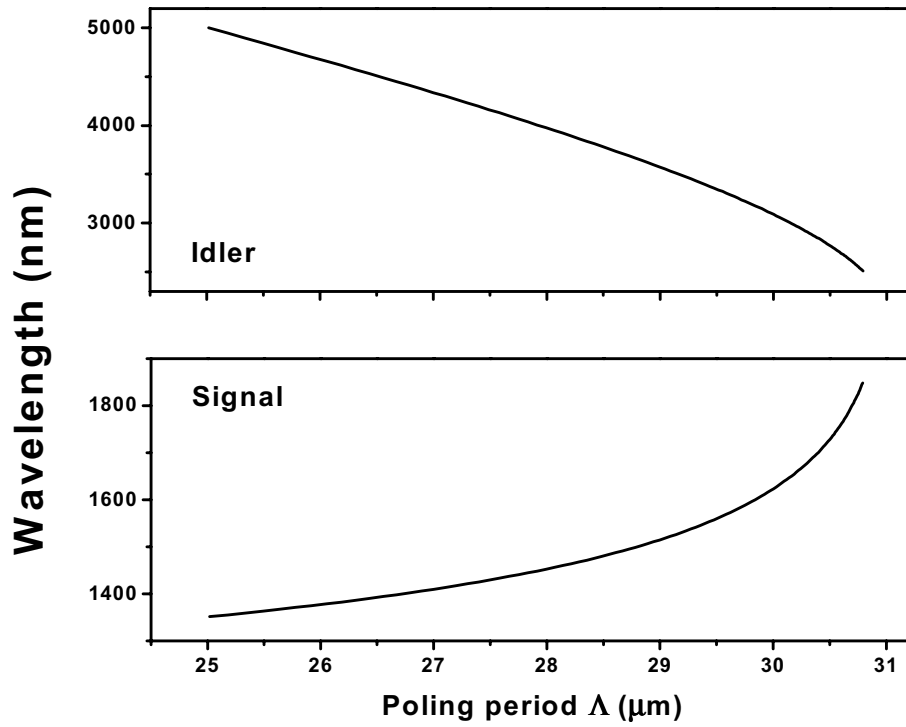


Fig. 8. Calculated signal and idler frequencies for poling periods ranging from 25 to 31 μm , when pumping with 1064 nm at a temperature of 180 $^{\circ}\text{C}$.

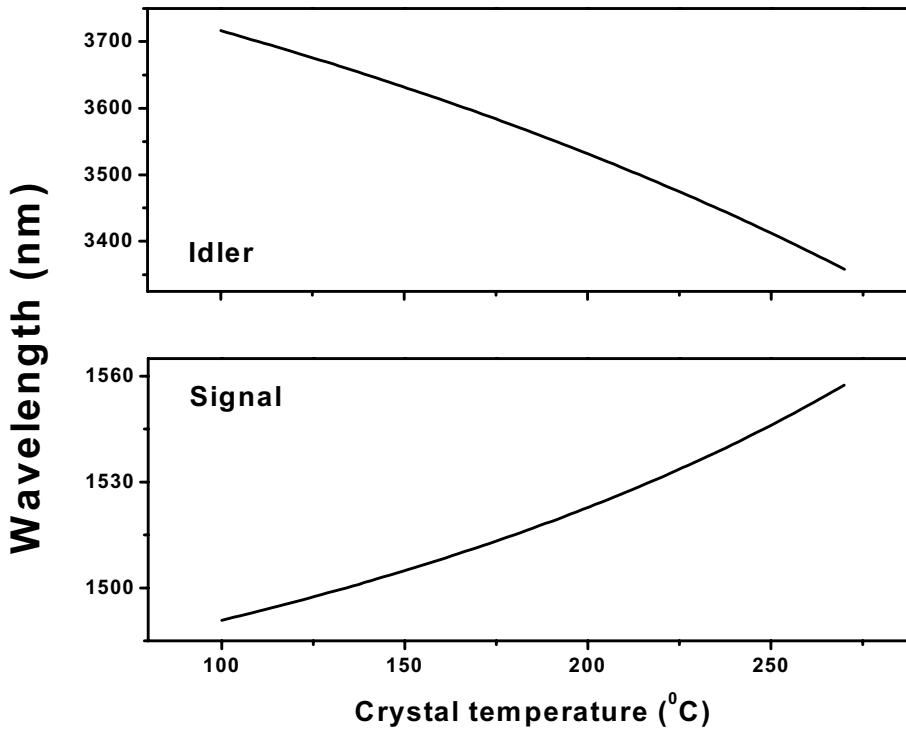


Fig. 9. Calculated signal and idler frequencies depending on temperature for a poling period of 29 μm , when pumping with 1064 nm.

Just like many other materials the PPLN crystal expands when it is heated, which will cause the poling periods to increase. For that reason it is common to always state the poling periods at room temperature. Figure 9 shows the calculated signal and idler wavelengths when the PPLN temperature is tuned from 100 to 270 °C, using a period of 29 μm and a pump frequency of 1064 nm. In this way a rather wide tuning range can be achieved for the idler frequency from 3400 to 3700 nm. In practice, the highest temperature that the crystal oven can reach limits the total temperature tuning range. As mentioned previously in paragraph 5, the crystal is heated in order to prevent photo-refractive damage. This places a lower limit on the temperature that can be used. Typically temperatures of at least 140 °C are used, but higher temperatures will significantly increase the lifetime of the PPLN crystal. Arbore and McHugh [19] have found that higher crystal temperatures (>180 °C) may even eliminate photo-refractive damage combined with an improvement in frequency stability.

Small variations in the temperature can be used to fine-tune the OPO system. In chapter 8 this is used to tune the OPO to the maximum of a CO₂ absorption. For example, with a PPLN period of 29 μm, a temperature change from 180 to 181 °C can tune the idler frequency over roughly 48 GHz. However, this method of tuning will not result in continuous tuning, because the signal frequency will be mode-hopping over the free spectral range of the OPO cavity (more about this in paragraph 8). When there are unwanted fluctuations in the temperature of the PPLN crystal, the generated idler wavelength will also tune and thus become unstable. Therefore it is important to have a very good (better than 0.01 °C) temperature stability of the crystal oven. In chapter 6 it will be shown how temperature fluctuations in the crystal can cause instabilities in the idler frequency.

2.8 Tuning with intra-cavity elements

An OPO consists of various optical elements. Many of these elements work as a multiple beam interferometer (in this case also referred to as Fabry-Perot interferometer). A Fabry-Perot interferometer basically consists of two surfaces of reflectivity R between which a laser beam can reflect, causing interference effects. For many frequencies of light there will be destructive interference, because the phases between the various passes through the interferometer are not matched. However, when the distance between the reflecting surfaces equals an integer number times the wavelength of the light, full transmission through the interferometer can be achieved. The transmission of such an interferometer is given by the *Airy formulas*. Neglecting absorption of light in the Fabry-Perot, they are written as [4]:

$$I_R = I_0 \frac{F \sin^2(\phi/2)}{1 + F \sin^2(\phi/2)} \quad (15)$$

$$I_T = I_0 \frac{1}{1 + F \sin^2(\phi/2)}$$

In which I_R and I_T are the reflected and transmitted intensities, respectively. I_0 is the incident intensity of the light. F is related to the finesse F^* and is given by:

$$F = \frac{4R}{(1-R)^2} \tag{16}$$

$$F^* = \frac{\pi}{2} \sqrt{F}$$

Finally, ϕ is the phase difference between alternating passes of the light:

$$\phi = 2\pi \frac{\Delta s}{\lambda} \tag{17}$$

In which λ is the wavelength of the light and Δs gives the optical path difference between two successively reflected waves. This is given by $\Delta s = 2nd \cos(\beta)$, with β as the angle between the light beam and the normal of the interferometer and d as the distance between the reflective surfaces. Figure 10 shows I_T for different values of the reflectivity R .

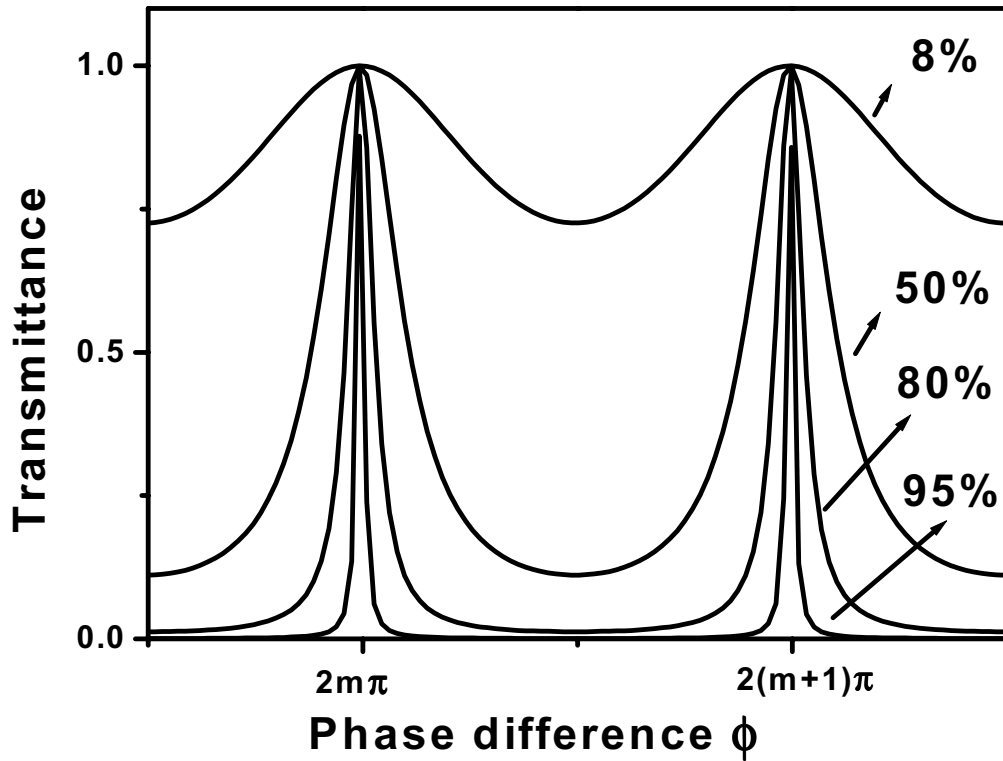


Fig. 10. Transmission of an absorption-free multiple beam interferometer as a function of the phase difference ϕ for different values of the reflectivity.

The higher the reflectivity, the sharper the transmission peak becomes. The *free spectral range* v_{FSR} gives the distance between two transmission peaks of the interferometer:

$$v_{FSR} = \frac{c}{\Delta s} = \frac{c}{2nd \cos(\beta)} \quad (18)$$

Figure 11 demonstrates the use of Fabry-Perot interferometers (FPIs) in an OPO. The OPO cavity consists of mirrors with a high reflectivity for the signal wavelength, so it is a high-finesse FPI. This restricts the signal frequencies of the OPO to a certain set of frequencies (called cavity modes), given by the transmission peaks of the cavity (fig 11c). Combined with the QPM gain curve (fig 11a), one cavity mode will be selected for OPO oscillation. However, if the restriction on the cavity modes is not strong enough, the signal frequency is able to hop from one cavity mode to another. This is called a cavity mode-hop.

The OPO cavity can be stabilized with an *air-spaced etalon* or *solid etalon* (fig. 12), which places an additional FPI (fig. 11b) restriction on the cavity-modes that can be used for oscillation. A solid etalon is a solid plane-parallel piece of material with two coated reflecting surfaces.

An air-spaced etalon consists of two separate plates, where one surface of each plate is coated with a reflection layer and the other surface is coated with an anti-reflection layer and has an angle against the inner surface (called wedge). The two reflective surfaces oppose each other and are aligned as parallel as possible.

Insertion of the etalon into the OPO cavity normally restricts the cavity modes enough to make the OPO operate at a single signal frequency and it is able to prevent mode-hops in the cavity. Figure 11d shows how the combined contributions of the cavity modes, etalon modes and QPM gain curve select one mode with the highest transmission.

If the location of the etalons transmission peaks can be tuned, the signal frequency can be tuned as well. Due to energy conservation, the tuning of the signal wavelength is then transferred to the idler wavelength. With an air-spaced etalon this can be accomplished by changing the distance between the reflective surfaces, which changes the free spectral range of the etalon and as a result will move the location of the transmission peaks. In order accurately tune the etalon, a piezo is normally used to move the mirrors. With a solid etalon the free spectral range can be tuned by rotating the etalon, for instance with a galvo-driver.

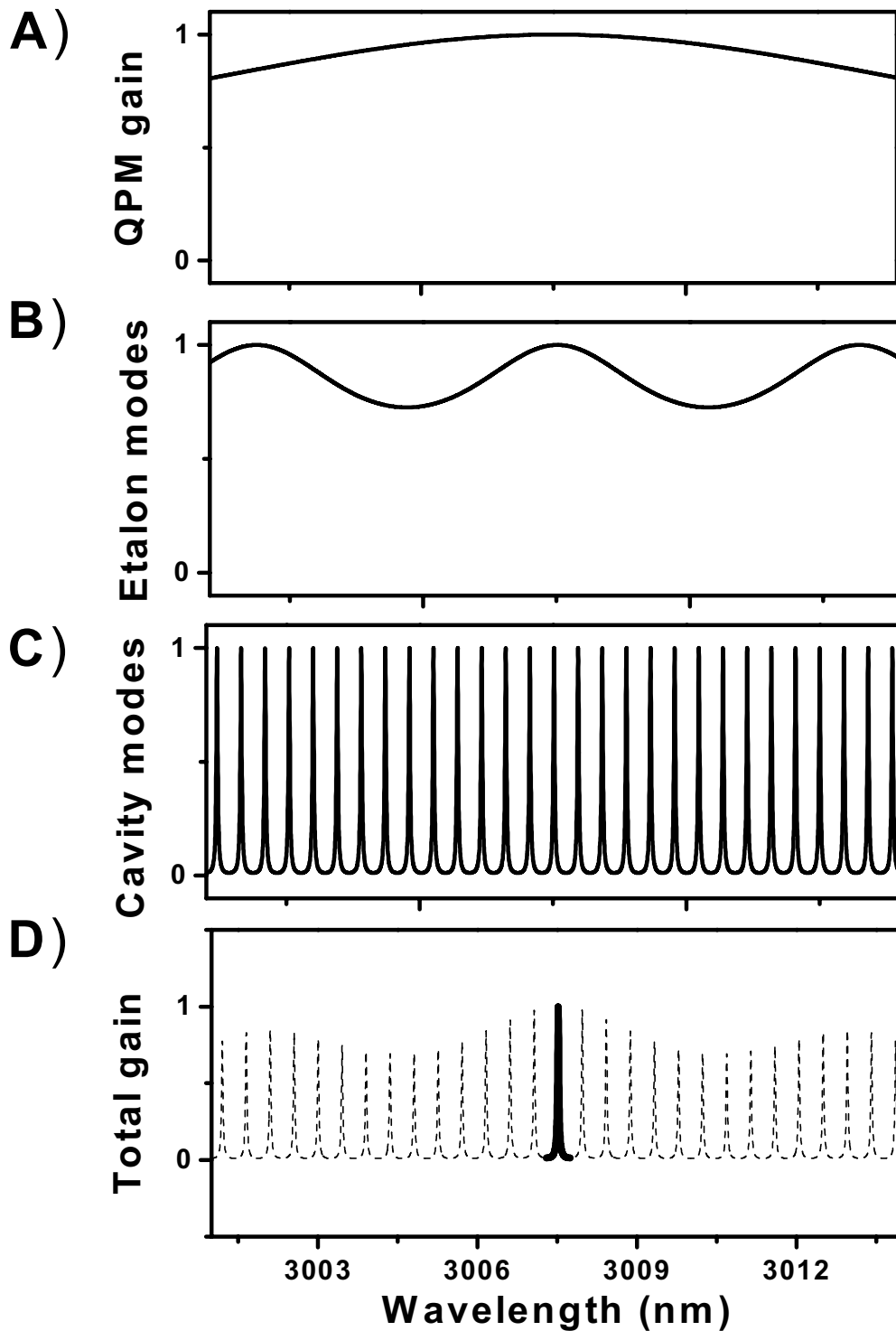


Fig. 11. Contributions to the total gain curve of the OPO due to a) the QPM phase-mismatch, b) the modes of the intra-cavity etalon in the OPO and c) the cavity modes of the OPO. The contributions from a), b) and c) are multiplied in order to get the total gain curve, shown in panel d), with the highest transmission is indicated by a thick solid line. The transmission of the cavity modes has been adjusted for better visibility. In reality they are closer together and very narrow.

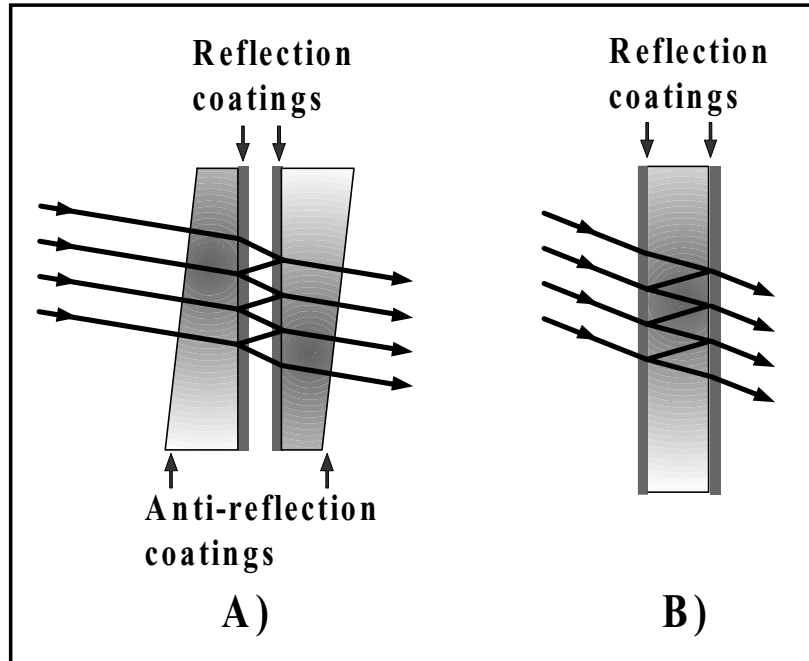


Fig. 12. Two realizations of a Fabry-Perot interferometer. A) air-spaced etalon. B) solid etalon.

2.9 Pump tuning

Due to energy conservation the generated signal and idler frequencies are widely tunable if the pump frequency is widely tunable as well. Figure 13 shows an example of this, where a PPLN crystal with period $29\ \mu\text{m}$ and temperature $180\ ^\circ\text{C}$ is pump tuned from 1020 to 1050 nm. This wavelength range can be provided by the type of pump laser that is used in chapter 9. The calculated total idler tuning range is from 2950 to 3430 nm, which is a larger range than can be realistically reached with temperature tuning (see paragraph 7).

The widest continuous tuning ranges for cw OPOs reported so far have all been achieved with continuously tunable pump sources [20-22]. With continuous pump tuning the OPO cavity is commonly stabilized with an intra-cavity etalon (see paragraph 8). This means that the signal frequency remains constant, while the idler frequency tunes by the same amount as the pump frequency is tuned. This method is used in Chapter 4 of this thesis, in order to build an OPO with a 24 GHz continuous pump-tuning range. At that time, this was the widest range ever reported for a Nd:YAG pumped OPO.

A problem appears if the pump frequency is tuned very far with a stabilized OPO cavity. At first the signal frequency is constant, but a mode-hop occurs if the difference between the calculated signal frequency (see fig. 13) and the generated signal frequency exceeds the free spectral range of the intra-cavity etalon. When the signal frequency makes a mode-hop, the idler frequency will also make a mode-hop, but in the opposite direction.

Normally, the direction of the idler-mode hop is the same as the direction of tuning, which means that the OPO is not able to generate all frequencies. The solution is to prevent mode-hops in the signal frequency by rotating the intra-cavity etalon, or by changing the temperature of the crystal. This problem will be described in more detail in chapter 9.

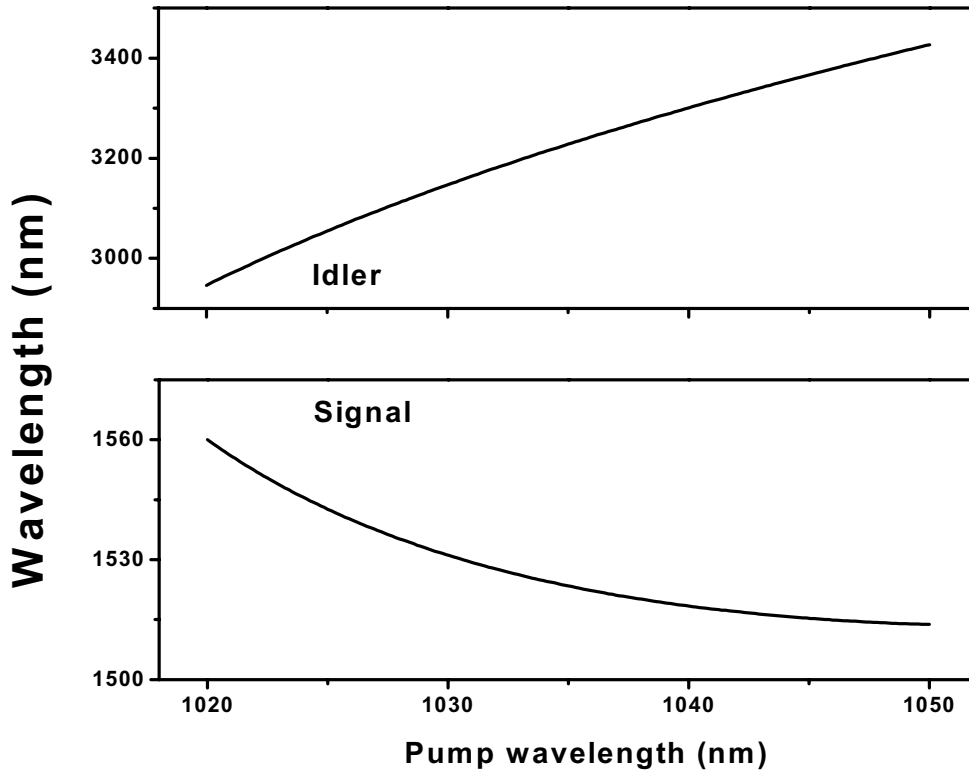


Fig. 13. Calculated signal and idler frequencies depending on pump wavelength at 180 °C, for a poling period of 29 μm .

2.10 OPO cavity design

There are several issues to take into account when designing the OPO cavity. One of the first considerations is for which wavelengths the cavity should be resonant. The simplest OPO cavity setup is the *singly resonant OPO* (SRO). In this design the OPO cavity mirrors are only reflective for the signal wavelength and have a high transmission for the pump and idler frequencies. The advantage of this setup is that it is easy to tune and simple to set up. The drawback is that an SRO has a very high *oscillation threshold*, which means that it requires a high pump power in order to start oscillating. A typical oscillation threshold for such devices is at least 3 Watts of pump power.

In order to reduce the oscillation threshold, the OPO cavity can be made resonant for the idler and/or pump frequencies. A *doubly resonant OPO* can be built that is resonant for

the signal and idler frequencies, but normally the cavity is made resonant for the signal and pump wavelengths. Such a design can be termed a *pump enhanced OPO*, *doubly resonant OPO*, or *pump resonant SRO*. An example is a 20 MHz line-width doubly resonant OPO with 18 mW idler output power covering the 2.2-3.7 μm region [20]. Another example is a 5 MHz linewidth OPO with 100 mW output power at idler frequencies between 2.3 and 4 μm [23]. The advantage of these systems is that they have a very low oscillation threshold (for the last example it could be as low as 135 mW), but the idler output power is rather low compared to an SRO setup (mainly because pump sources with lower power are used). When a pump resonant OPO is pump-tuned, the length of the cavity needs to be adjusted to keep the cavity resonant for the pump frequency. Due to this, a double resonant design does not allow very wide continuous pump tuning, since both the signal and pump wavelengths need to be kept in resonance. However, this problem can be solved by using two different cavities for the signal and pump wavelengths (see figure 14). The cavity then consists of three mirrors, with mirror 1 on one side of the crystal and mirror 2 and 3 on the other side. The first mirror is reflective for both the signal and pump wavelengths, the second mirror reflects the pump wave and transmits the signal light and the third mirror is reflective for the signal frequency only. In this way there are now two cavities, namely a signal resonant cavity between mirror 1 and 3 and a pump resonant cavity between mirror 1 and 2. When the pump source is now tuned, both cavities can be adjusted independently in order to keep both the pump and signal frequencies resonant [24,25].

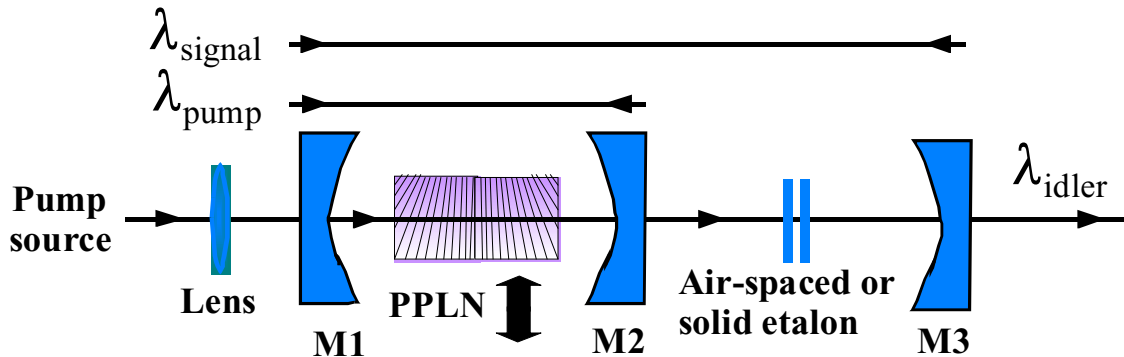


Fig. 14. Double resonant OPO cavity, with separate cavities for the signal and pump waves. The pump waves are reflected by mirror M1 and M2, and the signal waves by mirror M1 and M3. In this way an etalon can be used for the signal wave only.

In a triply resonant OPO the signal, idler and pump waves are all resonant. An example of such an OPO gives signal and idler radiation at 2.12 μm with a 1.06 μm pump source [26,27]. That system had an oscillation threshold below 0.5 mW and a signal + idler output power of several milliWatts. Clearly, the ultra-low threshold is an advantage, but in most cases the oscillation threshold of a doubly resonant OPO is low enough for the pump source that is used. Furthermore, one can expect even more problems with wavelength tuning and stability, since in this case also the idler frequency needs to be kept in resonance.

This thesis describes the development of a high-power OPO system, to be applied in trace-gas detection with photo acoustic spectroscopy. To obtain high output power a high power pump source is used, which means that a multi-resonant design is not required. For this reason all the OPOs reported in this thesis will be using a singly resonant OPO setup.

The next consideration to take into account when building an OPO system is whether to use a linear cavity or a ring cavity. This was studied in 1996 by Bosenberg *et al.* [14] by comparing the pump power versus idler output power of both a linear and a ring cavity. They found that the linear cavity had a higher oscillation threshold of 6.0 W compared to 3.6 Watts for the ring cavity. However, the conversion efficiency of the linear cavity went up faster and at 13.5 Watts of pump power the linear cavity produced 3.60 Watts compared to 3.55 Watts for the ring cavity. They also found that the linear cavity had quite different spectral properties than the ring cavity. Instead of running on a single mode of the OPO resonator, the linear cavity tended to run with linewidths of $\sim 2 \text{ cm}^{-1}$.

In this thesis a typical pump power of 10 Watts is used. Because a higher output power and a better stability are expected for the ring cavity, a bowtie ring cavity design will be used throughout this thesis.

The next important considerations for the OPO cavity design are its dimensions and the properties of the mirrors that are used. This will be discussed into detail in the next chapter (3).

2.11 Oscillation threshold for a singly resonant OPO

The oscillation threshold P_T for a singly resonant OPO is given by [3]:

$$P_T = A \frac{\lambda_p \lambda_s \lambda_i}{d_{\text{eff}}^2 L_c} \quad (19)$$

in which λ_p , λ_s and λ_i represent the wavelength of the respectively the pump, signal and idler waves. The effective nonlinear coefficient is given by d_{eff} and L_c gives the crystal length. A represents several other factors, such as for instance round-trip loss at the signal, transmission of the pump wave through the setup and the waist of the pump beam.

Important to note is that in equation (19) d_{eff} is represent as d_{eff}^2 , making it the most important factor for the threshold power. The effect of λ_p , λ_s and λ_i is important for generating very long wavelengths, because it turns out that the lowest threshold can be achieved with a pump wavelength that is as short as possible.

To demonstrate this, the value for $(\lambda_p \lambda_s \lambda_i)$ is compared for three ways of generating 10 μm radiation, namely using a 1 μm , 3 μm and 5 μm pump source. The results are shown in table 2:

Table 2: The effect of the pump wavelength on the oscillation threshold

Pump	Signal	Idler	$(\lambda_p\lambda_s\lambda_i)$
1 μm	1.11 μm	10 μm	11.1
3 μm	4.29 μm	10 μm	128.7
5 μm	10 μm	10 μm	500

What this shows is that the calculated oscillation threshold will be lower if a shorter pump wavelength is used. The difference between 1 and 5 μm pump wavelengths is roughly factor of 50 in this case. However, this does not mean that the output power will also be 50 times lower, because the ratio between the idler output power and the pump power is better for longer pump wavelengths due to the Manley Rowe relation (paragraph 4). The conclusion is that for high-power idler generation a long-wavelength pump source should be used, but for low power pump-sources a shorter wavelength will help to reduce the oscillation threshold.

2.12 Photo acoustic spectroscopy

Photo acoustic spectroscopy [28, 29] can be used for many applications, but is mainly applied to detect minute concentrations of molecular species in the presence of other components at higher pressure. It is a very sensitive technique for trace gas detection and will therefore be used frequently in this thesis.

The basic photo acoustic setup is shown in figure 15. A laser beam is sent through a rotating blade (termed chopper), which chops the beam into a series of light pulses at a certain frequency. These pulses of light are sent through the Photo Acoustic Cell (PAC), in which a gas sample has been enclosed. If the laser wavelength is tuned to an absorbing molecular transition, i.e. $E_I \rightarrow E_K$, some of the molecules in the lower level E_I will be excited into the upper level E_K . By collisions with other atoms or molecules these excited molecules may transfer their excitation energy into translational, rotational, or vibrational energy of the collision partners. At thermal equilibrium this causes an increase of thermal energy, resulting in a rise of the temperature and pressure inside the cell. This means that every pulse of light will cause an increase in pressure after which the pressure can reduce again, before the next pulse arrives. The pressure wave that is generated in this way is sound that can be heard provided that the sound has sufficient volume and that the frequency (determined by the chopping frequency) lies within the hearing range of the human ear. However, very often a chopping frequency outside this range is used.

The PAC acts like an organ tube with its resonance frequency matched to the chopping frequency of the laser beam. Due to this it amplifies the generated sound wave, after which it is transformed into an electronic signal with a microphone. A lock-in amplifier is used for further amplification and demodulation of this signal.

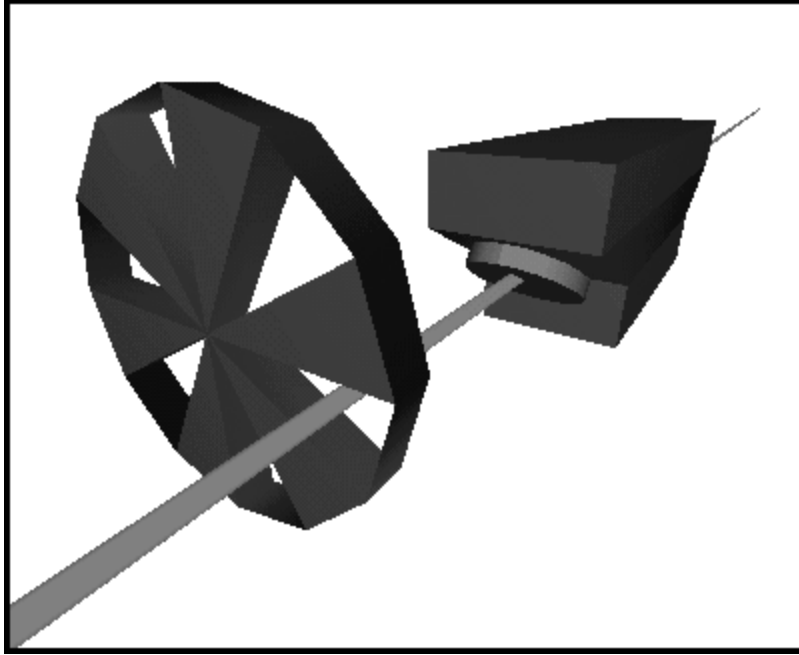


Fig. 14. A photo-acoustic spectroscopy setup. A chopper is used to modulate the laser beam. The light is then send through the photo-acoustic cell, where it will generate sound waves. These sound waves are detected with a microphone.

The lock-in amplifier is used to measure the amplitude and phase of the signal buried in noise. It achieves this by acting as a narrow bandpass filter, which removes much of the unwanted noise while allowing through the signal that is to be measured. The frequency of the signal to be measured and hence the bandpass region of the filter is set by a reference chopping frequency. In this way the sounds produced by the surroundings of the PAC can be suppressed. The strength of the photo acoustic signal is given by [4]:

$$S = \frac{2 N_i \sigma_{ik}}{fV} \Delta x (1 - \eta_k) P_L \Delta t S_m \quad (20)$$

in which N_i gives the density of the absorbing molecules in cm^{-3} , σ_{ik} gives the absorption cross section in cm^2 , Δx is the absorption pathlength, Δt the cycle period, P_L the laser power, η_k gives the quantum efficiency (the ratio of emitted fluorescence energy to absorbed laser energy), f is the number of degrees of freedom that are accessible for each of the N molecules at the temperature T , V is the volume of the PAC and S_m is the sensitivity of the microphone/PAC combination given in Volt/Pascal.

Important about equation 20 is that the photo acoustic signal linearly depends on the concentration of the molecules. Further more it also linearly depends on the power of the laser source, which means that a significant sensitivity can be gained using high power sources. The bandwidth of the laser should be smaller than the linewidth of the absorption. At one atmosphere this linewidth is typically in the order of 7-8 GHz.

References

1. A. Yariv, "Quantum Electronics", John Wiley & Sons, 3rd edition (1989)
2. S.E. Harris, "Tunable Optical Parametric Oscillators", Proc. IEEE **57**, 2096-2113 (1969)
3. M.M. Fejer, G.A. Magel, D.H. Jundt, and R.L. Byer, "Quasi-Phase-Matched Second Harmonic Generation: Tuning and Tolerances.", IEEE J. Quant. Elect. **28**, 263`-2653 (1992)
4. W. Demtröder, "Laser Spectroscopy", 2nd enlarged edition, Springer (1998)
5. J.A. Armstrong, N. Bloembergen, J. Bucuing, and P.S. Pershan, "Interactions between light waves in a nonlinear dielectric", Phys. Rev. **127**, pp 1918-1939 (1962).
6. P.A. Franken and J.F. Ward, "Optical harmonics and nonlinear phenomena", Rev. Mod. Phys. **35**, 23-39 (1963)
7. M.S. Piltch, C.D. Cantrell, and R.C. Sze, "Infrared second-harmonic generation in nonbirefringent cadmium telluride", J. Appl. Phys. **47**, pp 3514-3517 (1976)
8. A. Szilagyi, A. Hordvik, and H. Schollberg, "A quasi-phase-matching technique for efficient optical mixing and frequency doubling", J. Appl. Phys. **47**, pp 2025-2032 (1976)
9. D.E. Thompson, J.D. McMullen, and D.B. Anderson, "Second-harmonic generation in GaAs 'stack of plates' using high-power CO₂ laser radiation", Appl. Phys. Lett. **29**, pp 113-115 (1976)
10. M. Okada, K. Takizawa, and S. Leiri, "Second harmonic generation by periodic laminar structure of nonlinear optical crystal", Opt. Commun. **18**, pp 331-334 (1976)
11. A.A. Ballman, "Growth of piezoelectric and ferroelectric materials by Czochralski technique", J. Amer. Ceram. Soc. **48**, pp 112-113 (1965)
12. J.A. Giordmaine and R.C. Miller, "Tunable coherent parametric oscillation in LiNbO₃ at optical frequencies", Phys. Rev. Lett. **14**, pp 973-976 (1965)
13. W. R. Bosenberg, A. Drobshoff, J.I. Alexander, L.E. Myers and R.L. Byer, "Continuous-wave, singly resonant optical parametric oscillator based on periodically poled LiNbO₃", Opt. Lett. **21**, 713-715 (1996)
14. W. R. Bosenberg, A. Drobshoff, J.I. Alexander, L.E. Myers and R.L. Byer, "93% pump depletion, 3.5-W continuous-wave, singly resonant optical parametric oscillator", Opt. Lett. **21**, 1336-1338 (1996)
15. O. Levi, T.J. Pinguet, T. Skauli, L.A. Eyres, K.R. Parameswaran, J.S. Harris, M.M. Fejer, T.J. Kulp, S.E. Bisson, B. Gerard, E. Lallier and L. Becouarn, "Difference frequency generation of 8- μ m radiation in orientation-patterned GaAs", Opt. Lett. **27** 2091-2093 (2002)
16. P.E. Powers, T.J. Kulp, and S.E. Bisson, "Continuous tuning of a continuous-wave periodically poled lithium niobate optical parametric oscillator by use of a fan-out grating design", Opt. Lett. **23**, 159-161 (1998)
17. S.E. Bisson, K.M. Armstrong, T.J. Kulp, and M. Hartings, "Broadly tunable, mode-hop-tuned cw optical parametric oscillator based on periodically poled lithium niobate", Appl. Opt. **40** 6049-6055 (2001)

18. D.H. Jundt, "Temperature-dependent Sellmeier equation for the index of refraction, $n(e)$, in congruent lithium niobate", *Optics Lett.* **22** 1553 (1997)
19. M. Arbore and T. McHugh, "0.5 Watt, single-frequency, 1510-1630 nm, pump- and signal-resonant optical parametric oscillator", in *Conference on Laser and Electro-Optics*, in 2000 OSA Technical Digest Series (Optical Society of America, Washington, D.C., 2000), pp. 520-521
20. A.J. Henderson, P.M. Roper, L.A. Borschowa, and R.D. Mead, "Stable, continuously tunable operation of a diode-pumped doubly resonant optical parametric oscillator", *Opt. Lett.* **25**, 1264-1266 (2000).
21. M. E. Klein, C.K. Laue, D.-H. Lee, K.-J. Boller, and R. Wallenstein, "Diode-pumped singly resonant continuous-wave optical parametric oscillator with wide continuous tuning of the near-infrared idler wave", *Opt. Lett.* **25**, 490-492 (2000)
22. M.M.J.W. van Herpen, S. te Lintel Hekkert, S.E. Bisson, F.J.M. Harren, "Wide single-mode tuning of a 3.0-3.8- μm , 700-mW, continuous-wave Nd:YAG-pumped optical parametric oscillator based on periodically poled lithium niobate", *Opt. Lett.* **27**, 640-642 (2002)
23. F. Kühnemann, K. Scheider, A. Hecker, A.A.E. Martis, W. Urban, S. Schiller and J. Mlynek, "Photoacoustic trace-gas detection using a cw single-frequency parametric oscillator", *Appl. Phys. B* **66** 741-745 (1998)
24. F. Müller, A. Popp, F. Kühnemann, S. Schiller, "Transportable, highly sensitive photoacoustic spectrometer based on a continuous-wave dualcavity optical parametric oscillator", *Opt. Express* **11**, 2820-2825 (2003)
25. F. Müller, A. Popp, F. Kühnemann, S. Schiller, "A continuous-wave optical parametric oscillator for mid infrared photoacoustic trace gas detection", in *OSA TOPS Vol. 83 proceedings of ASSP meeting in San Antonio* (2003)
26. K.S. Zhang, T. Coudreau, M. Martinelli, A. Maître, and C. Fabre, "Generation of bright squeezed light at 1.06 μm using cascaded nonlinearities in a triply resonant cw periodically-poled lithium niobate optical parametric oscillator", *Phys. Rev. A* **64**, 033815 (2001)
27. M. Martinelli, K.S. Zhang, T. Coudreau, A. Maître, and C. Fabre, "Ultra-low threshold CW triply resonant OPO in the near infrared using periodically poled lithium niobate", *J. Opt. A: Pure Appl. Opt.* **3**, 300 (2001)
28. F.J.M. Harren, G. Cotti, J. Oomens, S. te Lintel Hekkert, "Photoacoustic spectroscopy in trace gas monitoring" in *Encyclopedia of Analytical Chemistry*, (Ed.) R.A. Meyers (John Wiley Ltd, Chichester, 2000), 2203-2226.
29. M.W. Sigrist, "Trace gas monitoring by laser photoacoustic spectroscopy and related techniques (plenary)", *Rev. of sci. inst.* **74**, 486-490 (2003)

3

Calculation of cavity dimensions

Abstract

This chapter discusses the theory needed to calculate the optimized dimensions of the OPO cavity. It starts with the basic theory of Gaussian beam transformation matrices, which is then used to calculate appropriate dimensions for an OPO cavity consisting of 4 mirrors in a bowtie cavity design, using a PPLN crystal as nonlinear crystal. The chapter concludes with a review of the effects of errors in the dimensions of the OPO cavity.

3.1 Introduction

The basic Optical Parametric Oscillator (OPO) setup is shown in Fig. 1.

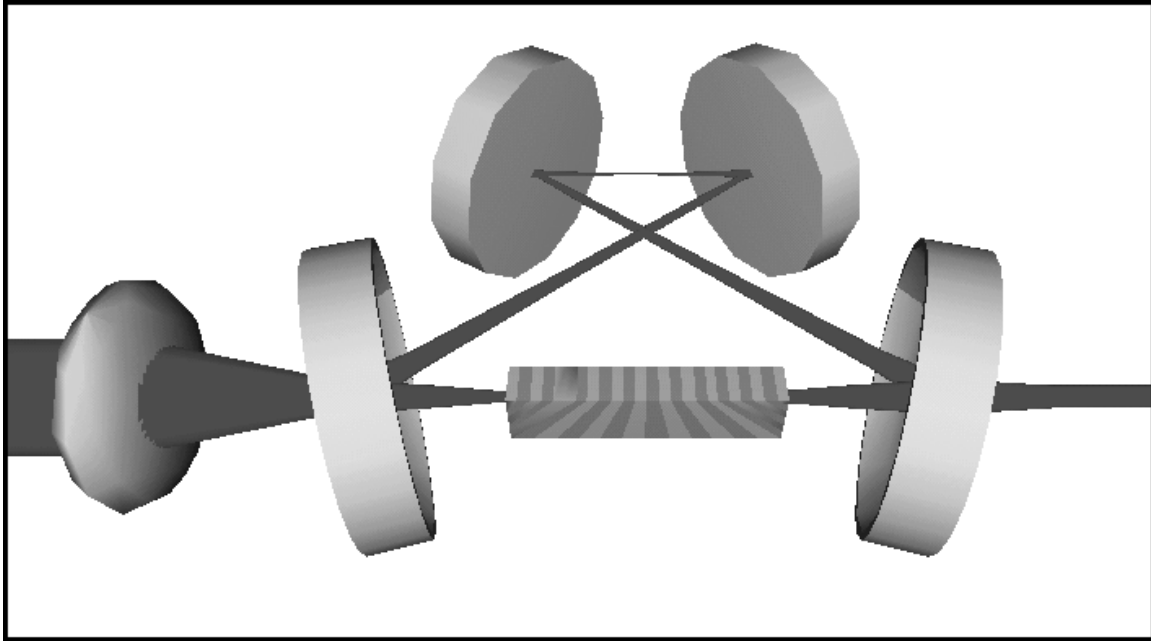


Fig. 1. The basic setup of the OPO, showing a Nd:YAG pump beam that is sent through a lens and is then focused into the fan-out PPLN crystal, which is placed inside the OPO cavity consisting of two curved and two flat mirrors. The remaining pump light and the generated idler light exits the cavity to the right, while the signal light is being resonated in the OPO cavity.

The Singly Resonant OPO (SRO) has a four-mirror bowtie ring cavity design that is resonant for the signal wavelength. The cavity consists of two curved (radius of curvature 10 cm) and 2 flat mirrors. Each mirror has a high reflectivity coating $R > 99.9\%$ for the signal wavelength (1.5-1.7 μm) with a high transmission $T > 80\%$ for the pump (1064 nm) and idler waves (3.0-3.8 μm). The input and output faces of the PPLN crystal are anti-reflection coated for the pump (1.064 μm), signal and idler wavelengths. The PPLN crystal is placed exactly between the two curved mirrors. A lens is used to focus the pump beam into the center of the PPLN.

The waist of the pump beam has to be chosen carefully. For the best OPO performance the pump and signal beams need to overlap as much as possible [19]. To achieve this, the focal point of the pump laser needs to be in the same place (the center of the PPLN crystal) as the focal point of the signal beam inside the stable ring resonator. In addition, the beam waist and divergence of the pump and signal beams need to be similar.

Using Gaussian beam transformation matrices the signal beam waist can be calculated as a function of cavity dimensions [20]. This can be used to decide which OPO cavity dimensions to use.

3.2 Basic Theory of Gaussian beam transformation matrices

A laser beam behaves like a Gaussian beam. An unaltered Gaussian beam is defined to travel in a straight line along the coordinate axis z and it has a minimum beam waist ω_0 at $z=0$. This means that:

$$\omega(0)=\omega_0 \quad (2.1)$$

If the beam waist $\omega(z)$ and the wavefront curvature $R(z)$ are known at a specific location of the Gaussian beam, they can be calculated at any position using equation 2.2 and 2.3:

$$R(z)=z\left(1+\frac{z_0^2}{z^2}\right) \quad (2.2)$$

$$\omega^2(z)=\omega_0^2\left(1+\frac{z^2}{z_0^2}\right) \quad (2.3)$$

in which z_0 is known as the *Rayleigh range*. An alternative term $b=2z_0$ is referred to as the *confocal parameter*. The rayleigh range is given by:

$$z_0 = \frac{\pi\omega_0^2}{\lambda} \quad (2.4)$$

The electrical field of a Gaussian beam can be written in a simple way, using the complex beam parameter $q(z)$:

$$q(z)=z-iz_0 \quad (2.5)$$

The relationship with $R(z)$ and $\omega(z)$ is given by:

$$\frac{1}{q(z)} = \frac{1}{z-iz_0} = \frac{z+iz_0}{z^2+z_0^2} = \frac{1}{z\left(1+z_0^2/z^2\right)} + i\frac{1}{z_0\left(1+z^2/z_0^2\right)} = \frac{1}{R(z)} - i\frac{\lambda}{\pi\omega^2(z)} \quad (2.6)$$

By taking the real and imaginary parts of eq. 2.6, this results in:

$$\frac{1}{R(z)} = \text{Re}\left(\frac{1}{q(z)}\right) \quad (2.7)$$

$$\frac{1}{\omega^2(z)} = -\frac{\pi}{\lambda} \cdot \text{Im}\left(\frac{1}{q(z)}\right) \quad (2.8)$$

The complex beam parameter can be used to calculate how a mirror or lens alters a Gaussian beam. Using a 2x2 ray matrix the transformation of $q(z)$ can be described with:

$$q' = \frac{Aq + B}{Cq + D} \quad (2.9)$$

Where A, B, C and D are the ray matrix elements. Table 1 shows some useful ray matrix operators.

Table 1: Ray Matrix Operators	
$\begin{pmatrix} 1 & d \\ 0 & 1 \end{pmatrix}$	Translation
$\begin{pmatrix} 1 & 0 \\ 0 & n_1/n_2 \end{pmatrix}$	Refraction on flat surface
$\begin{pmatrix} 1 & 0 \\ -1/f & 1 \end{pmatrix}$	Thin lens

Ray matrices, also known as ABCD matrices, offer a convenient form for describing the propagation of optical rays through various optical elements. Because they are matrix representations, a sequence of events can be combined by matrix multiplication to yield a final result. This means that it is possible, for example, to propagate radiation from an object to a lens, refract it through the lens and then propagate it to an image location, and describe all these events with a single matrix equation. This will be used to calculate the beam parameters in every position in our OPO cavity.

3.3 Calculation of q for OPO cavity

The propagation of the beam inside the cavity is split into 5 parts (figure 2), with the starting position at $z=0$. Part 1 starts at the position of the focus in the center of the PPLN crystal and ends at the right hand side of the PPLN crystal. The second part goes from the right edge of the PPLN crystal to the first curved mirror. Next is the propagation from the first curved mirror to the second curved mirror (passing 2 flat mirrors). From the second curved mirror to the left edge of the PPLN crystal is part 4, and finally part 5 goes from the left edge of the crystal to the starting point in the center.

In the starting position the beam will be in its focal point in the center of the PPLN crystal. This means that the wavefront curvature $R(0) = \infty$ and the beam waist $\omega(0) = \omega_0$. The complex beam parameter in the starting position q_0 follows from equation 2.6:

$$q_0 = i \frac{\pi \omega_0 n}{\lambda_0} = iz_0 \quad (3.1)$$

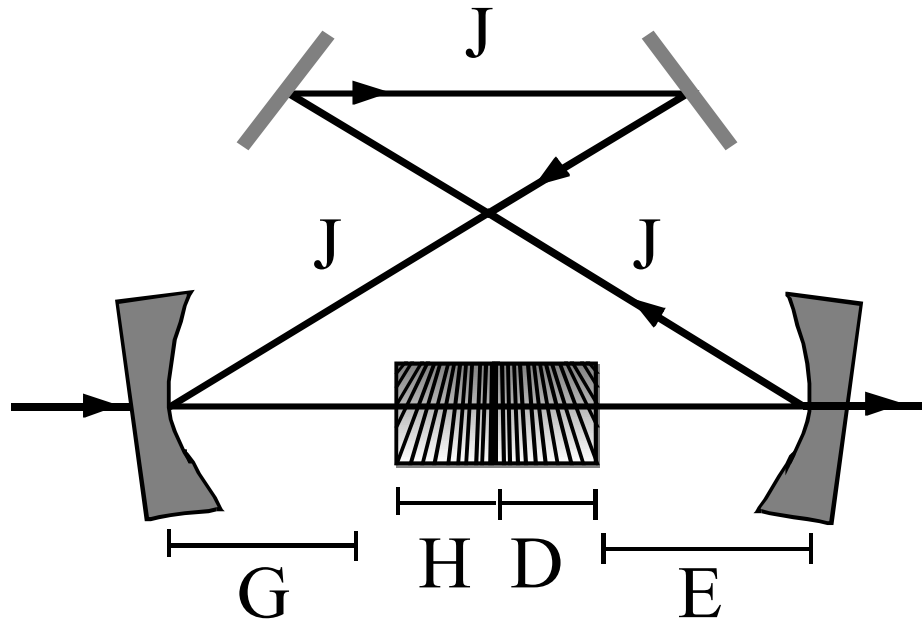


Fig. 2. The cavity is split up into 5 parts, with a length of D, E, J, G and H .

1.1 Part 1

The first part of the propagation through the cavity is the translation through the first half of the PPLN crystal over a distance d , with the edge of the PPLN crystal at distance D . The matrix representation is:

$$M_1 = \begin{pmatrix} 1 & d \\ 0 & 1 \end{pmatrix} \quad (3.2)$$

Where the edge of the PPLN crystal is reached at $z=D$. Using equation 2.9 this results in:

$$q_1 = \frac{Aq_0 + B}{Cq_0 + D} = q_0 + d \quad (3.3)$$

In order to calculate $R(d)$ and $\omega(d)$ this is re-written into:

$$\frac{1}{q_1} = \frac{1}{q_0 + d} = \frac{1}{iz_0 + d} = \frac{-iz_0 + d}{z_0^2 + d^2} \quad (3.4)$$

With equation 2.6 and 2.8 this gives:

$$\frac{1}{R(d)} = \text{Re} \left(\frac{1}{q_1} \right) = \frac{-d}{-z_0^2 - d^2} \quad (3.5)$$

$$\frac{1}{\omega(d)^2} = -\text{Im} \left(\frac{1}{q_1} \right) \frac{\pi}{\lambda} = \frac{-\pi z_0}{\lambda(-z_0^2 - d^2)} \quad (3.6)$$

$$\omega(d) = \sqrt{\omega_0^2 \left(\frac{z_0^2 + d^2}{z_0^2} \right)} = \omega_0 \sqrt{1 + \left(\frac{d}{z_0} \right)^2} \quad (3.7)$$

The distance d can be varied between 0 and D to calculate the beam waist at several locations. At z=D the edge of the crystal is reached and part 2 starts.

1.2 Part 2

For this part the beam will first go through an index of refraction change from PPLN (n=2.14) to air (n=1). After that there is another translation, until the curved mirror is reached at a distance of e=E. The matrix representation of these effects is:

$$M_2 = \begin{pmatrix} 1 & e \\ 0 & 1 \end{pmatrix} \begin{pmatrix} 1 & 0 \\ 0 & n_1/n_2 \end{pmatrix} \cdot M_1 = \begin{pmatrix} 1 & e \\ 0 & 1 \end{pmatrix} \begin{pmatrix} 1 & 0 \\ 0 & n_1/n_2 \end{pmatrix} \begin{pmatrix} 1 & D \\ 0 & 1 \end{pmatrix} = \begin{pmatrix} 1 & D + e \cdot n_1/n_2 \\ 0 & n_1/n_2 \end{pmatrix} \quad (3.8)$$

This leads to:

$$q_2 = \frac{Aq_0 + B}{Cq_0 + D} = \frac{q_0 + D + e \cdot n_1/n_2}{n_1/n_2} \quad (3.9)$$

$$\frac{1}{q_2} = \frac{n_1/n_2}{n_1/n_2} \left(\frac{1}{iz_0 + D + e \cdot n_1/n_2} \right) = \frac{n_1/n_2}{n_1/n_2} \left(\frac{\left(D + e \cdot n_1/n_2 \right) - iz_0}{\left(D + e \cdot n_1/n_2 \right)^2 + z_0^2} \right) \quad (3.10)$$

Which gives:

$$\frac{1}{\omega(e)^2} = \frac{\pi n_1}{\lambda_0} \left(\frac{z_0}{\left(D + e \cdot n_1/n_2 \right)^2 + z_0^2} \right) \quad (3.11)$$

Where e can be varied between 0 and E . At $e=0$ equation (3.11) should be the same as equation (3.7). This is indeed the case. The next part starts at $e=E$.

1.3 Part 3

To continue the third part there is a reflection on the curved mirror, after which there is another translation over a distance J . In this calculation the reflection by the curved mirror is assumed to be similar to transmission through a lens with a focal length f .

For the next calculation these values are defined:

$$\alpha = D + E \frac{n_1}{n_2} \quad (3.12)$$

$$\beta = j\alpha/f - j \frac{n_1}{n_2} \quad (3.13)$$

The matrix representation now looks like:

$$M_3 = \begin{pmatrix} 1 & j \\ 0 & 1 \end{pmatrix} \begin{pmatrix} 1 & 0 \\ -1/f & 1 \end{pmatrix} \begin{pmatrix} 1 & \alpha \\ 0 & n_1/n_2 \end{pmatrix} = \begin{pmatrix} 1 - j/f & \alpha - \beta \\ -1/f & n_1/n_2 - \alpha/f \end{pmatrix} \quad (3.14)$$

For the complex beam parameter, this yields:

$$\frac{1}{q_3} = \frac{-q_0/f - \beta/j}{(1 - j/f)q_0 - \beta + \alpha} = \frac{\left(-q_0/f - \beta/j\right)\left(-\left(1 - j/f\right)q_0 + \alpha - \beta\right)}{-\left(1 - j/f\right)^2 q_0^2 + \left(\alpha - \beta\right)^2} \quad (3.15)$$

From 3.15 the beam waist is found to be:

$$\frac{1}{\omega(j)^2} = \frac{\pi n_2}{\lambda_0} \left\{ \frac{-\left(\alpha - \beta\right)^2 / f + \beta^2 / j \left(1 - j/f\right)}{\left(1 - j/f\right)^2 z_0^2 + \left(\alpha - \beta\right)^2} \right\} = \frac{\pi n_1}{\lambda_0} \left\{ \frac{z_0}{\left(1 - j/f\right)^2 z_0^2 + \left(\alpha - \beta\right)^2} \right\} \quad (3.16)$$

Where j can be varied between 0 and J . As expected, at $j=0$ equation (3.16) turns into (3.11). At $j=J$ part 4 starts.

1.4 Part 4

The 4th part consists of another reflection of a curved mirror and another translation g until the left edge of the PPLN crystal is reached at $g=G$. The matrix representation is:

$$M_4 = \begin{pmatrix} 1 & g \\ 0 & 1 \end{pmatrix} \begin{pmatrix} 1 & 0 \\ -1/f & 1 \end{pmatrix} \begin{pmatrix} 1 - J/f & \alpha - \beta \\ -1/f & n_1/n_2 - \alpha/f \end{pmatrix} = \begin{pmatrix} 1 - J/f + g\delta & \alpha - \beta + g\gamma \\ \delta & \gamma \end{pmatrix} \quad (3.17)$$

where γ and δ are defined by:

$$\gamma = \frac{\beta}{f} - 2\frac{\alpha}{f} + \frac{n_1}{n_2} \quad (3.18)$$

$$\delta = \frac{j}{f^2} - \frac{2}{f} \quad (3.19)$$

The complex beam parameter is now very difficult to calculate in one step, therefore it is written like this:

$$\frac{1}{q_4} = \frac{Cq_0 + D}{Aq_0 + B} = \frac{(Cq_0 + d)(Aq_0 - B)}{A^2q_0^2 - B^2} \quad (3.20)$$

where A, B, C and D are the matrix elements of equation 3.17. To calculate the beam waist the imaginary part of (3.20) needs to be calculated:

$$\frac{1}{\omega(g)^2} = -\frac{\pi n_2}{\lambda_0} \text{Im} \left\{ \frac{1}{q_4} \right\} = -\frac{\pi n_2}{\lambda_0} \left(\frac{-BCz_0 + ADz_0}{-A^2z_0^2 - B^2} \right) \quad (3.21)$$

To make the calculation of $\omega(d)$ easier, the value for (AD-BC) can be calculated first:

$$AD - BC = \left((1 - J/f + g\delta)\gamma - (\alpha - \beta + g\gamma)\delta \right) = \frac{n_1}{n_2} \quad (3.22)$$

Combined with (3.21) this gives:

$$\frac{1}{\omega(g)^2} = \frac{\pi n_1}{\lambda_0} \left(\frac{z_0}{(1 - J/f + g\delta)^2 z_0^2 + (\alpha - \beta + g\gamma)^2} \right) \quad (3.23)$$

If $g=0$, then this equation turns into (3.16). At $g=G$ part 5 start.

1.5 Part 5

The final part of the calculation is an index of refraction change from air to PPLN and a translation h from the left edge of the crystal to the center of the crystal at $h=H$. The transformation matrix looks like this:

$$M_5 = \begin{pmatrix} 1 & h \\ 0 & 1 \end{pmatrix} \begin{pmatrix} 1 & 0 \\ 0 & n_2/n_1 \end{pmatrix} \begin{pmatrix} 1 - J/f + G\delta & \alpha - \beta + G\gamma \\ \delta & \gamma \end{pmatrix} = \begin{pmatrix} 1 - J/f + G\delta + h\delta n_2/n_1 & \alpha - \beta + G\gamma + h\gamma n_2/n_1 \\ \delta n_2/n_1 & \gamma n_2/n_1 \end{pmatrix} \quad (3.24)$$

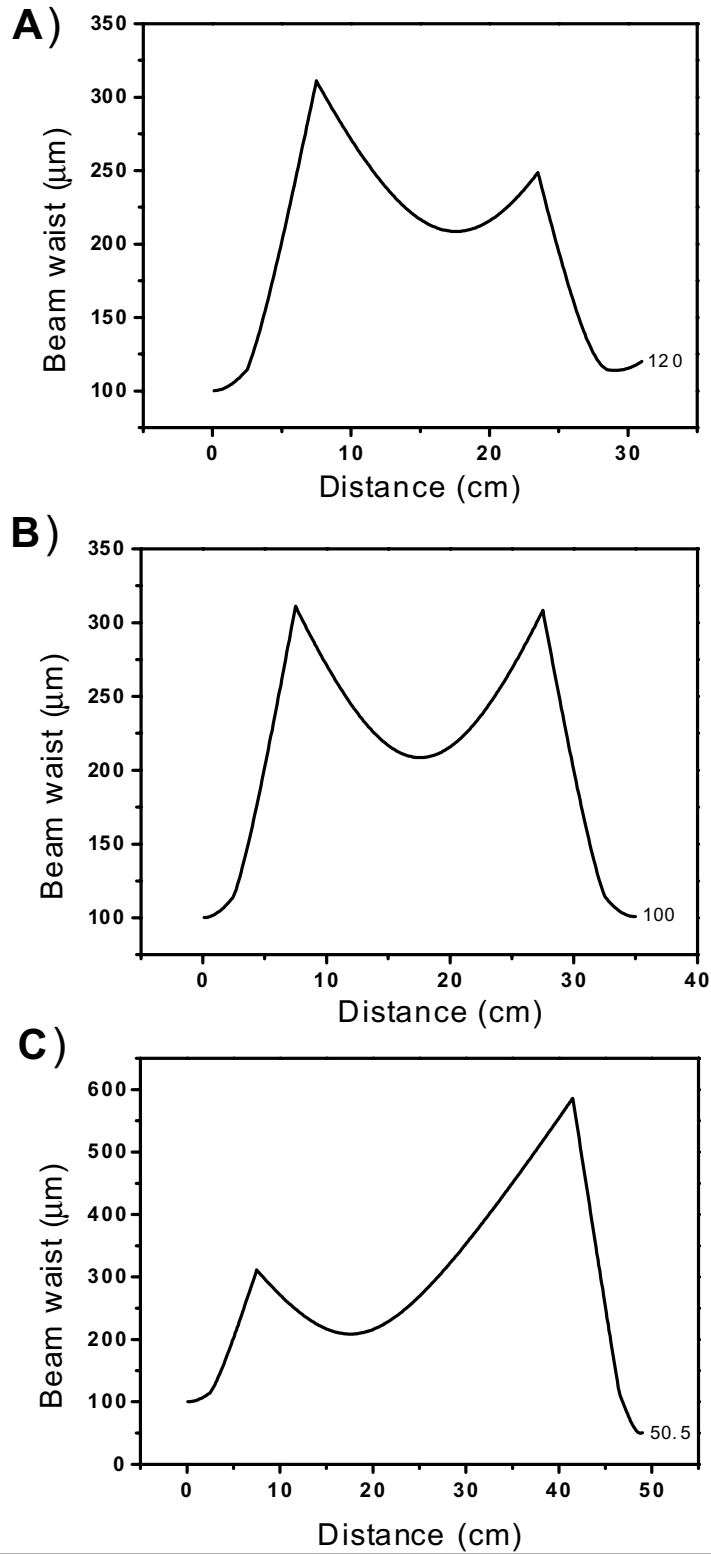


Figure 3: The beam waist starts at 100 μm in the center of the PPLN crystal and is then translated through the OPO cavity. The beam waist calculated in all positions within the OPO cavity for different values of the length J between the curved mirrors: A) Cavity length too short with $J=16$ cm B) Aligned cavity with $J=20$ cm. C) Cavity length too long with $J=34$ cm.

With A, B, C and D being the matrix elements of (3.24), equation (3.21) can be used again:

$$AD - BC = \frac{n_2}{n_1} \left(\gamma - J \gamma / f - \delta \alpha + \delta \beta \right) = \frac{n_2}{n_1} \cdot \frac{n_1}{n_2} = 1 \quad (3.25)$$

$$\frac{1}{\omega(h)^2} = \frac{\pi n_1}{\lambda_0} \left(\frac{z_0}{\left(1 - J/f + G \delta + h \delta \frac{n_2}{n_1} \right)^2 z_0^2 + \left(\alpha - \beta + G \gamma + h \gamma \frac{n_2}{n_1} \right)^2} \right) \quad (3.26)$$

with $h=0$, this equation turns into 3.23. At $h=H$ the beam has made one pass through the cavity.

3.4 Discussion

It is now possible to calculate the waist of the signal beam at any point in the cavity, but more importantly it is now also possible to calculate the cavity dimensions that are needed in order to get a good overlap between the pump-beam at 1.064 μm and the signal-beam at 1.5 μm . In order to get the best overlap between the pump-beam and the signal beam, the focal positions of the signal and pump beam need to be in the same place. In addition the beam waist of the signal beam needs to be similar to the beam waist of the pump laser.

Only for specific cavity dimensions the pump and signal beams will be overlapping inside a stable resonator. This will be demonstrated by an example. In this example a pump-beam with a beam waist in the center of the PPLN crystal of 100 μm is used. The crystal has a length of 5 cm (so $D=H=2.5$ cm) and on both sides there is 5 cm spacing between the crystal and the curved mirrors.

Like the pump beam, the beam waist starts at 100 μm in the center of the PPLN crystal, but is then translated through the OPO cavity. If the cavity is too short, for instance $J=16$ cm (fig. 2a) the focal point moves to the left of the PPLN crystal after one roundtrip. The beam waist also becomes bigger, namely 114 μm and the second focal point moves to the right. With $J=34$ cm (fig. 2c) the cavity length is too long. Here, the focal point moves to the right and is also considerably smaller, namely 50 μm , while the second focal point moves to the left. For this example, the cavity would be aligned with $J=20$ cm (fig. 2b). For this cavity length, the focal point stays in the center of the crystal and it also remains at 100 μm beam waist. The second focal point is also exactly in the middle, with a spot-size of 209 μm .

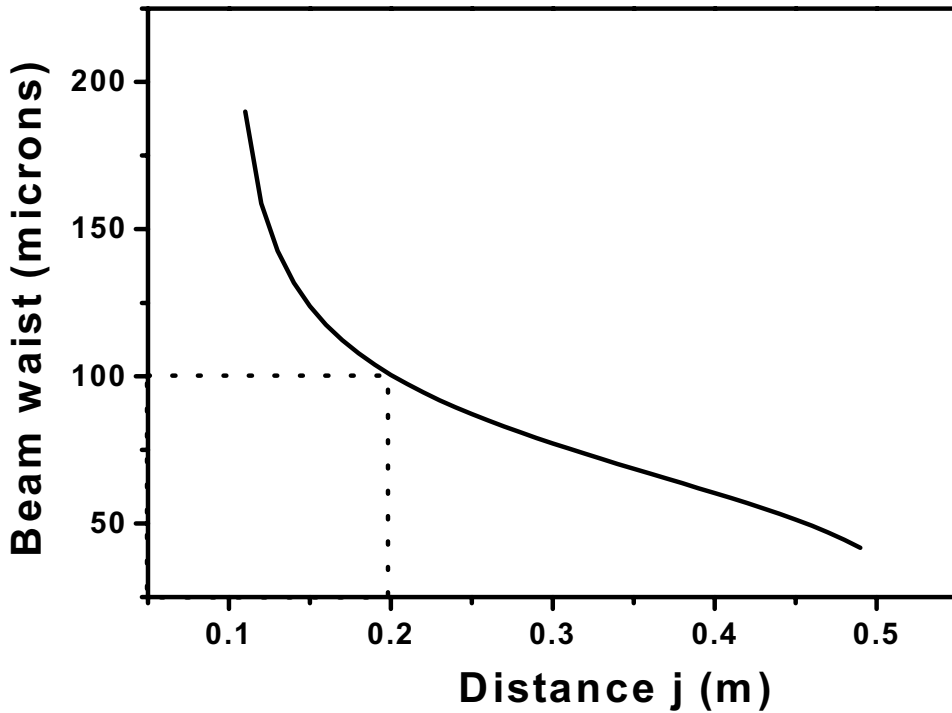


Figure 4: Using Gaussian beam transformation matrices, the signal beam waist in the center of the PPLN crystal has been calculated for a stable cavity with varying total cavity length. This picture shows that a longer cavity length leads to a smaller signal beam waist. A beam waist of $100\ \mu\text{m}$ gives a corresponding value of $J=20\ \text{cm}$.

The optimized cavity length depends on the signal beam waist in the center of the PPLN crystal. Figure 4 shows the relation between the beam waist and the length of J for the optimized cavity. As expected from figure 3, a beam waist of $100\ \mu\text{m}$ results in $J=20\ \text{cm}$.

It is now also possible to calculate the effects of misalignment of the OPO cavity. Some possibilities for misalignment are shown in figure 5.

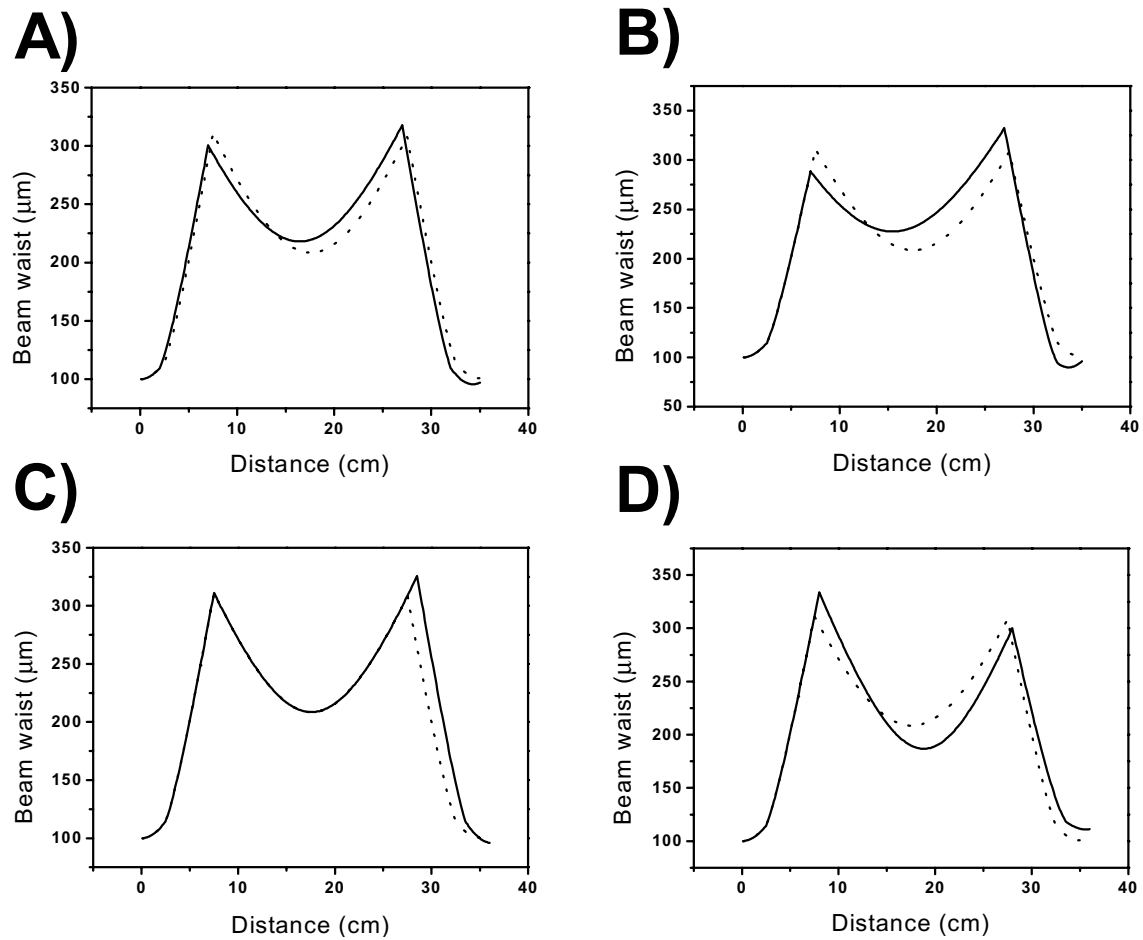


Figure 5: The effect of misalignment on the OPO cavity. Each panel shows the optimized cavity with a dotted line and compares it with the calculation of an un-optimized cavity. A) The focal position is displaced 0.5 cm to the right of the center of the PPLN crystal. B) The focal position is displaced 0.5 cm to the right and the PPLN crystal has been moved 0.5 cm to the right as well. C) The cavity length J is too long. D) The distance between the curved mirrors is 1 cm too long.

4

Continuous 34 GHz tuning of a singly resonant optical parametric oscillator using a skewed bowtie ring cavity

Abstract

We describe a continuous-wave, single frequency optical parametric oscillator (OPO) that was continuously tuned over 34 GHz by tuning the cavity length, while a low-finesse air-spaced intra-cavity etalon was locked to the signal frequency with an electronic feedback loop. To reduce misalignment as result of a large cavity mirror displacement a skewed (folded) bowtie ring cavity architecture was used. The intra-cavity etalon was able to suppress all mode-hops, but a 100 MHz in a few tenths of seconds frequency jitter was observed in the idler wavelength. The OPO operates at idler wavelengths between $2800\text{-}3100\text{ cm}^{-1}$ ($3.2 - 3.6\text{ }\mu\text{m}$) with an output power of $\sim 80\text{ mW}$.

4.1 Introduction

In 1996 Bosenberg *et al.* [1,2] demonstrated the first continuous-wave (cw) quasi phase-matched Optical Parametric Oscillator (OPO) using the nonlinear material Periodically Poled Lithium Niobate (PPLN). Even though other types of materials such as GaAs have great potential for the future [3-5], PPLN will probably remain one of the most widely used materials for cw OPOs operating within the PPLN transparency range of 0.33-4.5 μm . Even beyond this transparency range good performance of pulsed and recently also cw OPOs has been reported [6-9]. Over the years there have been many reports of improvements and changes that have been made to the original design. This paper will focus on one aspect of this, namely the continuous tunability in cw OPOs.

For many applications simple tuning approaches such as mode-hop tuning [10,11] are sufficient. Continuous mode-hop-free tuning of the OPO is useful for high-resolution spectroscopy at low pressures where absorption linewidths are narrow. The most commonly used method for this is continuous tuning of the pump source. With this technique the signal frequency is stabilized by means of an intra-cavity etalon, which yields idler tuning characteristics that mirror that of the pump source. The widest continuous pump tuning range ever reported for a cw OPO system was reported by Klein *et al.* [12], using a singly resonant OPO directly pumped by a diode laser. They achieved a continuous tuning range of 56 GHz with an idler operating range between 2.01-2.19 μm . However, for many spectroscopic applications, OPOs operating at idler wavelengths near 3 μm are desired and this system had a lower idler output power of 200 mW compared to other SRO systems.

For applications such as photo acoustic spectroscopy, both high power (>100's of mW) and wide tunability are required. Traditionally, Nd:YAG lasers have been used for pumping PPLN OPOs but few single frequency pump sources are available and tunability is limited, thus requiring that the OPO be tuned. An alternative is Yb:YAG which has high power output (10's of Watts) and broad tuning, which enables much simpler and more robust pump tuning of the OPO. In 2002, a Nd:YAG pumped cw OPO system was reported that produced both high-power (2.2 Watt) idler radiation (3.0-3.7 μm) and could also be continuously tuned over 24 GHz [13-14]. Up to now, this is the highest continuous tunability ever reported for a Nd:YAG pumped OPO system. Henderson *et al.* [15] demonstrated pump tuning of a cw doubly resonant OPO with 10 GHz continuous tunability for 4 mW idler radiation (2.2-3.7 μm). Normally doubly resonant OPOs are difficult to tune, because both the signal and idler wavelengths need to be in resonance with the OPO cavity. However, Henderson *et al.* were able to solve this problem by locking the cavity length to the peak of a signal-idler double resonance, while continuously tuning the pump source.

The use of such a locking scheme combined with tuning the OPO cavity length is an alternative way to continuously tune the singly resonant OPO system. This is a well-established technique commonly used with other types of laser systems, but for cw single-frequency OPOs it has been rarely used. This is surprising, because this tuning technique provides a powerful alternative to pump tuning, which does not have the requirement of a tunable pump source such as a MOPA diode laser system [13] or tunable fiber laser [16].

Here we demonstrate 34 GHz of continuous tuning in a cw singly resonant OPO system operating at idler powers of 80 mW in the 3.2-3.6 μm range. To our knowledge, this is the widest continuous tuning range ever reported for a Nd:YAG pumped single-frequency cw OPO system operating in this wavelength range. This tuning is achieved by tuning the signal frequency with the OPO cavity length, while locking the mirror spacing of the intra-cavity etalon to the signal frequency that is resonating in the OPO cavity. In this way the intra-cavity etalon enforces stable single mode operation during continuous tuning of the signal frequency. A skewed bowtie ring cavity was used to reduce misalignment for large mirror displacements.

4.2 Experiment

The pump source is a customized Coherent Verdi, which generates 6.5 Watts of continuous-wave single-frequency 1064 nm radiation. Using a 100 mm focal lens, the pump-beam is focused into the PPLN crystal (Crystal Technology) as shown in figure 1. The OPO cavity consists of 2 curved and 2 flat mirrors, which all have coatings with high reflectivity (>99.8%) for the signal (1.6-1.7 μm) and high transmission for the pump (1064 nm) and idler (3.2 – 3.6 μm) frequencies.

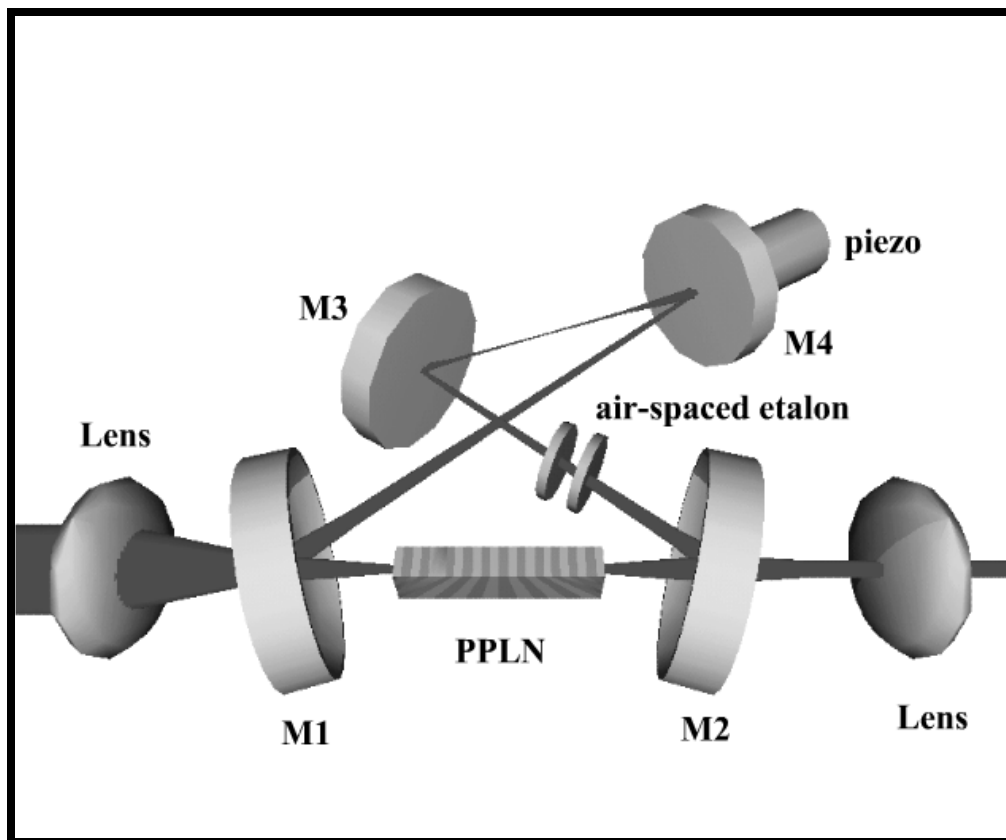


Fig. 1. Experimental setup for the cw singly resonant OPO. The cavity is resonant for the signal beam at 1.6-1.7 μm and consists of two curved (M1 and M2, both with 10 cm radii of curvature) and two flat mirrors (M3 and M4). Mirror M4 has been mounted onto a piezo, to be able to change the cavity length. To reduce misalignments for large mirror displacements, mirror M4 has been skewed away from the OPO cavity in order to reduce the angle between the incoming and reflected light beams. To stabilize the OPO an intra-cavity air-spaced etalon is used that is locked to the signal wavelength with an electronic feedback loop.

The shape of the cavity is similar to a bowtie ring cavity design developed by Bosenberg *et al.* [1,2], but now the second flat mirror position is skewed away from the beam path. For this reason two different flat mirrors are used, where the first one has its coating optimized for an angle of 45 degrees, and the other one for an angle of 6 degrees. The small-angle mirror has been mounted onto a long travel piezo (25 μ m), which can be used to tune the cavity length of the OPO. With a normal bowtie ring cavity this tuning method is limited due to misalignments that occur for large mirror displacements. However, the skewed cavity setup has a much smaller angle (3 instead of 16 degrees) between the light waves that travel towards and away from this mirror, which significantly reduces misalignment and therefore greatly extends the maximum tuning range.

To avoid photo-refractive damage, the PPLN crystal is heated and temperature stabilized at 130 ± 0.1 °C in a custom made oven. The input and output faces of the PPLN crystal have been anti-reflection coated for the pump, signal and idler frequencies. The crystal has a fan-out grating design [10], with poling periods ranging from 29.3 to 30.1 μ m.

The OPO cavity is frequency stabilized by means of an intra-cavity air-spaced etalon. This etalon consists of two 0.5" CaF₂ mirrors, where one surface of each mirror is coated with a 5% reflectivity layer for the signal wavelength whereas the rear face was anti-reflection coated. The two reflective surfaces oppose each other and are aligned as parallel as possible with a separation of 1.5 mm (free spectral range 100 GHz). The back surfaces of the mirrors are coated with an anti-reflection layer for the signal wavelength and they have a 30-minute wedge against the inner surface. When the air-spaced etalon is introduced into the OPO cavity it enforces stable single-mode operation for the signal frequency. Combined with the single-frequency pump source that is fixed in frequency, this yields a single-frequency idler beam with tuning characteristics similar (but opposite) to those of the signal frequency.

4.3 Results

The oscillation threshold of the OPO was ~ 3 Watt without the intracavity etalon and when pumping at full power (6.5W) a pump depletion of 85-90% could be achieved. With the air-spaced etalon inside the cavity the threshold increased to ~ 4 Watts and the output power was reduced from ~ 300 mW to ~ 80 mW.

One of the etalon mirrors has been mounted onto a circular ring piezo. This can be used to tune the spacing between the etalon mirrors and thus it can be used to tune the relative position of the transmission peaks of the etalon. Using an electronic feedback circuit the driving voltage of the etalon piezo is kept at a certain DC voltage with sine wave jitter added at 1.4 kHz frequency. This jitter generates an error signal from changes in OPO signal amplitude as measured by a photo-detector. The error signal is fed to the electronic circuit, which reduces the error signal to zero by altering the DC voltage on the etalon piezo. This locks the etalon position to the signal frequency and stabilizes the OPO to run at one single mode. The generated idler radiation is sent to a 2 GHz spectrum analyzer in order to check for single mode operation and to measure the total tuning range.

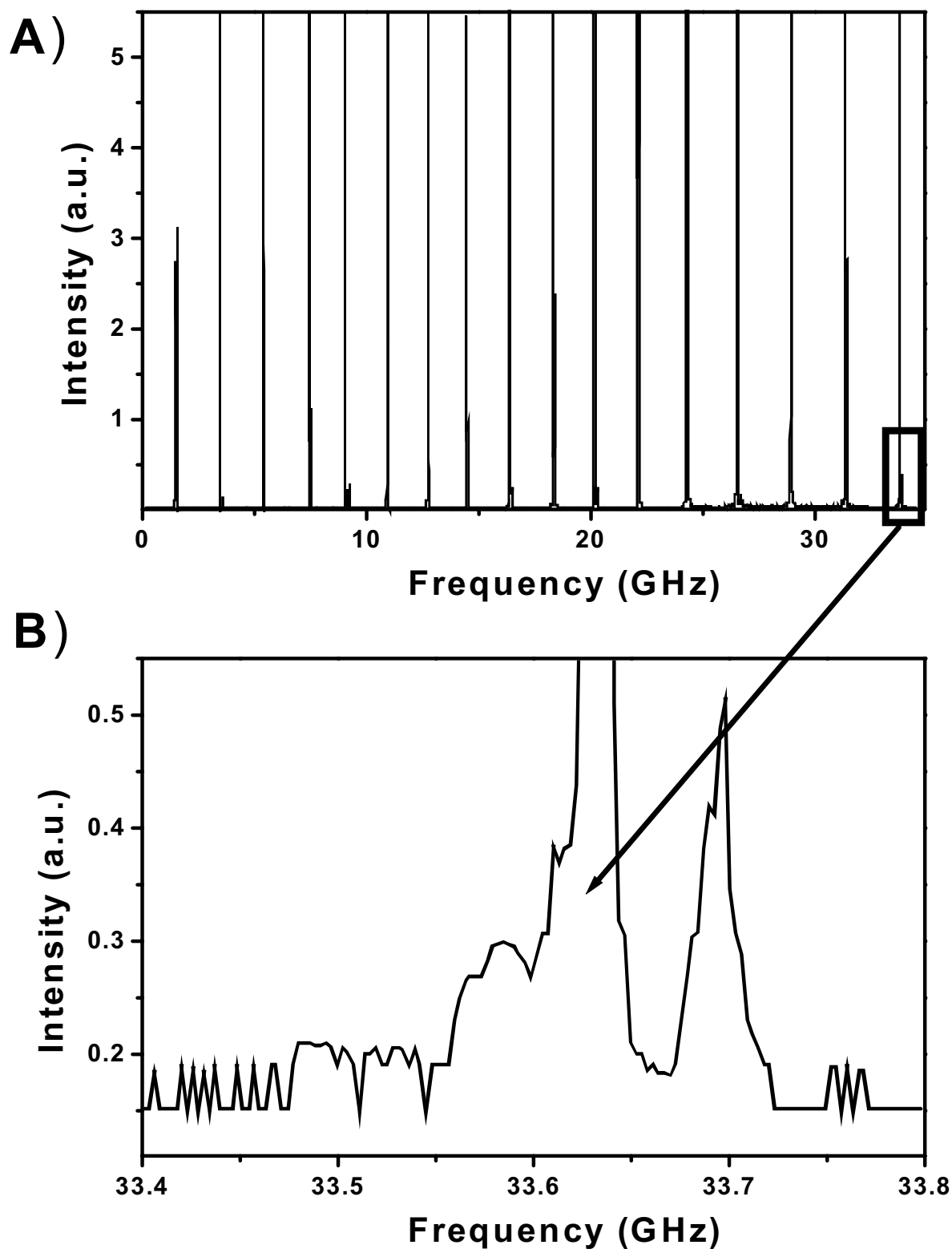


Fig. 2. Fringes of a 2 GHz spectrum analyzer as they were recorded during tuning. A) A total tuning range of 34 GHz is demonstrated by a scan that shows 17 recorded fringes. B) An expanded view of one of the fringes reveals a frequency jitter of up to 100 MHz in several tenths of seconds.

If the signal frequency is detuned, for instance due to changes in the OPO cavity length, the etalon lock will tune the etalon along with the signal frequency. Continuous tuning of the OPO can therefore be achieved by changing the cavity length with the piezo attached to one of the cavity mirrors. Figure 2a shows the recorded 2 GHz fringes that were observed from the spectrum analyzer during tuning. From the number of fringes a total continuous idler tuning range of 34 GHz is derived, which was limited by total travel range of the mirror piezo. We believe that longer scans in the order of the PPLN bandwidth (4 cm^{-1} @ $3.3 \text{ }\mu\text{m}$) will be possible in future.

Temperature fluctuations of the PPLN crystal were observed to cause minor fluctuations in the generated frequencies. This can be explained, because the PPLN crystal length (and with it the poling period and cavity length) depends on the temperature. An additional problem with these temperature fluctuations was that they introduced slow oscillations (40 seconds) in the idler output power that could be as high as $\pm 15\%$. Fortunately, the etalon lock loop is strong enough to hold the OPO on the same longitudinal mode. Under high resolution, a frequency jitter of up to 100 MHz in a few tenths of seconds is observed (fig. 2b). The thermal drift could be the cause for this, but also photo-refractive effects and air currents inside the OPO may play a role. Any secondary etaloning or wavelength dependent absorption or reflection can also influence the tuning, because the air-spaced etalon used here is of low finesse. Higher-finesse (10% or 20% reflectivity) air-spaced etalons were used to prevent this, but due to increasing walk-off losses with increasing reflectivity the insertion loss for these etalons was high. This made tuning difficult due to the higher OPO oscillation threshold.

4.4 Conclusion

In conclusion, we have demonstrated a total continuous tuning range of 34 GHz for a cw single-frequency OPO that was tuned with the cavity length, while an intra-cavity air-spaced etalon was locked to the signal frequency. The use of a skewed (folded) bowtie ring cavity reduced misalignment for large mirror displacements, increasing the total continuous tuning range. Currently the maximum tuning range is limited by the total travel range of the piezo used to increase the cavity length. In the future it should be possible to achieve a total continuous tuning range in the order of the PPLN OPO bandwidth (4 cm^{-1} @ $3.3 \text{ }\mu\text{m}$). The OPO runs without mode-hops, albeit with a frequency jitter of up to 100 MHz in a few tenths of seconds. This can probably be solved with a higher finesse intra-cavity etalon, but that also requires a more powerful pump source. This tuning method can be used with pump sources that are not continuously tunable themselves. Many high power pump sources (such as Nd:YAG and Yt:YAG) are not continuously tunable, but are very suitable pump sources for this configuration. Therefore skewed cavity tuning provides a powerful alternative to the commonly used pump tuning method.

References

1. W. R. Bosenberg, A. Drobshoff, J.I. Alexander, L.E. Myers and R.L. Byer, "Continuous-wave, singly resonant optical parametric oscillator based on periodically poled LiNbO_3 ", *Opt. Lett.* **21**, 713-715 (1996)

2. W. R. Bosenberg, A. Drobshoff, J.I. Alexander, L.E. Myers and R.L. Byer, "93% pump depletion, 3.5-W continuous-wave, singly resonant optical parametric oscillator", *Opt. Lett.* **21**, 1336-1338 (1996)
3. R. Haïdar, A. Mustelier, Ph. Kupecek, E. Rosencher, R. Triboulet, Ph. Lemasson and G. Mennerat, "Largely tunable midinfrared (8–12 μm) difference frequency generation in isotropic semiconductors", *J. Appl. Phys.* **91** 2550-2552 (2002)
4. O. Levi, T.J. Pinguet, T. Skauli, L.A. Eyres, K.R. Parameswaran, J.S. Harris, M.M. Fejer, T.J. Kulp, S.E. Bisson, B. Gerard, E. Lallier, L. Becouarn, "Difference frequency generation of 8- μm radiation in orientation-patterned GaAs", *Opt. Lett.* **27** 2091-2093 (2002)
5. T.J. Kulp, "The application of quasi-phase-matched parametric light sources to practical infrared chemical sensing systems", *Appl. Phys. B.* **75**, 317-327 (2002)
6. P. Loza-Alvarez, C.T.A. Brown, D.T. Reid, W. Sibbett, M. Missey, "High-repetition-rate ultrashort-pulse optical parametric oscillator continuously tunable from 2.8 to 6.8 μm ", *Opt. Lett.* **24**, 1523-1525 (1999)
7. M.A. Watson, M.V. O'Connor, P.S. Lloyd, D.P. Shepherd, D.C. Hanna, C.B.E. Gawith, L. Ming, P.G.R. Smith, O. Balachninaite, "Extended operation of synchronously pumped optical parametric oscillators to longer idler wavelengths", *Opt. Lett.* **27**, 2106-2108 (2002)
8. L.E. Myers and W.R. Bosenberg, "Periodically poled lithium niobate and quasi-phase-matched optical parametric oscillators", *IEEE J. Quantum Electron.* **33**, 1663-1672 (1997)
9. M.M.J.W. van Herpen, S.E. Bisson and F.J.M. Harren, "Continuous-wave operation of single frequency optical parametric oscillator between 4-5 μm based on periodically poled LiNbO_3 ", *Opt. Lett.*, submitted (2003)
10. P.E. Powers, T.J. Kulp, and S.E. Bisson, "Continuous tuning of a continuous-wave periodically poled lithium niobate optical parametric oscillator by use of a fan-out grating design", *Opt. Lett.* **23**, 159-161 (1998)
11. S.E. Bisson, K.M. Armstrong, T.J. Kulp, M. Hartings, "Broadly tunable, mode-hop-tuned cw optical parametric oscillator based on periodically poled lithium niobate", *Appl. Opt.* **40** 6049-6055 (2001)
12. M. E. Klein, C.K. Laue, D.-H. Lee, K.-J. Boller, and R. Wallenstein, "Diode-pumped singly resonant continuous-wave optical parametric oscillator with wide continuous tuning of the near-infrared idler wave", *Opt. Lett.* **25**, 490-492 (2000)
13. M.M.J.W. van Herpen, S. te Lintel Hekkert, S.E. Bisson, F.J.M. Harren, "Wide single-mode tuning of a 3.0-3.8- μm , 700-mW, continuous-wave Nd:YAG-pumped optical parametric oscillator based on periodically poled lithium niobate", *Opt. Lett.* **27**, 640-642 (2002)
14. M.M.J.W. van Herpen, S. Li, S.E. Bisson, S. te Lintel Hekkert, F.J.M. Harren, "Tuning and stability of a continuous-wave mid-infrared high-power single resonant optical parametric oscillator", *Appl. Phys. B* **75**, 329 (2002)
15. A.J. Henderson, P.M. Roper, L.A. Borschowa, and R.D. Mead, "Stable, continuously tunable operation of a diode-pumped doubly resonant optical parametric oscillator", *Opt. Lett.* **25**, 1264-1266 (2000).
16. M.E. Klein, P. Gross, K.-J. Boller, M. Auerbach, P. Wessels, C. Fallnich, "Rapidly tunable continuous-wave optical parametric oscillator pumped by a fiber laser", *Opt. Lett.* **28**, 920-922 (2003)

5

Wide single mode tuning of a 3.0-3.8 micron, 700 mW, continuous wave Nd:YAG-pumped optical parametric oscillator based on periodically poled lithium niobate

Abstract

A new Optical Parametric Oscillator (OPO) for the mid infrared wavelength region of 3-3.8 μm has been developed with an idler output power of up to 1.5 Watt. The singly resonant OPO (SRO) is pumped by a single mode, 10 Watt, cw, Nd:YAG laser and consists of a bowtie ring cavity with a fan-out periodically poled lithium niobate crystal and a low finesse intracavity air-spaced etalon. The single frequency idler output can be continuously tuned over 24 GHz with 700mW power, by tuning the pump laser. The tuning was demonstrated by recording an absorption line of ethane with photoacoustic spectroscopy.

M.M.J.W. van Herpen, S. te Lintel Hekkert, S.E. Bisson, F.J.M. Harren, "Wide single-mode tuning of a 3.0-3.8- μm , 700-mW, continuous-wave Nd:YAG-pumped optical parametric oscillator based on periodically poled lithium niobate", Opt. Lett. 27, 640-642 (2002)

5.1 Introduction

For spectroscopic applications in the mid-infrared (wavelength region 2.5-5 micron), continuous-wave (cw) optical parametric oscillators (OPO's) based on quasi-phasematched materials such as periodically poled lithium niobate (PPLN) can be very useful [1,2]. For direct absorption techniques, such as cavity ring down spectroscopy, low powers in the milliWatts region are sufficient [3]. However, for a number of spectroscopic applications such as molecular beam spectroscopy [4] and photoacoustic spectroscopy [5,6], high power combined with continuous single frequency tuning of the OPO is essential. For molecular spectroscopy an OPO linewidth of less than 10 MHz over a tuning range of tens of GHz for the mid infrared wavelength region is needed.

Bosenberg *et al.* were the first to show high power operation of a cw, single resonant optical parametric oscillator (SRO) based on PPLN in 1996 [1]. They demonstrated more than 1 W, tunable cw idler output power in the wavelength range of 3.3-3.9 μm . However, due to their pump laser they could not reach a linewidth better than 2.2 GHz for the idler.

SRO's have a high oscillation threshold and therefore need high pump powers. Double Resonant OPO's (DRO's) have much lower oscillation thresholds and can, therefore, be pumped by low power single frequency (diode) lasers. An additional advantage of diode pumping is the wide tunability of the pump wavelength, which can be used to tune the idler beam of the OPO. A recent example is a 20 MHz linewidth DRO with 18 mW idler output covering the 2.2-3.7 μm region [7] that has 10 GHz continuous tunability.

The first SRO directly pumped by a diode laser was reported by Klein *et al.* [8] and continuous tuning with a diode-pumped SRO system was also demonstrated by this group [9]. In this last study, their pump system was a master oscillator power amplifier (MOPA) with 4 MHz linewidth, tunable over 60 GHz. They were able to demonstrate a 56 GHz continuous tuning for the idler wave. However, this system covered the 2.01-2.19 μm wavelength region that is much easier to operate in compared to the widely used 3 μm idler region. Furthermore, this system has a small operating range and a lower idler output power of 200 mW compared to other SRO systems.

In this study, we aim for a high power (>1 Watt) single frequency idler output SRO with wide operating range (3.0-3.8 μm), a large continuous pump-tuning range (tens of GHz) and a small linewidth. The continuous pump-tuning range of 24 GHz that is demonstrated in this study is only surpassed by Klein *et al.* [9] and to our knowledge it is the highest continuous pump-tuning range ever reported with a Nd:YAG-pumped SRO system. The tuning of this Nd:YAG source makes our system unique.

5.2 Experiment

The OPO is pumped with a cw single-longitudinal-mode (SLM) Master Oscillator - Power Amplifier system (Lightwave M6000). From this system the Master Oscillator (MO) is a state-of-the-art Non-Planar Ring Oscillator (NPRO), which produces frequency-stable, narrow

linewidth, single-longitudinal-mode output at a Nd:YAG wavelength of 1064 nm. The MO is continuously tuned over 24 GHz by changing the temperature of the NPRO crystal. The Power Amplifier (PA) uses 160W of diode pump power to amplify the output of the MO, while contributing nearly undetectable changes in noise or beam quality. The complete system produces an output power of up to 15W, with narrow linewidth (<5 kHz over 1 ms) and low noise, which can be frequency-tuned over 24 GHz.

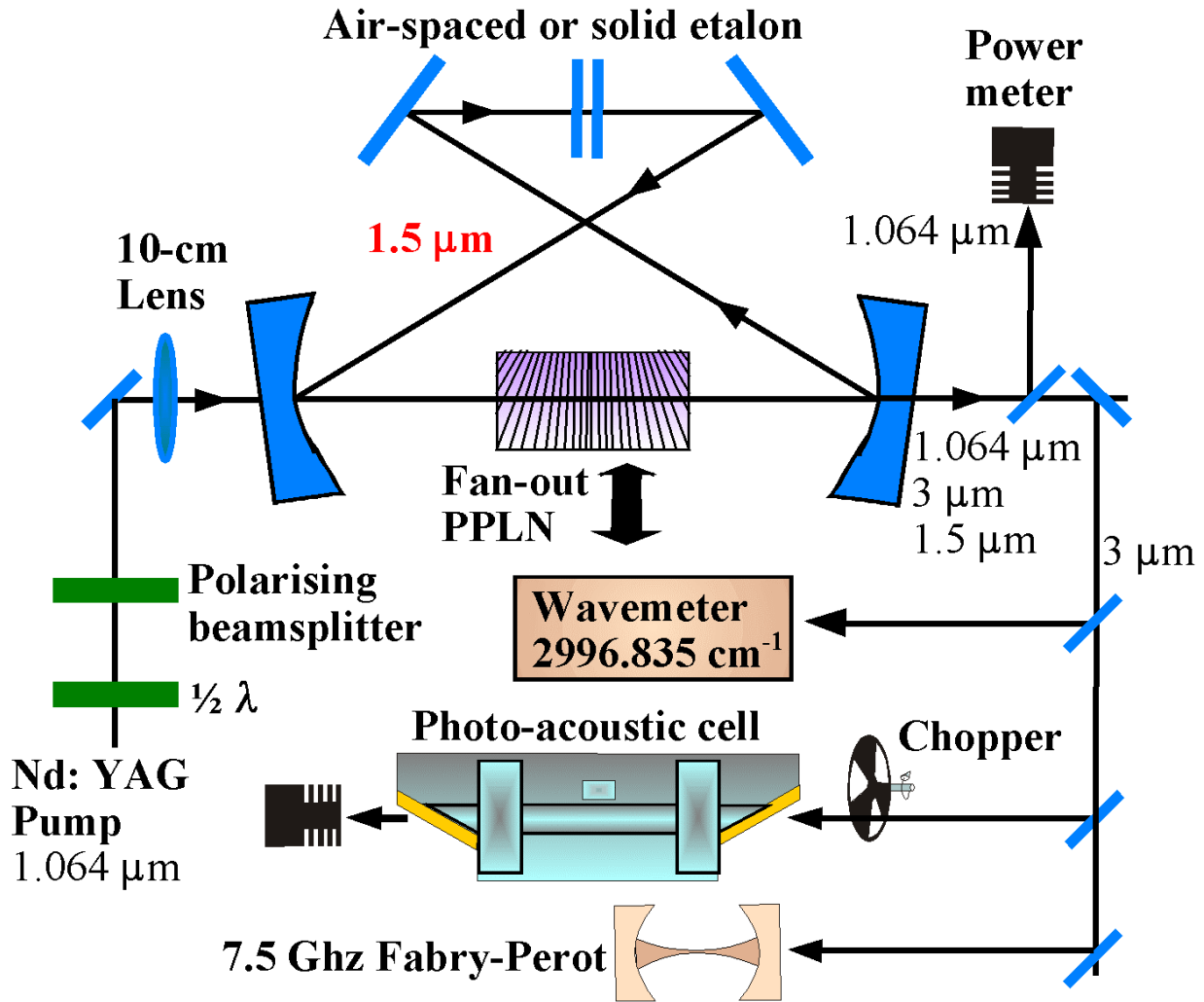


Fig. 1. Experimental setup for the cw singly resonant OPO. The pump beam is focussed into the 50 mm long fan-out PPLN with a 10 cm lens. A combination of a half wave plate and polarizing beam splitter is used to change pump power. The cavity is resonant for the signal beam at 1.5-1.7 μm and consists of two flat mirrors and two curved mirrors with 10 cm radii of curvature. The idler wavelength at 3.0-3.8 μm is sent to a photo-acoustic cell and a wavemeter. An intra-cavity air-spaced etalon is used to enhance frequency stability.

When changing pump powers the laser beam characteristics (i.e. divergence, pointing) change significantly. For that reason a combination of a half wave plate (New Focus, Santa Clara, CA, USA) and a polarizing beam splitter (OFR, Caldwell, NJ, USA) was used to change laser power without affecting the beam characteristics (Fig. 1).

The basic set-up for the cavity design of the OPO is similar to the one used earlier [2,10]. The PPLN crystal (Crystal Technology Inc., Palo Alto, CA, USA), which is 5 cm long and 0.5 mm thick, has a fan-out grating design as described earlier [2], with periodicities ranging from 29.3 - 30.1 μm . To prevent photo-refractive damage, the crystal is kept at 180 $^{\circ}\text{C}$ within a commercially available oven (Super Optronics, Gardena, CA, USA) and is temperature stabilized at 0.1 $^{\circ}\text{C}$. The input and output faces of the PPLN are anti-reflection coated for 1.064 μm , 1.5-1.7 μm and 3.0-3.8 μm . The PPLN is placed into a four-mirror ring cavity in which the signal beam at 1.5-1.7 μm is resonating (Free Spectral Range cavity 400 MHz). In this SRO the two curved mirrors (radius of curvature 10 cm, VLOC, New Port Richey, FL, USA) and the two flat mirrors (QTF, Oldsmar, FL, USA) have high reflectivity R for the signal wave ($R > 99.9\%$ at 1.5-1.7 μm), but high transmission T for the pump and idler waves ($T > 90\%$ and $R < 0.25\%$ at 1064 nm and $T > 80\%$ at 3.0-3.8 μm).

The combination of a single mode pump source and a single mode ring cavity resonating at the signal wavelength produces a non-resonant, but single frequency idler beam of which the tuning characteristics are similar to the pump laser.

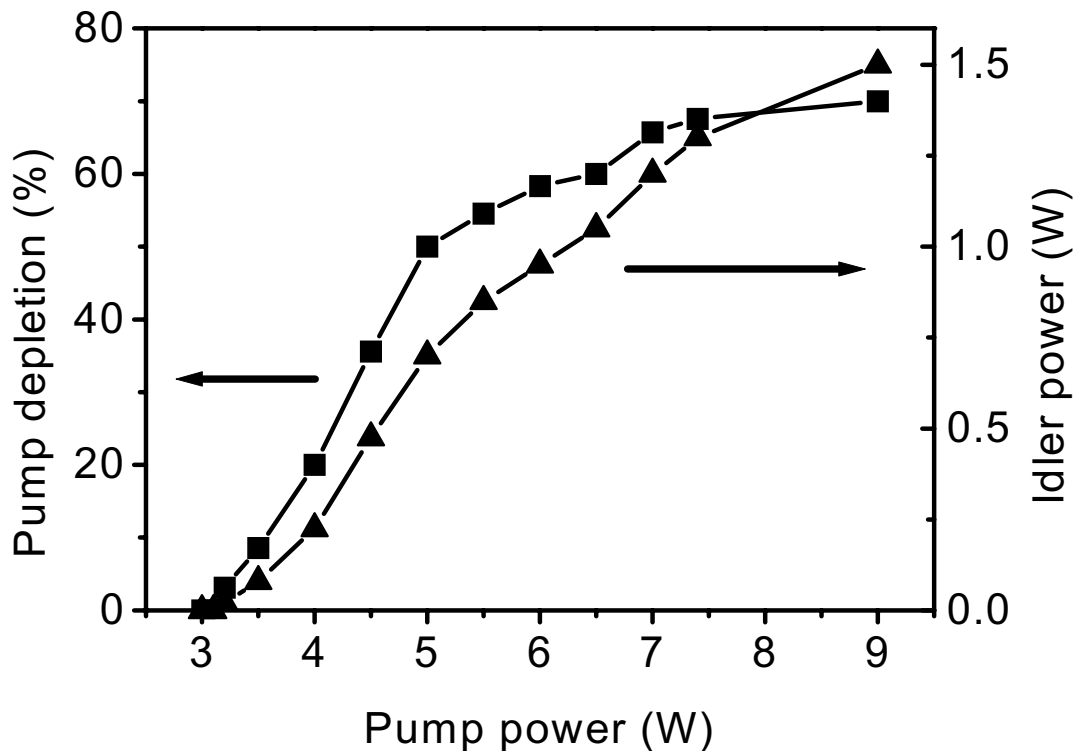


Fig. 2. Idler output and pump depletion versus pump input power for the SRO operating at an idler wavelength of 3.3 μm . The oscillation threshold is 3.0W and a maximum idler power of 1.5W is observed with a pump power of 9 W.

5.3 Results

The idler output and pump depletion are shown in Fig. 2. The oscillation threshold was found to be 3 W for the pump, while the pump depletion went up to 70% for 9 W pump power (maximum idler power 1.5 W). The pump depletion was highly dependent on proper focusing of the pump beam into the PPLN crystal. Using a 10 cm lens the pump beam was focused to a waist of 100 μm in the center of the crystal. The pump depletion is still low compared to other SRO systems; a possible reason for this is that the mirrors are not reflective enough. Rotating the pump polarization and PPLN crystal orientation by 90° might improve the performance of the mirror coatings in future.

With this setup the OPO cavity works fairly stable with infrequent mode-hops. Even though it is not absolutely necessary, single mode operation is enhanced by means of an intra-cavity etalon. This will also allow cavity mode-hop tuning in future [2]. We used either an uncoated 0.4 mm thick solid-state YAG etalon (VLOC), or an air-spaced etalon with a Free-Spectral-Range (FSR) of about 150 GHz and a reflectivity of 10% (Laser Optik, Garbsen, Germany). To minimize the losses, the first experiments were carried out using the solid state YAG etalon.

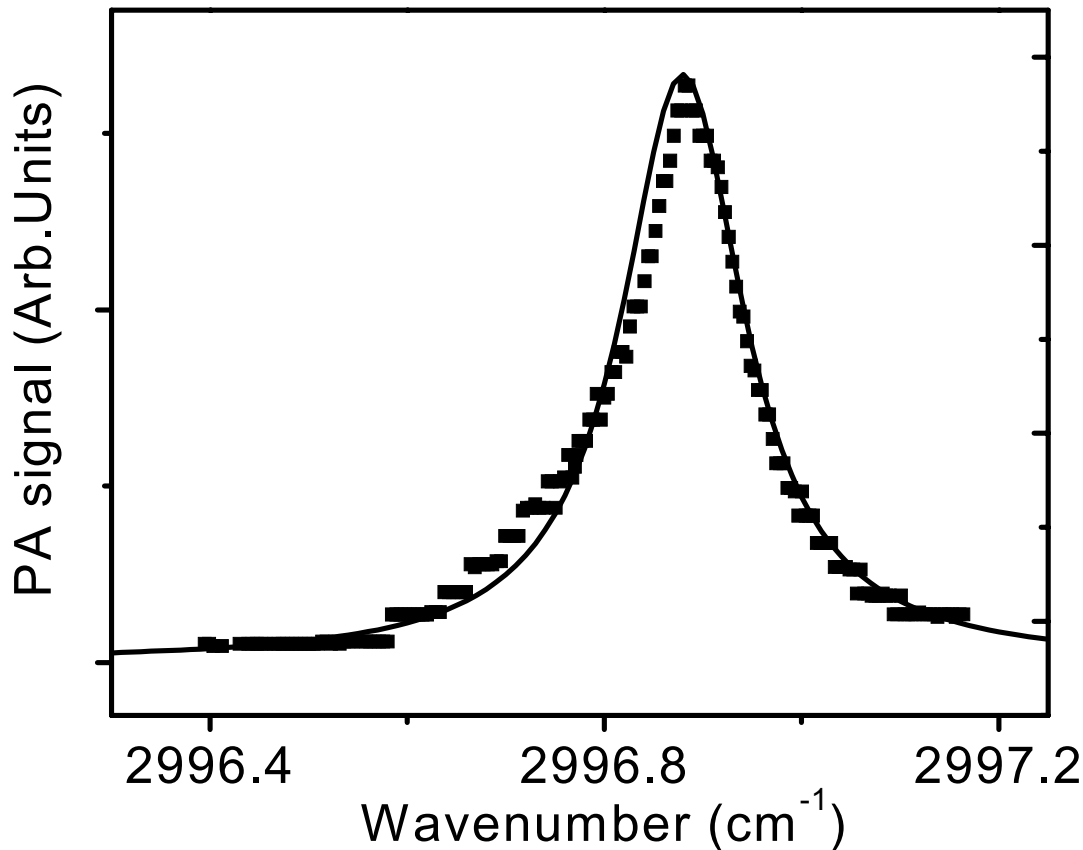


Fig. 3. Single frequency tuning is demonstrated by the pressure-broadened (0.75 atm) ν_7 , $\nu=1 \leftarrow 0$, $K=4 \leftarrow 3$, Q branch transition ($J=4-3$) of ethane, using photoacoustic spectroscopy. The experimental results are shown with the scatter graph, while the spectrum from the Hitran database is showed with the solid line.

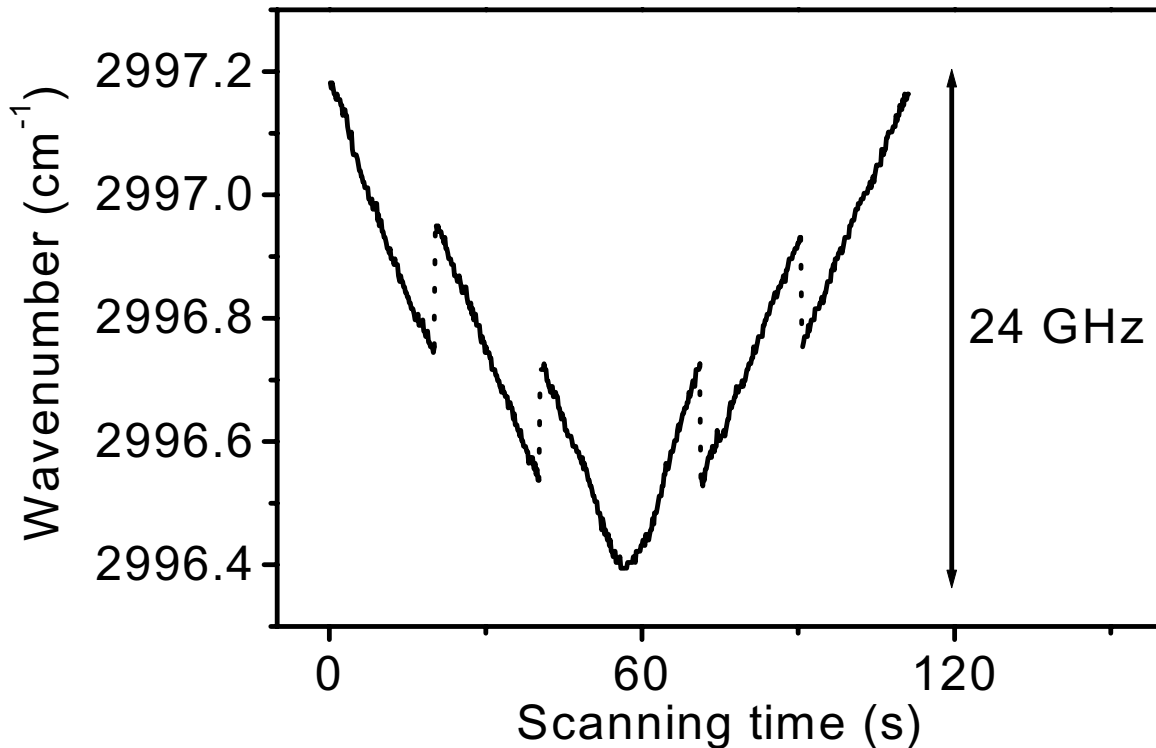


Fig. 4. While monitoring the idler wavelength with a wavemeter, the pump source of the OPO was tuned by changing its driving voltage. The whole range of the pump laser is scanned and after about 60 seconds it is scanned back. The mode-hops in the idler wavelength, which are indicated with a dashed line, are caused by mode-hops in the pump-source. A total tuning range of 24 GHz is found. The resolution of the picture was limited due to the resolution of the wavemeter and of the data acquisition card of the computer.

The output power of the OPO with and without this etalon was similar, but unfortunately the etalon was not selective enough to prevent all mode-hops in the OPO cavity. Next to that, mode-hop-tuning the cavity with this etalon was very limited due to walk-off losses when rotating the solid-state etalon.

Instead of this we decided to use a 10% reflectivity air-spaced etalon. Even though this etalon gave more losses, the advantage of better OPO stability and longer mode-hop-tuning range was found to be more important. Walk-off losses are minimized by placing the air-spaced etalon between the two flat mirrors in the second focal point of the SRO. Inserting the air-spaced etalon caused the output power to go down from 1.5 W to about 700 mW.

Single frequency tuning is demonstrated by recording the pressure-broadened (0.75 atm) ν_7 , $\nu=1\leftarrow 0$, $K=4\leftarrow 3$, Q branch transition of ethane, using photoacoustic spectroscopy [6]. Fig. 3 shows the absorption line of 10 parts per million of ethane in nitrogen, which is compared to the Hitran database. The idler wavelength (Fig. 4) is monitored by means of an infrared wavemeter (Burleigh WA1000 IR, NY, USA). The total idler tuning was found to be 24 GHz, with modehops after 12 GHz of tuning. The two mode hops observed in the idler wavelength are not caused by mode hops in the SRO, but by mode hops in the master oscillator of the pump laser. These hops in the pump source cause no troubles, because they are predictable and because the pump laser always hops back compared to the direction of tuning (Fig. 4). This means some parts of the scan are done twice, but no part of the scan is skipped. If the mode hops of the pump laser could be eliminated, then truly continuous tuning over 24 GHz could be achieved. From the noise in the measured absorption line we estimate the frequency stability of our system to be better than 50 MHz. In the near future we will demonstrate this by using a 300 MHz high finesse etalon; we expect a stability of better than 1 MHz.

5.4 Conclusion

The next two chapters concentrate on further improvements to the OPO setup. Optimizing the reflectivity and FSR of the air-spaced etalon should improve long-term stability of the SRO. By rotating the polarization or our pump source and the PPLN crystal orientation by 90° , a better pump depletion with a higher output power is expected. Furthermore, by combining our pump-tuning with mode-hop-tuning [2] the total continuous tuning range will be increased considerably. With these improvements this OPO will certainly be a very good source for most spectroscopic applications. We will apply this system in Life Science by combining it with photoacoustic spectroscopy [6] in order to develop a sensitive trace gas detector. Ethane, which was measured in this study, is emitted from biological samples due to lipid peroxidation when cell walls membranes are damaged and is therefore an important gas in biological studies [11]. We expect the lowest detectable concentration of ethane in air to be at sub part-per-billion levels.

References

1. W. R. Bosenberg, A. Drobshoff, and J.I. Alexander, "93% pump depletion, 3.5-W continuous-wave, singly resonant optical parametric oscillator", *Opt. Lett.* **21**, 1336-1338 (1996).
2. P.E. Powers, T.J. Kulp, and S.E. Bisson, "Continuous tuning of a continuous-wave periodically poled lithium niobate optical parametric oscillator by use of a fan-out grating design", *Opt. Lett.* **23**, 159-161 (1998).
3. G. Berden, R. Peeters, G. Meijer, "Cavity ring-down spectroscopy: Experimental schemes and applications", *Int. Rev. Phys. Chem.* **19**, 293-299 (2000).
4. K. Nauta and R.E. Miller, "The hydrogen fluoride dimer in liquid helium: A prototype system for studying solvent effects on hydrogen bonding", *Journal of Chem. Phys.* **113**, 10158-10168 (2000)
5. S.T. Persijn, R.H. Veltman, J. Oomens, F.J.M. Harren, and D.H. Parker, "CO laser absorption coefficients of biological relevance: H₂O, CO₂, ethanol, acetaldehyde and ethylene", *Appl. Spec* **54**, 62 (2000).
6. F.J.M. Harren, G. Cotti, J. Oomens, S. te Lintel Hekkert, "Photoacoustic spectroscopy in trace gas monitoring" in *Encyclopedia of Analytical Chemistry*, (Ed.) R.A. Meyers (John Wiley Ltd, Chichester, 2000), 2203-2226.
7. A.J. Henderson, P.M. Roper, L.A. Borschowa, and R.D. Mead, "Stable, continuously tunable operation of a diode-pumped doubly resonant optical parametric oscillator", *Opt. Lett.* **25**, 1264-1266 (2000).
8. M.E. Klein, D.-H. Lee, J.-P. Meyn, K.-J. Boller, and R. Wallenstein, "Singly resonant continuous-wave optical parametric oscillator pumped by a diode laser", *Opt. Lett.* **24**, 1142-1144 (1999).
9. M. E. Klein, C.K. Laue, D.-H. Lee, K.-J. Boller, and R. Wallenstein, "Diode-pumped singly resonant continuous-wave optical parametric oscillator with wide continuous tuning of the near-infrared idler wave", *Opt. Lett.* **25**, 490-492 (2000).
10. J. Oomens, S. Bisson, M. Harting, T. Kulp, F. J.M. Harren, "New laser sources for photoacoustic trace gas detection with applications in biomedical science" in *Proceedings SPIE* **3916** (Bellingham, USA, 2000) 295-302.
11. C.M.F. Kneepkens, G. Lepage, C.C. Roy, "The potential of the hydrocarbon breath test as a measure of lipid peroxidation", *Free Radical Biol. & Med.* **17**, 127-160 (1994).

6

Tuning and stability of a continuous-wave mid infrared high power single resonant optical parametric oscillator.

Abstract

A 2.2-Watt continuous wave, continuously tunable, single frequency OPO has been developed in the 3.0 - 3.8 μm wavelength range for the detection of molecular trace gasses. The oscillation threshold, output power and stability of the singly resonant OPO were improved by optimizing pump beamwaist and OPO cavity length. Both an air-spaced and solid etalon were tested to frequency stabilize and tune the OPO, from which the solid etalon gave a better performance. Temperature oscillations in the PPLN crystal caused oscillations in the idler wavelength of better than 200 MHz over 300 seconds, the short term stability was less than 3 MHz over 1 second. The high laser power in combination with photoacoustic spectroscopy achieved a detection limit of 10 parts per trillion for ethane in nitrogen.

This work has been published in:

M.M.J.W. van Herpen, S. Li, S.E. Bisson, S. te Lintel Hekkert, F.J.M. Harren, "Tuning and stability of a continuous-wave mid infrared high power singly resonant optical parametric oscillator", *Appl. Phys. B* **75**, 329 (2002)

6.1. Introduction

In recent years, the development of novel IR laser sources such as quantum cascade lasers [1,2], near IR telecom diode lasers [3] and sources based on quasi-phase matched materials [4] have made infrared optical detection a powerful method for both detecting and speciating gases at the ppb (1 ppb = 1 part per billion = $1:10^9$) to mid-ppt (1 ppt = 1 part per trillion = $1:10^{12}$) levels. While there is a wide range of laser sources that are well suited for trace gas detection, the method of detection combined with the species to be measured places important requirements on the laser. These include the operating wavelength range, tunability (continuous or step), stability, linewidth and power.

Continuous wave (cw) cavity ring-down spectroscopy is a particularly attractive method for trace gas detection as it is highly sensitive with possible detection limits as low as $1 \times 10^{-11} \text{ cm}^{-1}$ [5]. Moreover, the laser power requirements are extremely modest, often requiring only microwatts of power for a reasonable signal to noise ratio. The drawback however is that the stability and linewidth requirements can be quite stringent. These requirements can be relaxed somewhat albeit with a slight penalty in sensitivity through the use of cavity-enhanced-absorption (CEA) spectroscopy [6]. The advantage of CEA spectroscopy is the ability to achieve routine detection limits of $2 \times 10^{-8} \text{ cm}^{-1}$ with a technically simpler setup [6]. However, as in cavity ring-down spectroscopy, a high finesse cavity is required (mirror reflectivity $>99.98\%$), resulting in a strong dependence of the sensitivity on the performance of the high-reflectivity coating on the cavity mirrors. Normally the high reflectivity of these coatings is limited to a small wavelength region and these coatings are not always commercially available for a given wavelength region.

Photoacoustic spectroscopy is an alternative trace gas detection technique that does not depend on high reflectivity mirror coatings, but is still able to reach extremely low detection limits down to 10^{-9} cm^{-1} [7]. The photoacoustic effect linearly depends on the applied laser power; therefore the usefulness of photoacoustic trace gas detection is limited by the availability of high power lasers. Lasers such as the CO_2 laser (9-11 μm) [8,9], the CO laser (5-8 μm) [10,11] and the CO overtone laser (2.8-4 μm) [12] have proven their usefulness for trace gas detection in atmospheric physics, biology and medicine. The drawback of these lasers lies in their line-tunability, which means that they rely on accidental coincidences between the laser line and the infrared rotational-vibrational absorption lines of the gas under study.

Recently, cw optical parametric oscillators (OPOs) based on periodically poled lithium niobate (PPLN) have been developed [4,13-18] and have proved to be quite suitable for photoacoustic trace gas detection, as they offer a high output power (~ 1 Watt) combined with a wide, continuously tunable operating range and a narrow linewidth. When using a singly resonant OPO (SRO) setup pumped by a Nd:YAG laser, output powers of more than 100 milliWatts are achieved in a wavelength range of 1.5-4.0 μm .

Bosenberg *et al.* were the first to show more than 1 Watt operation of a cw, singly resonant optical parametric oscillator based on PPLN in the wavelength range of 3.3-3.9 μm [13]. However, due to their pump laser they could not reach a linewidth better than 2.2 GHz for the idler wavelength.

Singly resonant OPOs have a high oscillation threshold and therefore need high pump powers. This is in contrast to doubly resonant OPOs, which have a much lower oscillation threshold, making them amenable to pumping by low power single frequency (diode) lasers. An additional advantage of diode pumping is the wide tunability of the pump wavelength, which can be used to tune the idler beam of the OPO. A recent example is a 20 MHz linewidth double resonant OPO with 18 mW idler output covering the 2.2-3.7 μm region [14].

The first SRO directly pumped by a diode laser was reported by Klein *et al.* [15]. Subsequently, continuous tuning with a diode-pumped SRO system was also demonstrated by this group [16]. In this last study, their pump system was a master oscillator power amplifier (MOPA) with 4 MHz linewidth, tunable over 60 GHz. With this design they were able to demonstrate 56 GHz continuous tuning for the idler wave. However, this system had a fairly low output power of 200 mW and covered the 2.01-2.19 μm wavelength region that is much easier to operate on compared to the widely used 3 μm idler region. Kühnemann *et al.* have demonstrated the applicability of a cw pump-enhanced OPO for photoacoustic trace gas detection [17]. With this setup a detection limit as low as 0.5 ppb was achieved for ethane (C_2H_6) with a 10 seconds measurement time. Due to the pump-resonant cavity design the threshold pump power was low, but continuous tuning proved difficult.

Here, we demonstrate an SRO pumped by a 15W single frequency Nd:YAG laser with an output power in the idler wavelength region (3-3.8 μm) of up to 2.2 Watts. The performance with various types of intracavity etalons, frequency stability, tunability and the application of this system for trace gas detection will be discussed.

6.2. Experimental setup

The basic OPO setup is similar to what has been described before [18] (see chapter 5) and is shown in Fig. 1. The SRO is only resonant for the signal wavelength and has a four-mirror bowtie ring cavity design consisting of 2 curved (radius of curvature 10 cm) and 2 flat mirrors. The cavity mirrors have a high reflectivity $R > 99.9\%$ for the signal wavelength (1.5-1.7 μm) with a high transmission $T > 80\%$ for the pump (1064 nm) and idler waves (3.0-3.8 μm). The PPLN crystal (Crystal Technology Inc., Palo Alto, CA, USA) has a fan-out grating design [4] with periods ranging from 29.3-30.1 μm and is 50 mm long and 0.5 mm thick. To prevent photo-refractive damage the PPLN crystal is kept at a constant temperature of 190 ± 0.1 $^\circ\text{C}$ using a commercially available oven (Super Optronics, Gardena, CA, USA). The input and output faces of the PPLN are anti-reflection coated for 1.064 μm , 1.5-1.7 μm and 3.0-3.8 μm .

The Nd:YAG pump source is a 15 Watt Lightwave master oscillator power amplifier (MOPA) system with a linewidth of 5 kHz (over 1 ms) and a frequency stability of 50 MHz/hour. The laser beam has a spatially TEM_{00} mode with a beam quality of $M^2 < 1.1$. In addition, it can be continuously tuned over 24 GHz by changing the temperature of the master oscillator. During tuning two reproducible mode hops are observed that occur opposite to the direction of tuning [18]. When the output power of the pump laser was changed, both beam divergence and beam pointing changed. This can be avoided by keeping the pump laser power constant and instead using a half-wave plate and a polarizing beam splitter to vary the pump power (see Fig. 1).

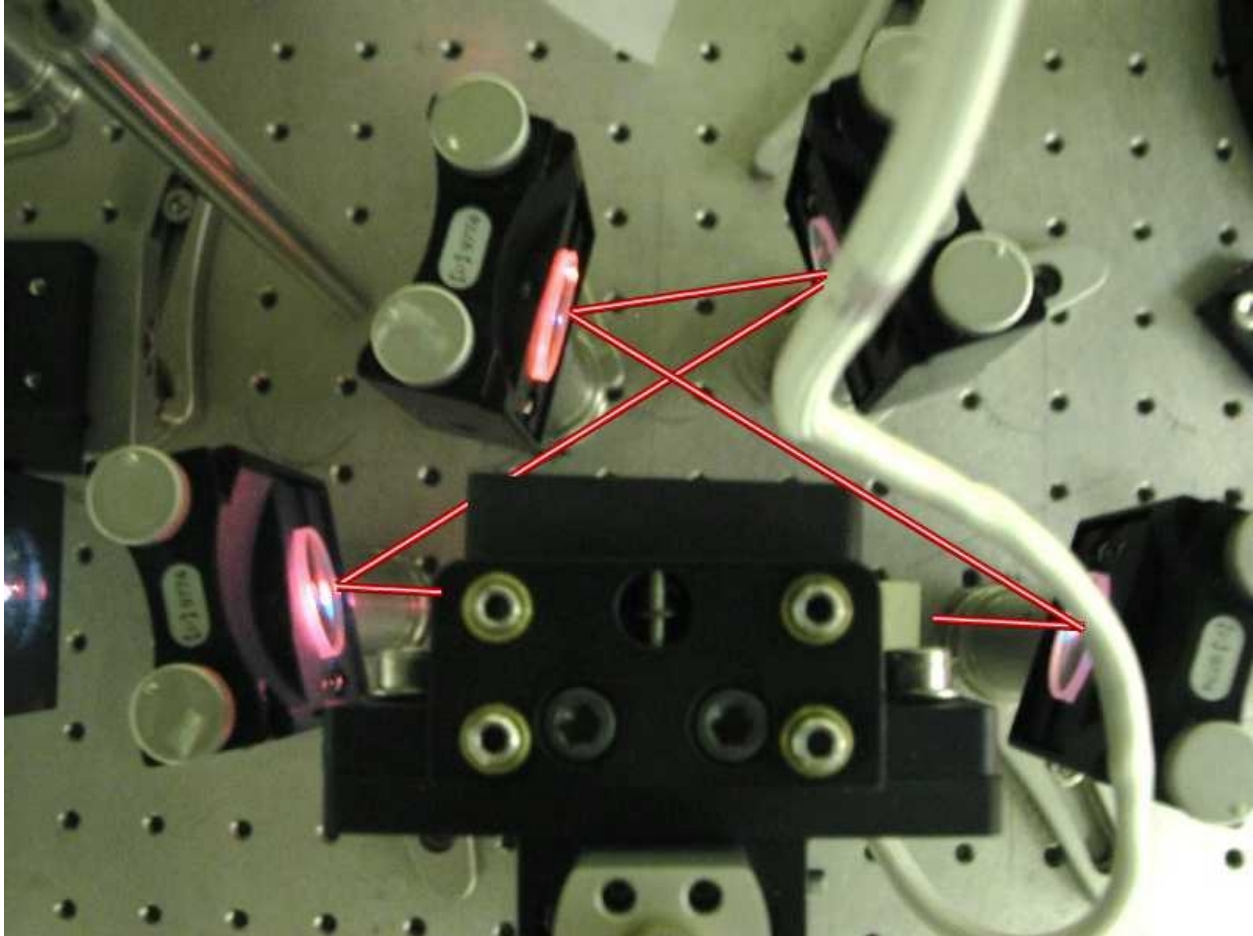


Fig. 1. Photograph of the OPO cavity during operation. The path of the signal beam (which is not visible to the human eye) is indicated with a red-white line. When the OPO is not oscillating a green tracer beam is visible due to second harmonic generation of the 1064 nm pump wave. When the OPO turns on a red beam is visible along the path of the signal beam. This is caused by higher order non-linear effects between the signal and pump waves. Sometimes it is also possible to observe a violet color.

The combination of a single mode pump source and a single mode ring cavity resonating at the signal wavelength produced a non-resonant, but single frequency idler beam with tuning characteristics similar to the pump laser.

A 10-cm lens was used to focus the pump beam into the center of PPLN. The waist of the pump beam has to be chosen carefully. For the best OPO performance the pump and signal beams need to overlap as much as possible [19]. To achieve this, the focal point of the pump laser needs to be in the same place (the center of the PPLN crystal) as the focal point of the signal beam inside the stable ring resonator. In addition, the beam waist and divergence of the pump and signal beams need to be similar. Using Gaussian beam transformation matrices the signal beam waist can be calculated as a function of cavity dimensions [20] (chapter 3). In our case the 5 cm long PPLN crystal has a distance of 5.5 cm between the crystal edges and the curved mirrors. By fixing these

lengths the only parameter left is the position of the flat mirrors, which can be used to vary the total cavity length. Fig. 2 shows that a longer cavity length results in a smaller signal beam waist for a stable cavity.

Because higher intensity increases the conversion efficiency, the beam waist normally needs to be as small as possible for the best OPO performance [19]. The pump intensity is restricted on the high end by photo-refractive damage effects and also by diffractive effects at the crystal faces. For a pump power of approximately 10 Watts, the smallest beam waist that can be achieved without causing too much crystal damage is found to be 80-100 μm . Fig. 2 shows that for a pump beam waist of 80 μm and a fixed distance of 21 cm between the curved mirrors, a total cavity length of 44 cm is required.

By optimizing the cavity length accordingly we have been able to improve the OPO performance considerably as compared to our previous report in chapter 5 [18], which had an output power of 1.5 Watt and a pump depletion of 70%. Fig. 3 shows that the oscillation threshold was 3 Watt while the idler output power was improved to 2.2 Watt with a pump depletion of 90 %. This pump depletion is comparable to other reported OPOs [4,13], but our output power is very high compared to other narrow bandwidth single frequency OPO systems [4,15-17].

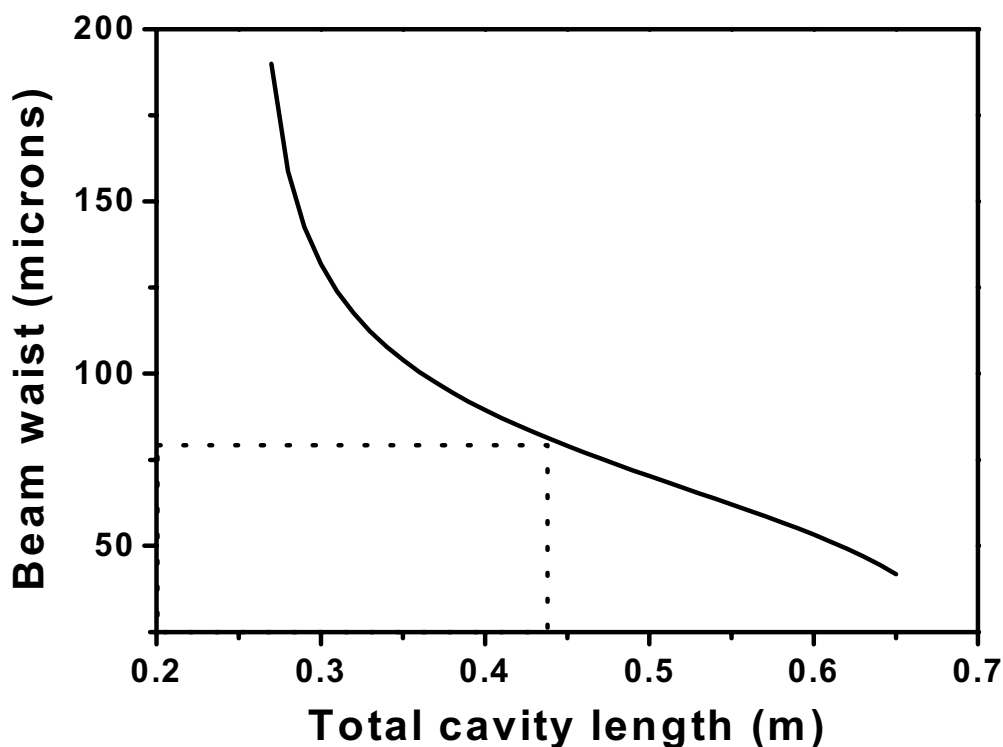


Fig. 2. Using Gaussian beam transformation matrices, the signal beam waist in the center of the PPLN crystal has been calculated for a stable cavity with varying total cavity length. In this calculation the PPLN crystal length was fixed at 5 cm and the distance between the crystal and the 10-cm curvature mirrors was 5.5 cm on both sides. This picture shows that a longer cavity length leads to a smaller beam waist.

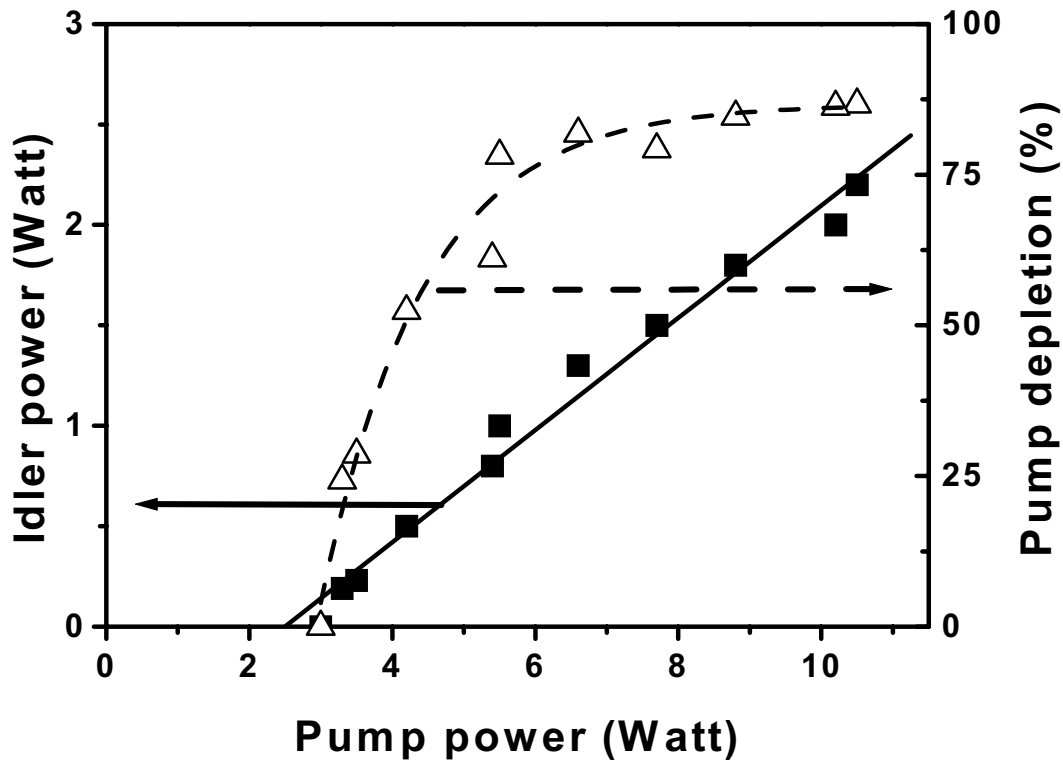


Fig. 3. The idler output power versus the pump power shows a maximum output power (solid line, solid squares) of 2.2 Watt, with a pump depletion (dashed line, open triangles) of 90%. The oscillation threshold is found at 3 Watts.

To ensure single-longitudinal-mode operation, an intracavity etalon was placed in the path between the two flat mirrors. An important consideration was whether to use an air-spaced etalon or a solid etalon. The advantage of using an air-spaced etalon is that it has a constant insertion loss, which reduces the possibility of etalon mode hops [21]. However, the oscillation threshold of the cavity with such an air-spaced etalon was much higher as compared to a solid etalon, resulting in lower output powers. Another drawback of an air-spaced etalon is that it is experimentally difficult to align and therefore is more likely to have additional losses due to misalignment. An air-spaced etalon also uses more space in the OPO cavity, as the mounting is significantly larger than for a solid etalon.

6.3. Air-spaced etalon

We have tested four different air-spaced etalons within our OPO cavity. All etalons consisted of two wedged (30 arc minutes wedge angle) substrates that were anti-reflection coated on one side and had a 10%, 20% or 30% reflectivity coating or no coating (reflectivity $\sim 3\%$) on the other side for the signal wavelength. The 20% reflectivity etalon gave the best results, because the 3% and 10% etalons were not selective enough to stabilize the frequency of the OPO, while the 30% etalon gave too much loss in the OPO cavity. The etalon mirror spacing could be varied between 0.2 and 3 mm (free spectral range from 50 - 750 GHz). The wedges of the substrates were

oriented such that the thin edge of one substrate was adjacent to the thick edge of the other substrate. The distance between the etalon mirrors could be varied over small distances by means of a circular piezo (a ring with a transparent center) attached to one of the substrates.

Unfortunately, the etalon was too large to fit inside the optimized 44cm long cavity, so the cavity length was extended to 52cm. This resulted in a slight increase in the OPO threshold (without the etalon) but the idler output was still high, approximately 1.5W. With the etalon placed in the cavity at the second signal focus, and with a spacing of 1 mm, the idler output dropped from 1.5 W to 400mW for the 20% reflectivity etalon. This drop can be attributed to a slight misalignment of the etalon faces, beam walk-off, coating and substrate losses. Both alignment losses and walk-off losses increase with increasing mirror separation.

Tuning of the OPO was accomplished by continuously tuning the etalon spacing, which resulted in mode-hop tuning of the OPO. Mode-hop tuning is attractive in that it is simple, requiring only one controllable element, and doesn't require complicated lock loops. The disadvantage is that the frequency is tuning in steps of at least one cavity-mode (about 300 MHz).

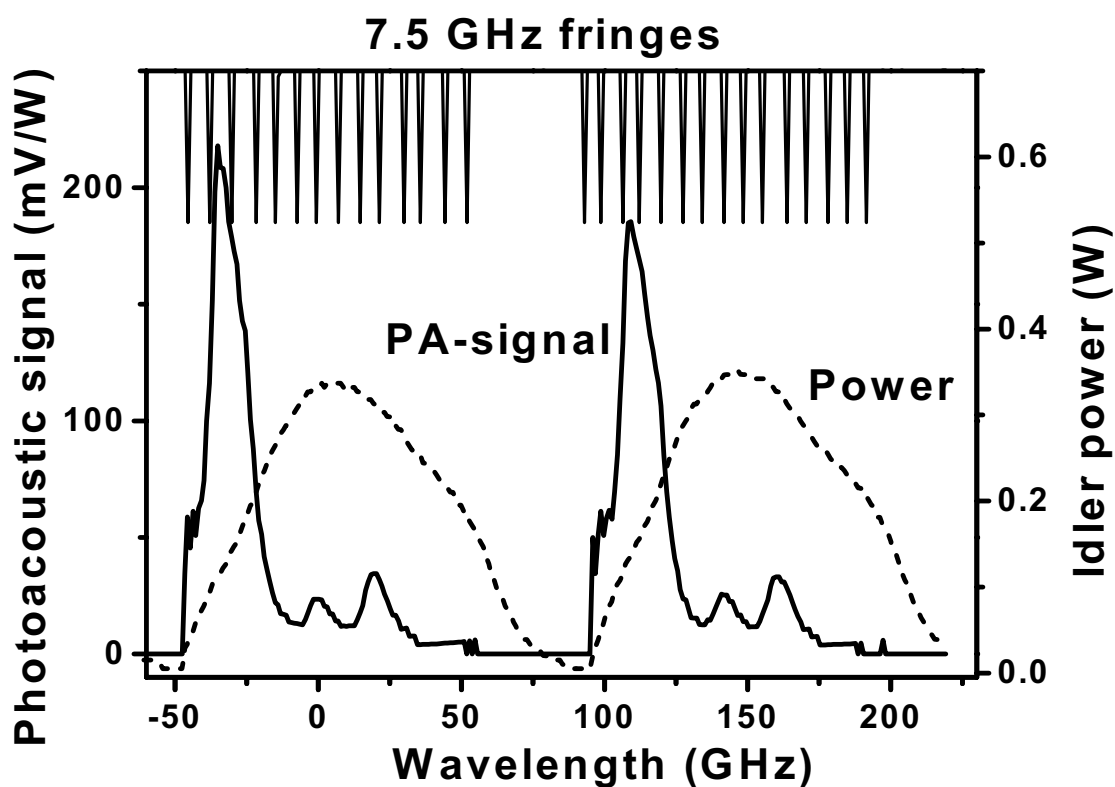


Fig. 4. By changing the distance between the mirrors of the intra-cavity air-spaced etalon a 100 GHz wide mode-hop scan of 10-ppm ethane in nitrogen was made around 2996.9 cm^{-1} . The solid line at the bottom shows the photoacoustic signal, the dashed line the idler power and the solid line at the top the fringes from a 7.5 GHz external Fabry Perot.

Figure 4 illustrates a scan of the OPO over two etalon free spectral ranges around 2996.9 cm^{-1} using the 20% reflectivity etalon. The data shows a repeating, reproducible spectrum with low resolution. Using the fringes of an external 7.5 GHz spectrum analyzer, the total tuning range was found to be 100 GHz, which could be extended by simultaneously tuning the PPLN crystal period and air-spaced etalon.

We observed a strong dependence of the idler output power on the piezo voltage. This was unexpected, because the air-spaced etalon is supposed to have a constant insertion loss [21]. This is most likely caused by steering of the etalon piezo element with voltage, causing a misalignment of the etalon. If we were able to improve the pump-signal overlap we would probably be able to improve the performance of the air-spaced etalon technique. Unfortunately the dimensions of our cavity do not allow this at the moment.

6.4. Solid Etalon

For a solid etalon, Bisson *et al.* [21] reported the best performance with a plane parallel (<10 arc seconds), uncoated $400\text{ }\mu\text{m}$ thick solid YAG etalon (Free Spectral Range 207 GHz). We have also tested an etalon of this type in our OPO, although given the much higher pump power it was not clear if the finesse would be high enough to stabilize the cavity. However, the uncoated YAG etalon appeared to be selective enough to stabilize the OPO cavity to a single mode without causing a large decrease of the idler output power (from 1.6 Watt to 1.5 Watt). A galvo-driver was used to rotate the etalon over several degrees to tune the free spectral range of the etalon, which mode-hop tuned the idler wave over approximately 10 cm^{-1} . This range can be extended by synchronously tuning the PPLN crystal period. The OPO mode-hop-tuned in a similar way as described by Bisson *et al.* [21]. When rotating the etalon the idler wavelength mode-hopped with steps varying from 0.02 to 0.1 cm^{-1} ($0.6 - 3\text{ GHz}$) depending on the number of cavity modes jumped. During rotation, large mode-hops with steps of more than 1 cm^{-1} occurred regularly. Rotating the etalon caused significant changes in the output power of the OPO, which could be explained by walk-off losses within the solid etalon.

6.5. Trace gas detection

Since the solid-etalon gave a better performance in idler output power, a broader tuning range and better cavity stability, we decided to use the solid etalon for our trace gas detection experiments. To measure at a specific absorption line, e.g. of ethane at 2996.9 cm^{-1} , we first tuned the OPO to the center of the absorption peak by moving the fan-out PPLN crystal and rotating the solid etalon. Then we continuously tuned over the entire absorption peak by continuously tuning the pump laser over 24 GHz, while recording the absorption using photoacoustic spectroscopy [7]. During such a scan we did not move the PPLN crystal and solid etalon. The photoacoustic cell was similar to a design described earlier [22], but in this case we increased the length of the acoustic resonator to 300 mm and equipped the cell with 3 electret microphones for improved sensitivity. A Burleigh wavemeter was used to monitor the idler wavelength. A strong absorption-peak of ethane in nitrogen at 2996.9 cm^{-1} was used for our ethane trace gas experiments.

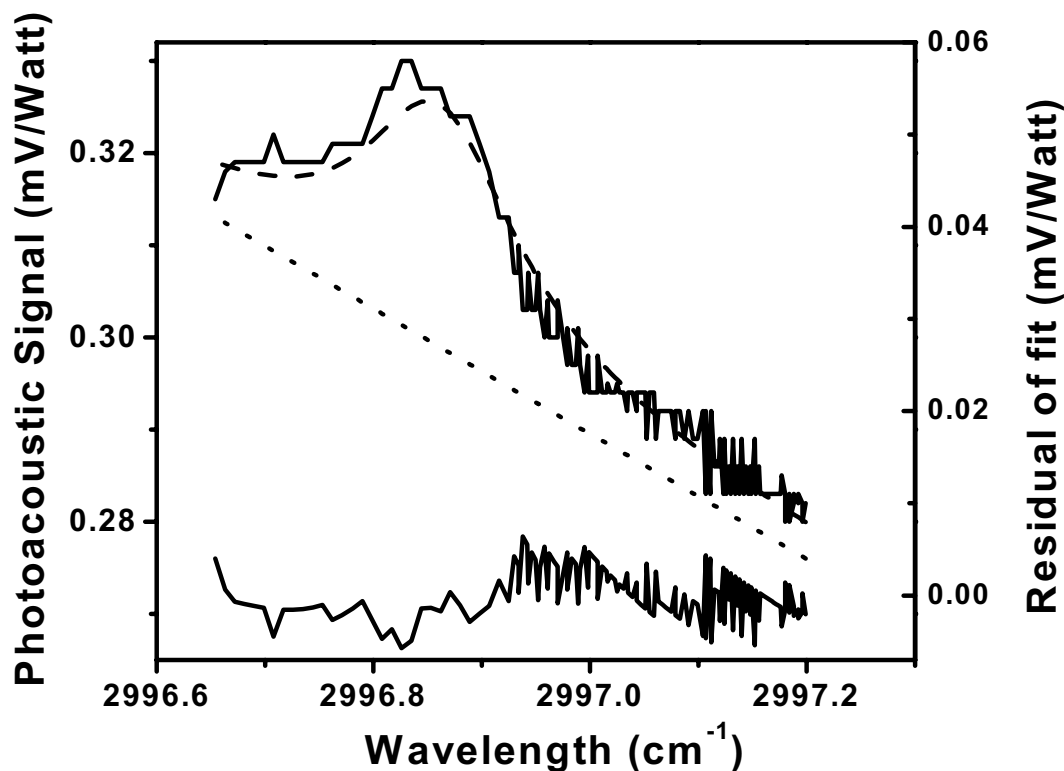


Fig. 5. Pump-scan around 2996.9 cm^{-1} of 0.6-ppb ethane in nitrogen at atmospheric pressure. A Lorentzian fit with linearly decreasing background has been plotted through the data (dashed line). The linearly decreasing background is also shown separately with a dotted line. The bottom of the picture shows the residual if the fit is subtracted from the data.

Fig. 5 shows a one atmosphere (at STP) pressure broadened absorption line of a concentration of 0.6 ppb of ethane in nitrogen. A Lorentzian fit over the absorption peak is added to the figure. Such a fit can be used very well to find the linearly decreasing background signal originating from other absorptions. As can be seen in fig. 5 the residual of the fit stayed within the microphone noise of $5 \mu\text{V}/\text{Hz}^{1/2}$. With the background signal subtracted, the total area beneath the Lorentzian curve can be used as a value for the strength of the absorption and thus the gas concentration.

To find the detection limit for ethane we varied its concentration in nitrogen from 10 ppm to 0.1 ppb in a previous study and reported it in reference [23] (see the next chapter 7). For both the peak values of the absorption line and the Lorentzian fit area values we found a linear relation with the concentration, giving detection limits of respectively 0.1 ppb and 0.01 ppb. This is a huge improvement compared to the detection limit of 1 ppb for commonly used CO lasers [7]. Because the Lorentzian fit helps to find the background signal a much better detection limit and specificity is found using the Lorentzian fit area values. The lowest detectable absorption strengths were calculated to be $3 \times 10^{-10} \text{ cm}^{-1}$ for this system with a scan time of 40 seconds over the absorption peak.

6.6. OPO wavelength stability

To demonstrate the wavelength stability and high-resolution performance of the OPO a low-pressure (60 milliBar) photoacoustic spectrum of 10 ppm ethane in nitrogen is measured (fig. 6).

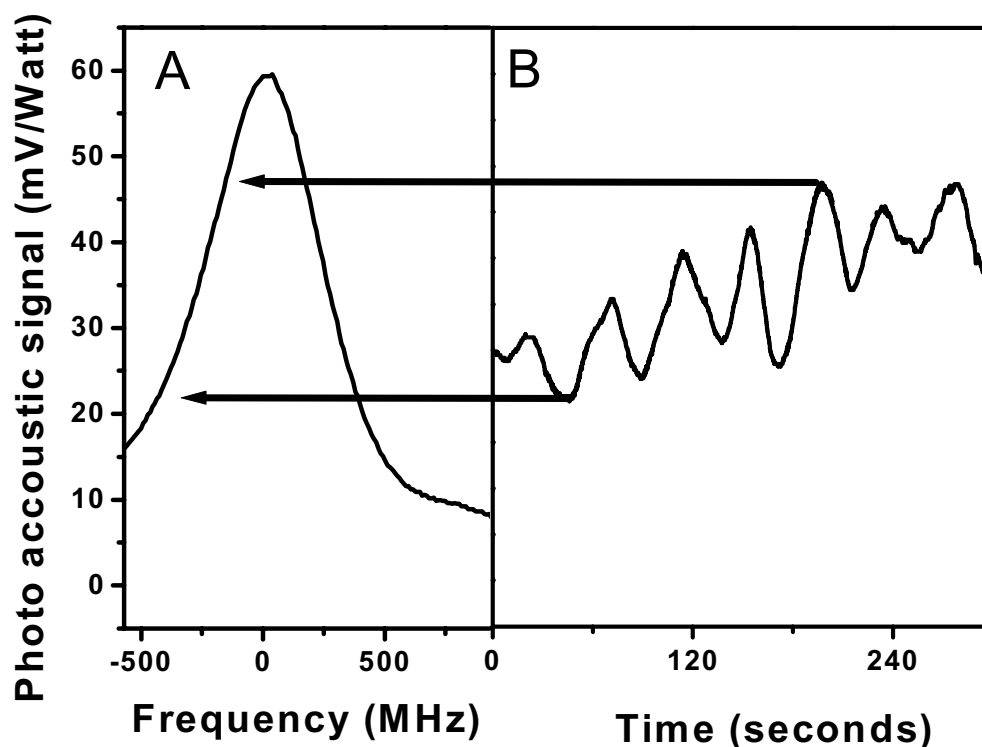


Fig. 6. The wavelength stability of the system is demonstrated by recording the photoacoustic signal coming from the half maximum of a 60 mBar pressure broadened absorption line of 10 ppm of ethane in nitrogen at 2996.9 cm^{-1} . Without tuning the OPO, a 45-seconds oscillation is observed, corresponding to temperature oscillations in the oven of the PPLN crystal. The frequency stability was found to be $<200 \text{ MHz}$ over 300 seconds and $<3 \text{ MHz}$ over 1 second.

The full width half maximum of the absorption line at this pressure was found to be 575 MHz. By placing the laser emission at the half maximum of this absorption line it is possible to estimate the frequency stability of the idler wavelength by the change of the photoacoustic signal over time. When not tuning the OPO we observed a periodical oscillation in the photoacoustic signal with a period around 45 seconds. During the total observation time of 300 seconds this caused an idler frequency drift of 200 MHz. This periodical change was induced by a temperature oscillation of $\pm 0.1 \text{ }^{\circ}\text{C}$ inside the PPLN oven. When the temperature was at its lowest value the photoacoustic signal was also at its lowest point. This corresponds with a decrease of the wavelength in nm, which is in agreement with PPLN temperature tuning theory.

Fortunately, because the instabilities caused by the PPLN oven temperature are rather slow ($<200 \text{ MHz}$ in 300 seconds) the idler wavelength is quite stable over a small time interval (<3

MHz over 1s). Thus, by improving the oven stability temperature a frequency stability of less than 3 MHz can be easily achieved.

6.7. Conclusion

Photoacoustic trace gas detection has been demonstrated using a high-power cw single-frequency, singly resonant OPO. The system gives continuously tunable radiation over 24 GHz in the range of 3.0-3.8 μm with a power of up to 2.2 Watts. Oscillations of ± 0.1 $^{\circ}\text{C}$ in the PPLN temperature induced a long-term idler frequency drift of less than 200 MHz over 300 s. Over 1 s the stability is < 3 MHz.

The air-spaced etalon proved to be useful for OPO tuning and could mode-hop-tune the OPO over a tuning range of 100 GHz. However, the air-spaced etalon gave high losses probably caused by a not fully optimized OPO cavity. A different cavity design would probably give a better performance for an air-spaced etalon. The solid etalon worked very well and could be used to mode-hop tune the laser over 10 cm^{-1} without losing a substantial amount of idler power. The combination of this OPO system with photoacoustic spectroscopy was used for trace gas detection of ethane. Using a Lorentzian fit with a linearly decreasing background a detection limit of 0.01 ppb was found.

References

1. R. Claps, F.V. Englich, D.P. Leleux, D. Richter, F.K. Tittel, R.F. Curl, "Ammonia detection by use of near-infrared diode-laser-based overtone spectroscopy", *Appl. Opt.* 40 4387-4394 (2001)
2. C. Gmachl, D.L. Sivco, R. Colombelli, F. Capasso, A.Y. Cho, "Ultra-broadband semiconductor laser", *Nature* 415, 883-887 (2002)
3. M. Beck, D. Hofstetter, T. Aellen, J. Faist, U. Oesterle, M. Ilegems, E. Gini, H. Melchior, "Continuous wave operation of a mid-infrared semiconductor laser at room temperature", *Science* 295, 301-305 (2002)
4. P.E. Powers, T.J. Kulp, and S.E. Bisson, "Continuous tuning of a continuous-wave periodically poled lithium niobate optical parametric oscillator by use of a fan-out grating design", *Opt. Lett.* 23, 159-161 (1998).
5. G. Berden, R. Peters, G. Meijer, "Cavity ring-down spectroscopy: Experimental schemes and applications", *International Reviews in Physical Chemistry*, 19 565-607 (2000)
6. R. Engeln, G. Berden, R. Peeters, G. Meijer, "Cavity enhanced absorption and cavity enhanced magnetic rotation spectroscopy", *Rev. Sci. Instrum.* 69 3763 (1998)
7. F.J.M. Harren, G. Cotti, J. Oomens, S. te Lintel Hekkert, "Photoacoustic spectroscopy in trace gas monitoring" in *Encyclopedia of Analytical Chemistry*, (Ed.) R.A. Meyers (John Wiley Ltd, Chichester, 2000), 2203-2226.

8. M.W. Sigrist: Air Monitoring by Laser Photoacoustic Spectroscopy, in Air Monitoring by Spectroscopic Techniques, Éd. By M.W. Sigrist, Chemical Analysis, Vol. 27, (John Wiley, New York, 1994) pp.163-238
9. F.J.M. Harren, R. Berkelmans, K. Kuiper, S. te Lintel Hekkert, P. Scheepers, P. Hollander, R. Dekhuijzen, D. H. Parker, "On-line laser photoacoustic detection of ethene in exhaled air as biomarker of ultraviolet radiation damage of the human skin", *Appl. Phys. Lett.* 74, 1761-1763 (1999)
10. H. Zuckermann, F.J.M. Harren, J. Reuss, D.H. Parker, "Dynamics of acetaldehyde production during anoxia and post-anoxia in red bell pepper studied by photoacoustic techniques", *Plant Physiol.*, 113 925-932 (1997)
11. S.T. Persijn, R.H. Veltman, J. Oomens, F.J.M. Harren, D.H. Parker, "CO laser absorption coefficients for gases of biological relevance: H₂O, CO₂, ethanol, acetaldehyde, and ethylene", *Appl. Spectros.* 54 62-71 (2000)
12. A.A.E. Martis, S. Büscher, F. Kuhnemann, W. Urban, "Simultaneous ethane and ethylene detection using a co-overtone laser photoacoustic spectrometer: A new tool for stress/damage studies in plant physiology", *Instrum. Sci. Technol.* 26, 177-187 (1998).
13. W. R. Bosenberg, A. Drobshoff, and J.I. Alexander, "93% pump depletion, 3.5-W continuous-wave, singly resonant optical parametric oscillator", *Opt. Lett.* 21, 1336-1338 (1996).
14. A.J. Henderson, P.M. Roper, L.A. Borschowa, and R.D. Mead, "Stable, continuously tunable operation of a diode-pumped doubly resonant optical parametric oscillator", *Opt. Lett.* 25, 1264-1266 (2000).
15. M.E. Klein, D.-H. Lee, J.-P. Meyn, K.-J. Boller, and R. Wallenstein, "Singly resonant continuous-wave optical parametric oscillator pumped by a diode laser", *Opt. Lett.* 24, 1142-1144 (1999).
16. M. E. Klein, C.K. Laue, D.-H. Lee, K.-J. Boller, and R. Wallenstein, "Diode-pumped singly resonant continuous-wave optical parametric oscillator with wide continuous tuning of the near-infrared idler wave", *Opt. Lett.* 25, 490-492 (2000).
17. F. Kühnemann, K. Scheider, A. Hecker, A.A.E. Martis, W. Urban, S. Schiller, J. Mlynek, "Photoacoustic trace-gas detection using a cw single-frequency parametric oscillator", *Appl. Phys. B* 66, 741-745 (1998)
18. M.M.J.W. van Herpen, S. te Lintel Hekkert, S.E. Bisson, F.J.M. Harren, "Wide single mode tuning of a 3.0-3.8 micron, 700 mW, continuous wave Nd:YAG-pumped optical parametric oscillator based on periodically poled lithium niobate", *Opt. Lett.* 27, issue 8, (2002)
19. G.D. Boyd and D.A. Kleinman, *J. Appl. Phys.* 39 3597-3639 (1968)
20. *Lasers and Electro-Optics*, Ed. C.C. Davis (Cambridge University Press, 1996 Cambridge)
21. S.E. Bisson, K.M. Armstrong, T.J. Kulp, M. Hartings, "Broadly tunable, mode-hop-tuned cw optical parametric oscillator based on periodically poled lithium niobate", *Appl. Opt.* 40, 6049-6055 (2001)
22. F.G.C. Bijnen, J. Reuss, F.J.M. Harren, "Geometrical optimization of a longitudinal resonant photoacoustic cell for sensitive and fast trace gas detection", *Rev. Sci. Instrum.* 67, 2914-2923 (1996)
23. M.M.J.W. van Herpen, S. Li, S.E. Bisson, F.J.M. Harren, "Photoacoustic trace gas detection of ethane using a continuously tunable, continuous-wave optical parametric oscillator based on periodically poled lithium niobate", *Appl. Phys. Lett.* 81, 1157-1159 (2002)

7

Photoacoustic trace gas detection of ethane using a continuously tunable, continuous-wave optical parametric oscillator based on periodically poled lithium niobate

Abstract

A 1.2-Watt, continuous-wave, continuously-tunable, singly-resonant optical parametric oscillator (idler tuning range 3.0-3.8 μm), pumped by a 10-W continuous-wave Nd:YAG laser, is used in combination with a photoacoustic cell for the detection of ethane. An intra-cavity solid-state etalon (thickness 400 μm) was used to stabilize the OPO cavity and could be used to mode-hop tune the idler wavelength over 10 cm^{-1} . The applicability of the system was demonstrated by determining a detection limit for ethane down to 10 parts per trillion. The selectivity was achieved by making a 24 GHz wide pump laser scan over the ethane absorption line at 2996.9 cm^{-1} , after which a Lorentzian fit determined the total area of the absorption signal. Both area value and peak value proved to be linearly depending on the ethane concentration.

This work has been published in:

M.M.J.W. van Herpen, S. Li, S.E. Bisson & F.J.M. Harren, "Photoacoustic trace gas detection of ethane using a continuously tunable, continuous-wave optical parametric oscillator based on periodically poled lithium niobate", *Appl. Phys. Lett.* **81**, 1157-1159 (2002)

7.1 Introduction

The advantage of infrared laser-based trace gas detection lies in its extreme sensitivity and specificity to trace gaseous molecules with the possibility of rapid detection [1,2]. For example, using laser-based photoacoustic spectroscopy, concentrations down to 10 ppt (1-ppt = part per trillion = $1:10^{12}$) for ethylene (C_2H_4) and 100 ppt for acetaldehyde [3,4] can be measured. These features render infrared spectroscopic methods superior to gas chromatographs, mass spectrometry and classical infrared absorption techniques, which have orders of magnitude less sensitivity (5-10 ppb for ethylene and 100 ppb for acetaldehyde, 1-ppb = part per billion = $1:10^9$). The performance of photoacoustic trace gas detection improves with higher laser power. That is why in the past high power gas lasers such as the CO_2 laser (9-11 μm) [5,6], the CO laser (5-8 μm) [4,7] and the CO overtone laser (2.8-4 μm) [8] were used. These lasers allow the detection of a large number of environmentally, biologically and medically relevant gases [1,5], but their disadvantage lies in their discrete line tunability. A continuously tunable laser source would allow more gases to be measured with increased sensitivity and would have a better selectivity between gases that have absorption lines close to each other. Good examples of tunable, mid-infrared sources are the quantum cascade distributed feedback lasers [9,10]. For photoacoustic spectroscopy, optical parametric oscillators (OPOs) are a better choice, because they can give continuous tunability next to a high output power [11]. Kühnemann *et al.* have demonstrated a detection limit of 0.5 ppb for ethane with a low power (40 mWatt) singly resonant OPO (SRO) that is not continuously tuned during the trace gas measurements [12]. Here we demonstrate a detection limit of 0.01 ppb with a high power OPO that is continuously tuned over 24 GHz during the trace gas measurements.

7.2 Experiment

The OPO is similar to what has been described before [11,13] (see chapter 5 and 6). Using a periodically poled lithium niobate (PPLN) crystal with a fan out grating design (periods ranging from 29.3 to 30.1 μm) a signal beam (wavelength 1.5 - 1.7 μm) and an idler beam (3.0-3.8 μm) are generated via optical parametric conversion from a 1064 nm pump source. The pump source is a Nd:YAG Master Oscillator Power Amplifier system (M6000, Lightwave, CA) generating more than 10 Watts cw at 1064 nm. The pump-laser linewidth is 5 kHz (over 1 ms) with a frequency stability of 50 MHz/hour and it has a TEM_{00} spatial mode with a beam quality of $M^2 < 1.1$. The pump laser can be continuously tuned over 24 GHz with two reproducing mode-hops occurring backwards compared to the direction of tuning [11]. For our singly resonant OPO (SRO), a bowtie ring cavity is used to resonate the signal wavelength, while transmitting the idler and pump wavelengths. Single mode operation of this cavity is enhanced by means of an intra-cavity etalon.

An important consideration is whether to use an air-spaced or solid state etalon. The advantage of using an air-spaced etalon is that the losses are constant after inserting it, which reduces etalon mode hopping [14]. The drawback of the air-spaced etalon is that (in our case) the OPO oscillation threshold increased considerably, resulting in a lower output power. Proper alignment of such an etalon is experimentally difficult and also very important to reduce losses. In addition, an air spaced etalon requires more intra-cavity space as compared to a solid etalon. For our

actual spectroscopic trace gas experiments we do not tune the intra-cavity etalon, but instead we tune the Nd:YAG pump source, which will cause the idler frequency to tune as well. This means that the constant losses during etalon tuning are of minor importance to us, so we have decided to use a solid state etalon as this gives a higher output power.

7.3 Results

According to previous attempts [14] we used a 400- μm thick solid YAG etalon with a free spectral range of 207 GHz (VLOC, New Port Richey, FL). The plane parallel (<10 arc seconds), uncoated ($R = 8\%$) YAG etalon appeared to be selective enough to stabilize the OPO cavity to a single mode, without increasing the threshold power much (from 3 to 4 Watt). The idler output power went down from 1.5 Watt to 1.2 Watt.

To mode-hop tune the OPO wavelength the YAG etalon can be angle rotated with a galvo driver. When the PPLN crystal is kept at a fixed periodicity during rotation of the etalon, a tuning range of 10 cm^{-1} can be covered for the idler wavelength. A significant change in idler output power is observed during rotation, which can be explained by walk off losses within the solid etalon. The mode-hop-tuning behavior of the OPO is similar to what has been described by Bisson *et al.* [14]. When rotating the etalon the idler wavelength tunes in steps of $0.02\text{-}0.1\text{ cm}^{-1}$ ($0.6\text{ - }3\text{ GHz}$), depending on the number of cavity modes jumped. Sometimes, several mode hops are observed giving steps of more than 1-cm^{-1} . In future experiments we plan to use higher finesse YAG etalons (reflectivity $R>20\%$) to decrease the mode-hop step-size.

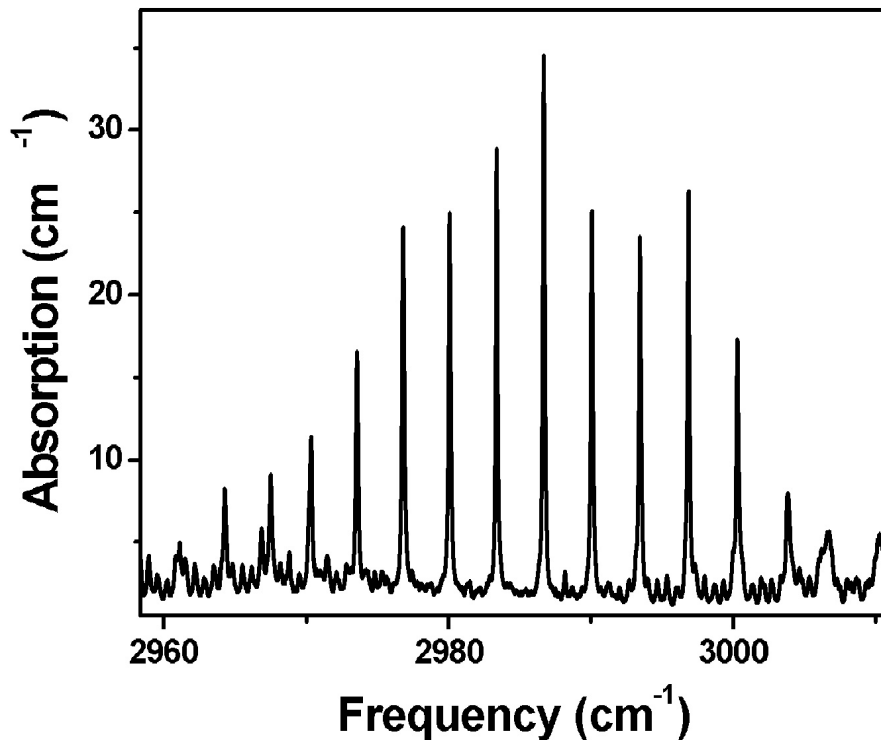


Fig. 1. Ethane spectrum measured with an FTIR spectrometer at standard room temperature and pressure [15].

Figure 1 shows the absorption spectrum of Ethane near 3000 cm^{-1} , which was measured with an FTIR spectrometer [15]. For photoacoustic detection of ethane (C_2H_6), we coarse tuned the OPO to the center of the absorption line at 2996.9 cm^{-1} by adjusting the fan-out PPLN crystal and by tuning the intra-cavity solid-state etalon. The pump laser was then continuously tuned over 24-GHz to record the entire absorption peak (Fig. 2). A wavemeter (Burleigh WA-1000 IR) was used to record the idler wavelength with a resolution of 0.01 cm^{-1} .

The OPO idler beam was directed through a photoacoustic cell in which a mixture of ethane in nitrogen was kept at atmospheric pressure (STP). The photoacoustic cell is similar to a design described earlier [3], but we increased the length of the acoustic resonator from 100 mm to 300 mm and reduced the radius from 3 mm to 2 mm, which improved the sensitivity by a factor of 2.6 [3]. The acoustic resonator is excited in the first longitudinal mode at a resonance frequency of 560 Hz. In addition, we used 3 Knowless IK3024 electret microphones instead of one.

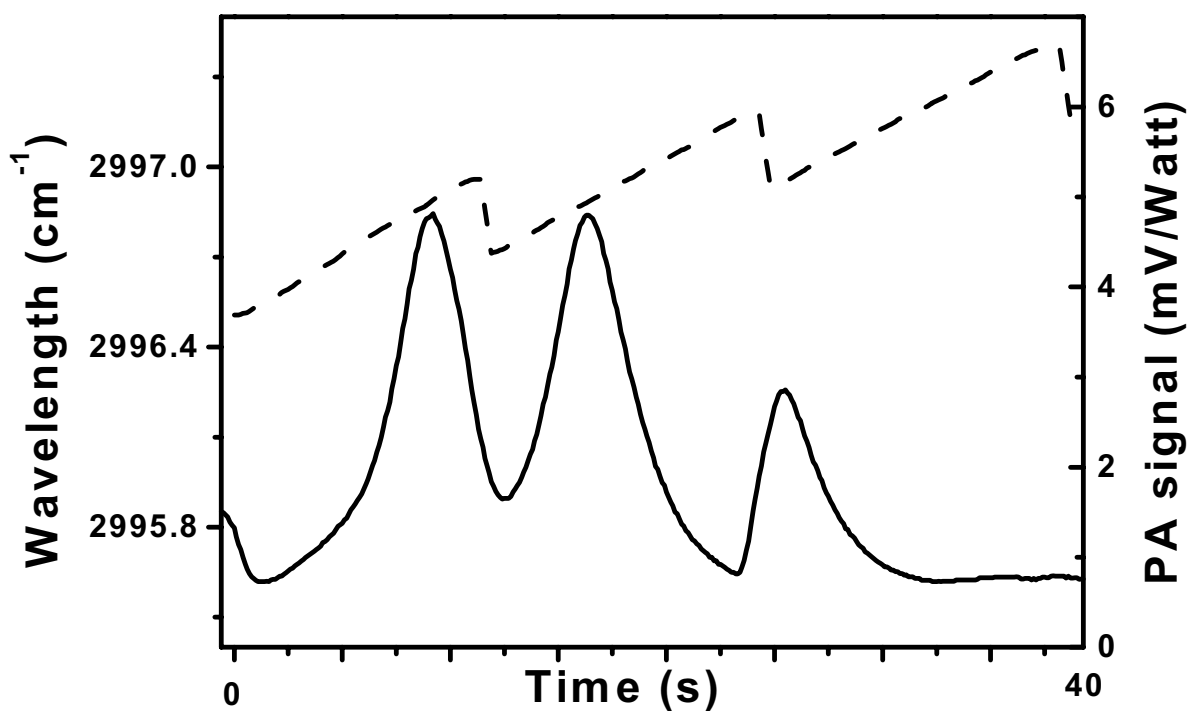


Fig. 2. A 24-GHz pump scan of the OPO at the idler wavelength. The solid line shows the photoacoustic signal of a mixture of 3-ppm ethane in nitrogen. The wavelength (dashed line) shows two mode-hops which are caused by reproducible mode-hops of the pump laser, which are always backwards compared to the direction of tuning.

Figure 2 shows an example of an OPO scan acquired by tuning of the pump source. Although two mode-hops were observed in this scan, they were reproducible from scan to scan and could be removed from the data by plotting the measured photo-acoustic signal against the recorded wavelength. These mode hops always occurred opposite to the direction of tuning and were attributed to mode hops in the pump source. An example of a scan of 0.4-ppb ethane in nitrogen is shown in figure 3, which shows the Lorentzian least-squares fit of the pressure broadened ethane absorption peak. For this fit, a linearly decreasing background signal was added to the Lorentzian profile. The picture shows that this fit can be used very well to find the background signal and to fit the actual absorption signal. With the fitted background subtracted, the total area under the Lorentzian curve can be used as a value for the absorbance and thus the concentration.

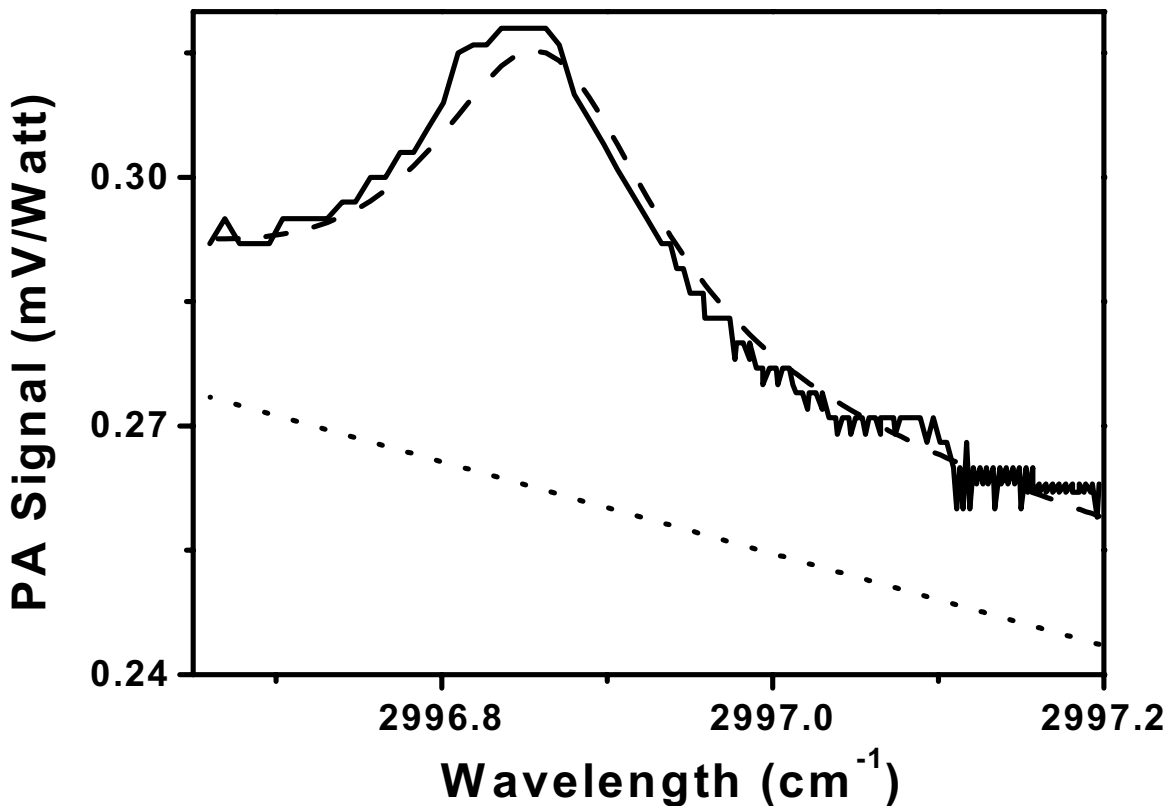


Fig. 3. Photoacoustic signal of the ethane absorption line at 2996.9 cm^{-1} for a mixture of 0.4 ppb ethane in nitrogen. A Lorentzian fit (dashed line) with a linearly decreasing background (dotted line) has been plotted through the experimental data (solid line). Evident are the microphone noise ($5 \mu\text{V}/\text{Hz}^{1/2}$) and the high background signal (0.3 mV/Watt). Due to this wavelength-dependent background signal it is hard to use solely the peak value of the absorption at this ethane concentration, but the Lorentzian fit is able to find the background signal very well. With background subtracted the photoacoustic signal is 0.04 mV/Watt.

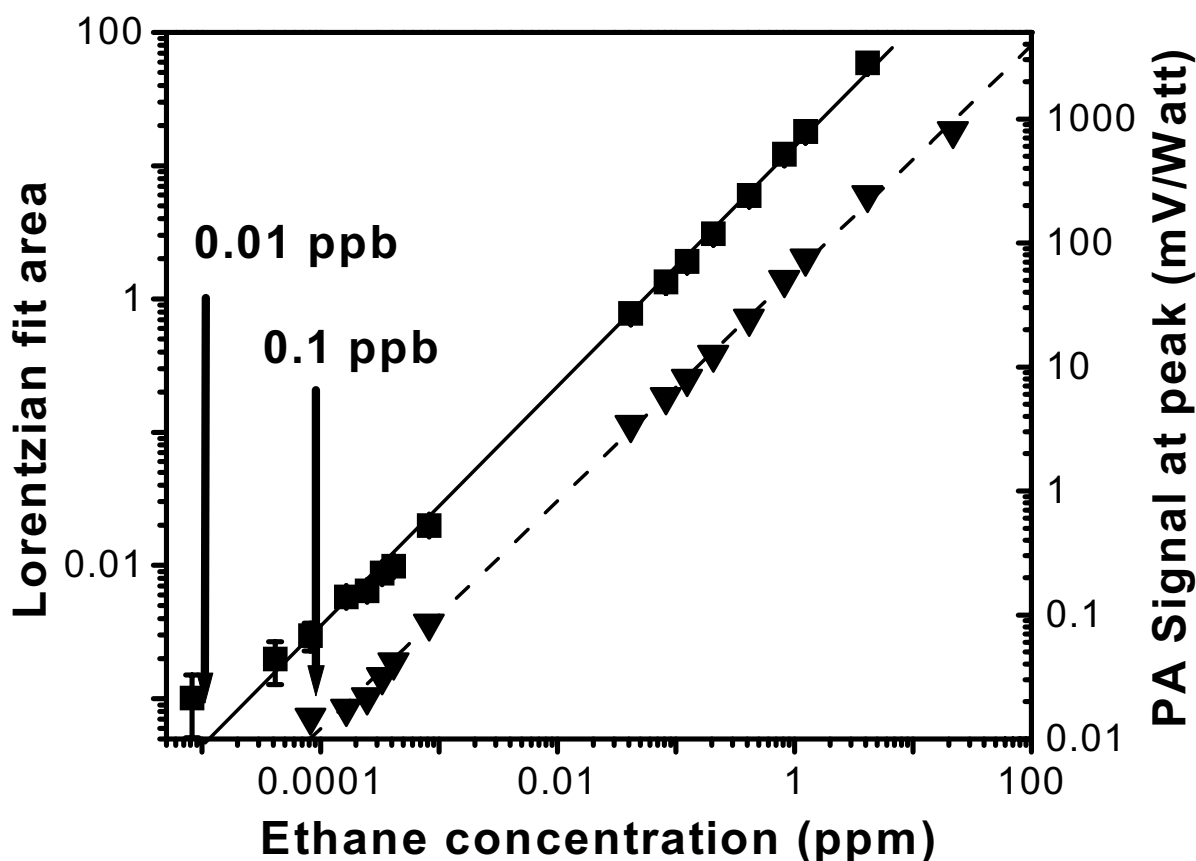


Fig. 4. The detection limit of ethane is determined by measuring the peak height (triangles + dotted line) and the area of the fit of the absorption (squares + solid line) at 2996.9 cm^{-1} for different concentrations of ethane in nitrogen. The detection limit is determined by the noise of the system, which is used as the horizontal axis. Using the peak values a detection limit of 0.1 ppb was found. With the Lorentzian fit area a detection limit of 0.01 ppb is found.

To find the ethane detection limit for our system we have measured the absorption of ethane at 2996.9 cm^{-1} for different concentrations of ethane in nitrogen. Using two mass flow controllers, pure nitrogen gas was mixed with 20-ppm and 0.8-ppb ethane / nitrogen mixtures to obtain ethane concentrations ranging from 20 ppm to 0.01 ppb. Figure 4 shows two calibration lines; one for the peak values of the absorption line and one for the total area under the Lorentzian fit. Both values show a linear behavior with the concentration, until it reaches the noise level and turns into a horizontal line. The detection limit (signal-to-noise ratio $\text{SNR}=1$) using the peak values was found to be 0.1 ppb and was limited by the microphone noise of $5 \mu\text{V} / \text{Hz}^{1/2}$. Using the peak height was difficult because of a varying background signal around 0.3 mV/Watt (Fig. 3). In this case the fitted background signal could be subtracted, but without continuous tuning this would not have been possible and would have resulted in a lower detection limit of 5 ppb. The detection limit using the Lorentzian fit was found to be 0.01 ppb ($\text{SNR}=1$), which was

limited by the noise of the total area under the Lorentzian curve (scan time 40 s). The noise in the area value was determined by measuring the area values for pure nitrogen. Because the Lorentzian fit helps to find the background signal, a much better detection limit was obtained using the Lorentzian fit area values. Using the Hitran database [16] the maximum absorption strength of ethane at 2996.9 cm⁻¹ was determined to be 33.4 atm⁻¹cm⁻¹. Combined with the detection limit of 0.01 ppb, this results in a detection limit of 3*10⁻¹⁰ cm⁻¹ (scan time 40 seconds).

7.4 Conclusion

While we have demonstrated the use of a PPLN OPO for trace gas detection of ethane, the broad tunability allows a wide range of different gases to be detected in the mid-IR (3.0-3.8 μm, e.g. vibrational C-H-stretch of molecules). Mainly due to the higher power, this system has a much better sensitivity compared to other OPO systems [12]. In addition this system has a better specificity, because it is continuously tunable. We demonstrated that the detection limit could still be reached if the background signal is varying. In future we expect to apply the system in various applications in biology and medicine [1,6,12].

References

1. F.J.M. Harren, G. Cotti, J. Oomens, S. te Lintel Hekkert, "Photoacoustic spectroscopy in trace gas monitoring", in *Encyclopedia of Analytical Chemistry*, Edited by R.A. Meyers (John Wiley Ltd, Chichester, 2000), pp. 2203-2226
2. G. Berden, R. Peters, G. Meijer, "Cavity ring-down spectroscopy: Experimental schemes and applications", *International Reviews in Physical Chemistry* 19, 565-607 (2000)
3. F.G.C. Bijnen, J. Reuss, F.J.M. Harren, "Geometrical optimization of a longitudinal resonant photoacoustic cell for sensitive and fast trace gas detection", *Rev. Sci. Instrum.* 67, 2914-2923 (1996)
4. H. Zuckermann, F.J.M. Harren, J. Reuss, D.H. Parker, "Dynamics of acetaldehyde production and post-anoxia in red bell peppers studied by photoacoustic techniques", *Plant Physiol.* 113, 925-932 (1997)
5. M.W. Sigrist, "Air Monitoring by Laser Photoacoustic Spectroscopy", in *Air Monitoring by Spectroscopic Techniques*, edited by M.W. Sigrist (John Wiley, New York, 1994), *Chemical Analysis* 27, pp.163-238
6. F.J.M. Harren, R. Berkelmans, K. Kuiper, S. te Lintel Hekkert, P. Scheepers, P. Hollander, R. Dekhuijzen, D. H. Parker, "On-line laser photoacoustic detection of ethene in exhaled air as biomarker of ultraviolet radiation damage of the human skin", *Appl. Phys. Lett.* 74, 1761-1763 (1999)
7. S.T. Persijn, R.H. Veltman, J. Oomens, F.J.M. Harren, D.H. Parker, "CO laser absorption coefficients of biological relevance: H₂O, CO₂, ethanol, acetaldehyde and ethylene", *Appl. Spectros.* 54, 62-71 (2000)
8. A.A.E. Martis, S. Büscher, F. Kühnemann, W. Urban, *Instrum. Sci. Technol.* 26, 177 (1998).
9. C. Gmachl, D.L. Sivco, R. Colombelli, F. Capasso, A.Y. Cho, "Ultra-broadband semiconductor laser", *Nature* 415, 883-887 (2002)
10. M. Beck, D. Hofstetter, T. Aellen, J. Faist, U. Oesterle, M. Illegems, E. Gini, H. Melchior, "Continuous wave operation of a mid-infrared semiconductor laser at room temperature", *Science* 295, 301-305 (2002)
11. M.M.J.W. van Herpen, S. te Lintel Hekkert, S.E. Bisson, F.J.M. Harren, "Wide single mode tuning of a 3.0-3.8 micron, 700 mW, continuous wave Nd:YAG-pumped optical parametric oscillator based on periodically poled lithium niobate", *Opt. Lett.* 27, issue 8, (2002)
12. F. Kühnemann, K. Scheider, A. Hecker, A.A.E. Martis, W. Urban, S. Schiller, J. Mlynek, "Photoacoustic trace-gas detection using a cw single-frequency parametric oscillator", *Appl. Phys. B* 66, 741-745 (1998)
13. P.E. Powers, T.J. Kulp, S.E. Bisson, "Continuous tuning of a continuous wave periodically poled lithium niobate optical parametric oscillator by use of a fan-out grating design", *Opt. Lett.* 23, 159-161 (1998)
14. S.E. Bisson, K.M. Armstrong, T.J. Kulp, M. Hartings, "Broadly tunable, mode-hop-tuned cw optical parametric oscillator based on periodically poled lithium niobate", *Appl. Opt.* 40, 6049-6055 (2001)
15. A. Popp, H. Dahnke, F. Kühnemann, J. Orphal, G. Basum, J.P. Burrows: unpublished work report, Institut für Angewandte Physik (Bonn) and Institut für Umweltphysik (Bremen) (1999)
16. The Hitran database: <http://cfa-www.harvard.edu/HITRAN/>

8

Continuous-wave operation of single frequency optical parametric oscillator between 4-5 μm based on periodically poled LiNbO_3

Abstract

We present a cw, Nd:YAG-pumped, singly resonant, single-frequency, narrow linewidth, high power optical parametric oscillator with idler tuning from 3.7-4.7 μm . In this spectral range, absorption of the idler wave in the LiNbO_3 crystal is significant, causing the oscillation threshold to increase with a subsequent decrease in output power from 1.2 Watts at 3.9 μm to 120 milliWatts at 4.7 μm . The OPO cavity was stabilized and mode-hop-tuned with a rotatable solid etalon, but this caused a reduction in idler power of up to 50%. The usefulness for spectroscopy was demonstrated by recording a photo-acoustic spectrum of a strong CO_2 absorption using a 24 GHz continuous idler scan.

This work has been published in:

*M.M.J.W. van Herpen, S.E. Bisson, F.J.M. Harren, "Continuous-wave operation of single frequency optical parametric oscillator between 4-5 μm based on periodically poled LiNbO_3 ", Opt. Lett. **28**, 2497-2499 (2003)*

8.1 Introduction

Optical Parametric Oscillators (OPO's) based on Periodically Poled Lithium Niobate (PPLN) are a powerful tool to generate mid-infrared radiation, due to their wide tunability, high power, high stability and narrow linewidth [1-8]. Because the transparency of Lithium Niobate decreases at wavelengths above 4 μm , generation of radiation with longer wavelengths is difficult. However, there is a strong interest in generating long mid-IR wavelengths for a number of applications such as spectroscopy and chemical sensing.

For pulsed OPO operation it has been shown that due to the high parametric gain, idler absorption loss in the PPLN crystal can be tolerated with operation extending far into the IR absorption edge of LiNbO₃ [1-2]. Recently, pulsed OPO operation has been shown at idler wavelengths out to 7.3 μm [2].

In continuous-wave (cw) operation, OPO generation of idler wavelengths above 4 μm has continued to be a problem. Lowenthal [9] has made an analysis of the effect of idler loss on the cw OPO pump threshold and output power. His model was able to predict these values accurately for OPO's without idler absorption, but there has not yet been a validation of this model with strong idler absorption. In 1997 Myers and Bosenberg [3] described an OPO operating between 3.6 and 4.7 μm pumped by a multi-mode YAG source with a linewidth of ~ 2.2 GHz. The authors found that for wavelengths above 4 μm the idler output power dropped significantly and they observed a 'modest rise' in the oscillation threshold. Unfortunately, the oscillation threshold was not measured as a function of the wavelength and no information was given about the pump depletion. In that study, the authors also did not stabilize the frequency of the OPO cavity with an intra-cavity etalon.

To be useful for many spectroscopic applications, the OPO must have a narrow linewidth (<10 MHz), good stability and broad tunability. Since the work of Myers and Bosenberg, no successful attempt has been made to develop a PPLN OPO operating with long idler wavelengths, probably due to a lack of suitable pump sources. Here, we present a Nd:YAG-pumped, cw, singly resonant OPO with single-frequency, narrow linewidth high power output. The OPO can be continuously tuned over 24 GHz within its operating range of 3.7-4.7 μm . The usefulness of this system for spectroscopy is demonstrated by recording a strong CO₂ absorption with photo-acoustic spectroscopy.

8.2 Experiment

The experimental setup is similar to the setup described before [7,8]. The pump laser was a cw Nd:YAG source (Lightwave M6000) operating at 1064nm, which generated up to 11 Watts of single-mode output power. This laser has a small linewidth (5 kHz over 1 ms) with high frequency stability (50 MHz/hour) and an excellent beam quality of $M^2 < 1.1$ in a TEM₀₀ spatial mode. The frequency of the pump source can be continuously tuned over 24 GHz [7].

The PPLN crystal used in this work was 5 cm long and had periods ranging from 25.9 to 28.7 μm and was initially operated at a temperature of 188.3 °C. The crystal was anti-reflection coated

for the signal ($<0.5\%$ R at 1400-1500 nm), idler ($<12\%$ R at 3000-4850 nm) and pump ($<0.5\%$ R at 1064 nm) wavelengths. The OPO used a bowtie ring-cavity design with two flat mirrors and two curved mirrors, all coated (VLOC, New Port Richey, FL, USA) for high reflectivity at the signal wavelength ($\geq 99.8\%$ R at 1350-1500 nm) and high transmission for the pump ($>90\%$ T at 1064 nm) and idler wavelengths ($\geq 85\%$ T at 3650-4850 nm). This gave a singly resonant OPO, which was resonant for the signal frequency only. For spectroscopic applications, single mode operation of this cavity could be enhanced by means of an intra-cavity 400- μm thick uncoated YAG etalon (reflectivity 8%). However, inserting this etalon into the OPO cavity caused a 50% reduction in idler power. The combination of a single mode pump source and a single mode ring cavity resonating at the signal wavelength produces a non-resonant, but single frequency idler beam with tuning characteristics that mirror the pump laser. Because the pump laser can be continuously tuned over 24 GHz, this tuning range can be used to tune the idler frequency as well. Additionally, the intra-cavity etalon can be rotated to mode-hop-tune the OPO [4].

When the pump-beam travels through the PPLN crystal green light is generated due to non-phase matched second harmonic generation. In previous experiments [7], this green light was used as tracer beam to align the OPO cavity. However, in this case this was not possible, because the cavity mirror coatings transmitted most of the visible light. To solve this problem, the OPO cavity was first constructed with cavity mirrors suitable for generating idler wavelengths between 3 and 4 μm , which coincidentally reflect green light [7]. With these mirrors and a pump power of 11W, it was possible to generate 450 mW of idler power at a wavelength of 3.683 μm with a PPLN period of 28.7 μm . Next, the 3-4 μm cavity mirrors were replaced one-by-one with mirrors suitable for 4-5 μm operation. After replacing each mirror, the mirror alignment was adjusted until the OPO started to oscillate again.

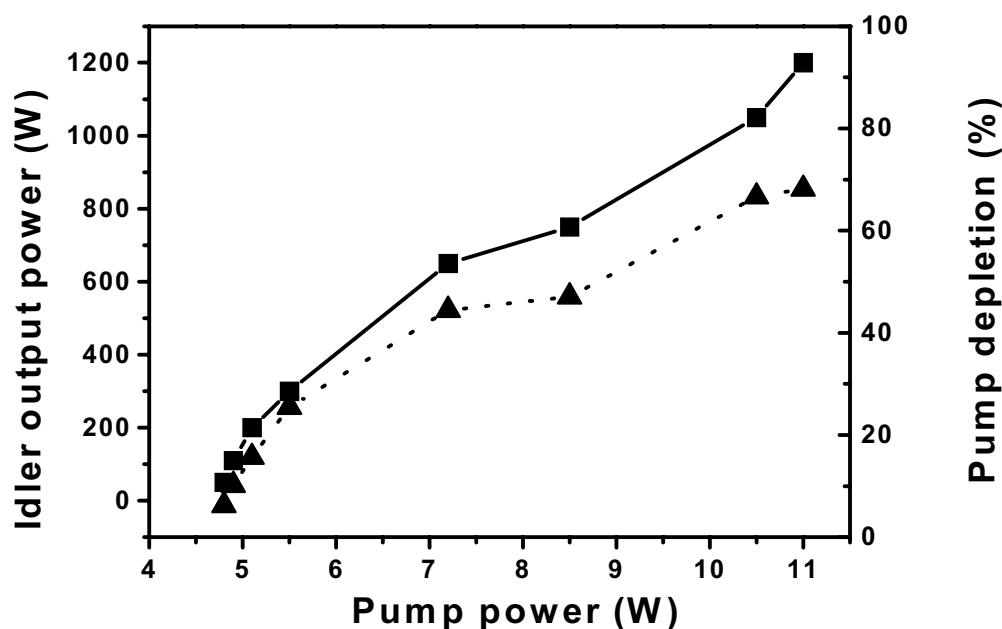


Fig. 1. Idler output (solid line) and pump depletion (dotted line) versus pump input power for the SRO operating at an idle wavelength of 3.9 μm . The oscillation threshold is 5.0 W and a maximum idler power of 1.2 W with 70% pump depletion is observed with a pump power of 11W.

8.3 Results

Figure 1 shows the 3.9 μm idler output power and pump depletion of the OPO with all mirrors replaced. The OPO oscillation threshold at 3.9 μm was found at 5 Watts, and with full pump power of 11 Watts an idler output of 1.2 Watts was achieved, with 70% pump depletion. The low pump depletion may be explained in part by low reflectivity of the cavity mirrors at the short signal wavelengths and low transmission of the PPLN coatings at the edge of its specified range at 1.5 μm . In addition this could also indicate that the cavity length was not optimized [8] or that there were thermal lensing effects.

The OPO was able to generate light with idler wavelengths ranging from 3.6 to 4.7 μm . For a pump power of 11 Watts and without the intra-cavity etalon, the output power varied from 1.2 Watts at 3.9 μm to 120 milliWatts at 4.7 μm (fig. 2), which is similar to the output powers reported by Myers and Bosenberg [3]. Because idler photons with a longer wavelength have a lower quantum energy, the output power is therefore correspondingly lower at longer wavelengths. However the observed drop in output power with increased idler wavelength is due rather to intrinsic absorption of the idler wave in the PPLN crystal. At a pump power of 11W and an estimated idler absorption of up to 35% per cm [9] thermal (lensing) effects can be quite large, causing a misalignment of the OPO cavity. Fig. 2 shows the correspondence of idler output power with the transparency of LiNbO_3 . The oscillation threshold appeared to be stable around 5 Watts for idler wavelengths up to 4.2 μm , but for longer idler wavelengths the oscillation threshold increased significantly and became as high as 7.5 Watts at 4.7 μm (fig. 3). At this wavelength the pump depletion is 10% with 11 Watts of pump power.

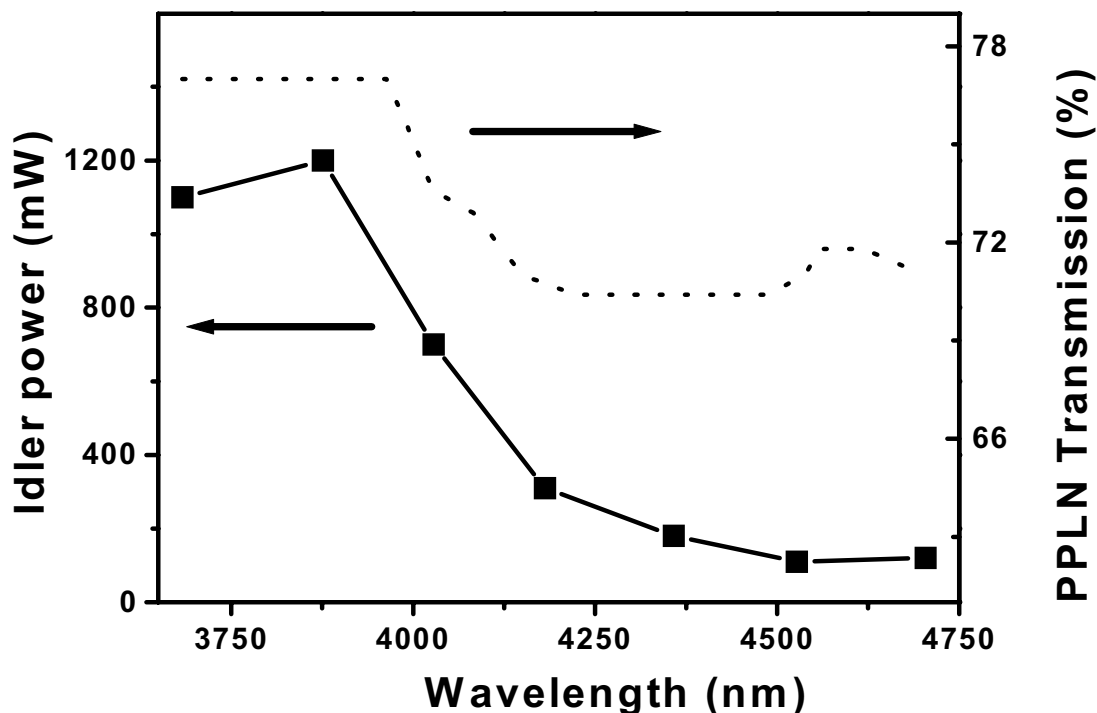


Fig. 2. OPO idler tuning with a multi-grating crystal. The idler power (solid line) correlates strongly with PPLN transparency (dots).

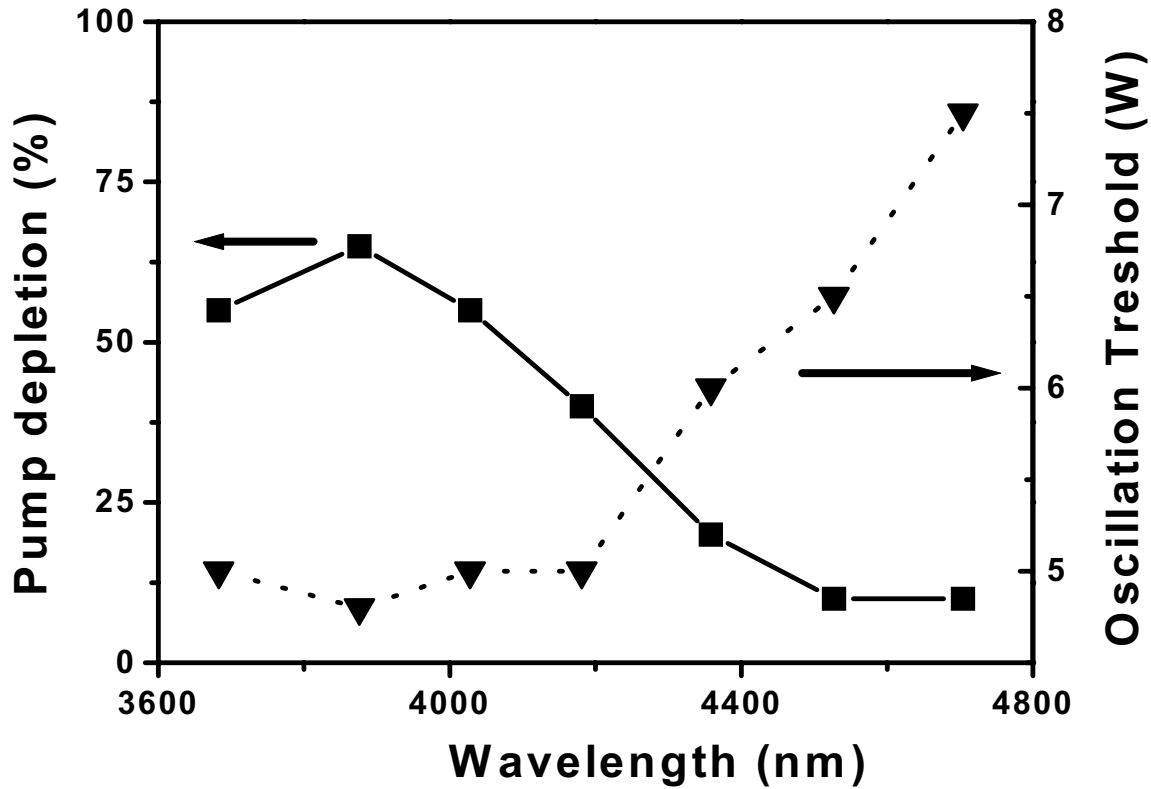


Fig. 3. Pump depletion (solid line) and oscillation threshold (dotted line) as a function of the idler wavelength with 11 W of pump power.

For the case of no idler absorption, Lowenthal's analysis [9] predicted an oscillation threshold of around 5 Watts at 4.5 μm , which is in agreement with our findings with low idler absorption. With an idler absorption of 35% per cm at 4.5 μm the oscillation threshold is predicted to increase to 7.3W according Lowenthal's model, which is consistent with the observed value of 6.5W. With 11 Watts of pump power Lowenthal predicts an idler output power of 1.0 Watt and a pump depletion around 80% at 4.5 μm . However, our experimental values were much lower than this with the idler output power around 110 mW (in agreement with [3]) and a pump depletion of 10%. Because the pump depletion at 3.9 μm was also lower than predicted, it was also expected that it would also be lower at 4.5 μm . However, this is not enough to explain the large discrepancy with the model, especially since it was able to accurately predict the oscillation threshold. The difference can be explained by thermally induced focusing effects, which can significantly reduce OPO performance, but are ignored in Lowenthal's analysis. With the high pump power of 11 Watts and the high idler absorption is it likely that these effects are present.

For a particular PPLN grating period and temperature, the idler wavelength could be calculated using the Sellmeier equations of Jundt [10] (fig. 4). To demonstrate the accuracy of this wavelength calculation in cases where there was significant absorption, we measured the

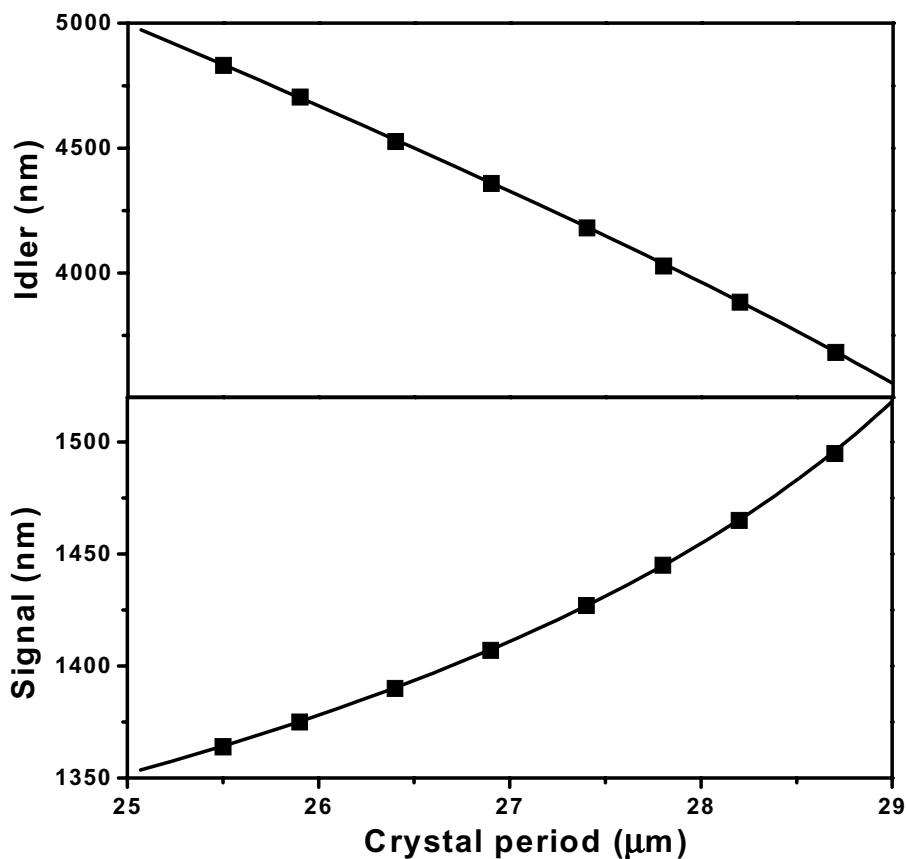


Fig. 4. Calculated signal and idler wavelengths at 188 °C. The squares indicate the crystal periods available on the PPLN crystal. By changing the crystal temperature the full wavelength range from 3.8 to 4.8 μm can be covered.

absorption of a known CO_2 line in air ($340\text{ppm}\pm 10\text{ ppm}$) at a wavelength of $4.201\mu\text{m}$ (2380.72 cm^{-1}). For this measurement, the coarse wavelength was set by translating the PPLN crystal to a period of $27.4\mu\text{m}$ and operating the PPLN crystal at a temperature of $176\text{ }^\circ\text{C}$. Fine tuning to the peak of the CO_2 absorption line was achieved by mode-hop tuning [4] the OPO with an intra-cavity etalon. Continuous pump-tuning over 24 GHz was used to tune the idler frequency over the CO_2 absorption line. A maximum absorption of $52\pm 4\%$ was found with a path-length of 135 cm, giving an experimental absorption coefficient of $\alpha=16\pm 2\text{ atm}^{-1}\text{cm}^{-1}$. From the Hitran database a CO_2 absorption strength of $\alpha=16.9\text{ atm}^{-1}\text{cm}^{-1}$ was calculated at this wavelength. Since the calculated value is in agreement with the experimental value, this result can be used as confirmation that the calculated wavelength can be used to accurately set the OPO wavelength.

The combined attributes of high power and broad tunability make this system an ideal source for spectroscopic and chemical sensing applications. The high power of this system makes it

particularly well suited for photoacoustic spectroscopy. To demonstrate the use of this system for spectroscopy in the 4.0-5.0 μm range, we recorded photoacoustic spectra of a very strong CO_2 absorption ($378.8 \text{ atm}^{-1}\text{cm}^{-1}$) at 2361.47 cm^{-1} (4235 nm).

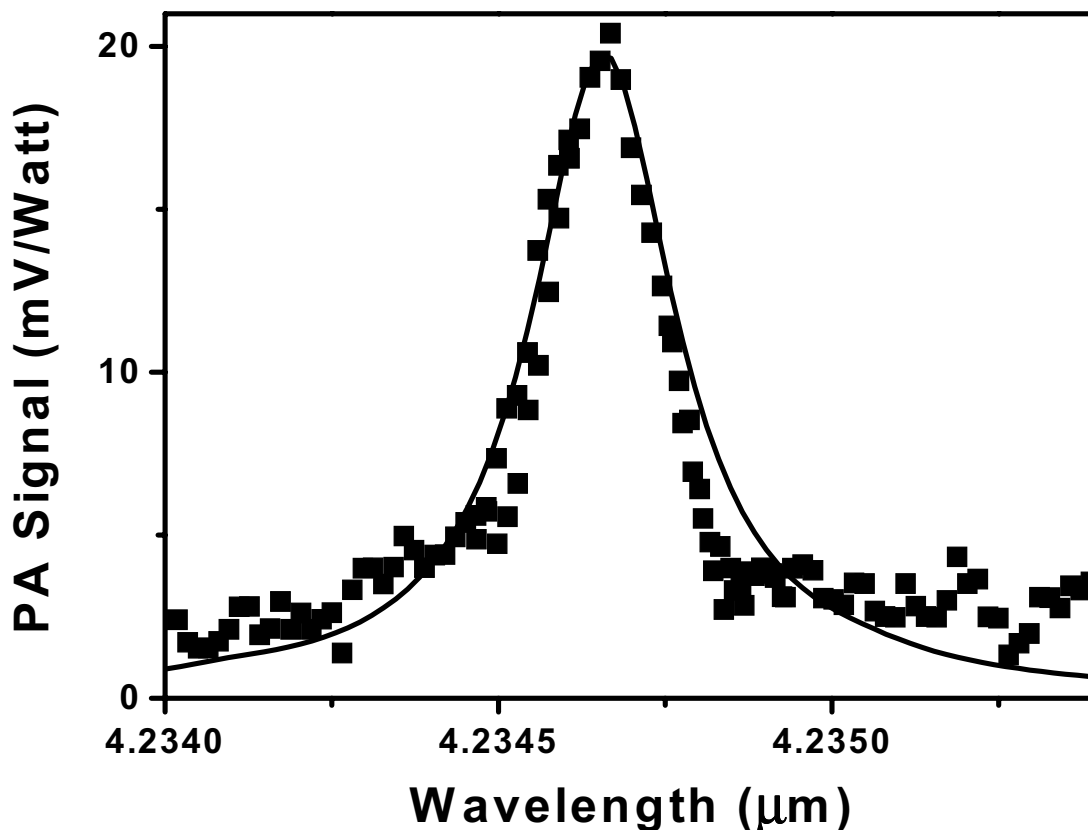


Fig. 5. Photoacoustic spectrum (squares) of the 4235 nm (2361.47 cm^{-1}) CO_2 line acquired by pump tuning the OPO over 24 GHz. For this measurement, the CO_2 concentration was 7 ppm in nitrogen. A Hitran calculation (solid line) is shown for comparison.

To tune the OPO to this wavelength, the same crystal period of $27.4 \mu\text{m}$ was used, but with a temperature of $152.5 \text{ }^\circ\text{C}$. Figure 5 shows a 24 GHz pump scan over the CO_2 absorption line at a concentration of 7 ppm in nitrogen. The OPO cavity was covered with a box and flushed with pure nitrogen gas to minimize losses due to atmospheric absorption. However, at the peak of the CO_2 absorption there was still a loss of at least 30% in the idler power due to residual absorptions in the OPO environment. Despite these losses and the losses due to the intra-cavity etalon there was still 40 milliWatts of idler power at the peak of the CO_2 absorption.

8.3 Conclusion

In conclusion, we have successfully developed a cw YAG-pumped, singly resonant, single-frequency, high power OPO operating from 3.7-4.7 μm . We have found that at longer idler

wavelengths, absorption of the idler wave in the LiNbO₃ crystal significantly increased the oscillation threshold by as much as 2.5 W, which was in agreement with this part of Lowenthal's theoretical analysis [9]. For idler wavelengths longer than 3.9 μm, the idler output power was considerably reduced due to intrinsic absorption within the LiNbO₃ crystal. Due to the high pump power and idler absorption, it was likely that there have been induced thermal focusing effects. Our values for output power and pump depletion were not in agreement with Lowenthal's analysis, probably because this analysis excludes these effects. Despite of this, the OPO cavity could be stabilized quite well and mode-hop-tuned with a solid-state intra-cavity etalon. However, insertion of the solid etalon reduced the idler power by as much as 50%. For truly continuous tuning, the Nd:YAG pump laser was tuned over 24GHz, which correspondingly tuned the idler frequency by the same amount. These features make the system very useful for spectroscopic applications, which was demonstrated by recording a strong CO₂ absorption with photo-acoustic spectroscopy.

References

1. P. Loza-Alvarez, C.T.A. Brown, D.T. Reid, W. Sibbett, M. Missey, *Opt. Lett.* **24**, 1523-1525 (1999)
2. M.A. Watson, M.V. O'Connor, P.S. Lloyd, D.P. Shepherd, D.C. Hanna, C.B.E. Gawith, L. Ming, P.G.R. Smith, O. Balachninaite, *Opt. Lett.* **27**, 2106-2108 (2002)
3. L.E. Myers and W.R. Bosenberg, *IEEE J. Quantum Electron.* **33**, 1663-1672 (1997)
4. P.E. Powers, T.J. Kulp, and S.E. Bisson, *Opt. Lett.* **23**, 159-161 (1998)
5. M. E. Klein, C.K. Laue, D.-H. Lee, K.-J. Boller, and R. Wallenstein, *Opt. Lett.* **25**, 490-492 (2000)
6. W. R. Bosenberg, A. Drobshoff, and J.I. Alexander, *Opt. Lett.* **21**, 1336-1338 (1996)
7. M.M.J.W. van Herpen, S. te Lintel Hekkert, S.E. Bisson, F.J.M. Harren, *Opt. Lett.* **27** 640-642 (2002)
8. M.M.J.W. van Herpen, S. Li, S.E. Bisson, S. te Lintel Hekkert, F.J.M. Harren, *Appl. Phys. B* **75**, 329 (2002)
9. D.D. Lowenthal, *IEEE J. Quantum Electron.* **34**, 1356-1366 (1998)
10. D.H. Jundt, *Optics Lett.* **22** 1553 (1997)

9

Wide pump tuning and high power of a continuous-wave single resonant optical parametric oscillator

Abstract

A new singly resonant, single-frequency optical parametric oscillator (OPO) has been developed for the 2.6-4.7 μm infrared wavelength region, using a high power (> 20 W), widely tunable (1024-1034 nm) Yb:YAG pump source. With the OPO frequency stabilized with an intracavity etalon, the OPO achieved an idler output power of 3 W at 2.954 μm . Tuning of the idler frequency was achieved by longitudinal mode-hop tuning of the pump source (FSR 100 MHz). In this way an idler frequency scan of 100-150 GHz could be obtained, after which the signal frequency hops ahead over the FSR of the intracavity etalon of the OPO (207 GHz). Due to un-optimized mirror coatings for the OPO cavity and PPLN crystal, the frequency stability was limited to 90 MHz over 1s, with an unaffected long-term frequency stability of 250 MHz over 200 seconds.

This work has been published in:

M.M.J.W. van Herpen, S. te Lintel Hekkert, S.E. Bisson, F.J.M. Harren, "Combined wide pump tuning and high power of a continuous-wave, singly resonant optical parametric oscillator", Submitted to Appl. Phys. B. (2003)

9.1 Introduction

In a typical Optical Parametric Oscillator (OPO) a fixed frequency or tunable pump source is used to convert one laser frequency into two new tunable frequencies, with the restriction that energy conservation and phase matching (momentum) conditions are fulfilled. The generated frequency with the highest energy per photon is termed the signal, while the other is termed the idler with their sum equaling the pump energy. Since the performance and design of the OPO depend heavily on the pump specifications, some of the most determining factors for an OPO are the specifications of the pump source and its power.

For low pump powers, a pump-enhanced [1-3], doubly resonant [4], or triply resonant [5] OPO cavity is a good choice since the nonlinear conversion process can be enhanced by resonating one or more of the waves. The advantage of such a setup is that the oscillation threshold is reduced significantly, allowing OPO operation at milliWatt power levels. The main disadvantage of such a design is that wide continuous tuning is limited, because not one, but two or three frequencies need to be kept in resonance with the OPO cavity during tuning. In addition low idler output power limits the field of applications for such a system.

The use of quasi-phase matched materials such as periodically poled lithium niobate (PPLN) coupled with higher power pump sources (multi-watt) allow the practical use of singly resonant OPOs (SROs) [6-12]. This is an important advantage in that wide continuous tuning is relatively easy, because the OPO cavity only needs to be resonant for a single wavelength. Bosenberg *et al.* [6,7] demonstrated the first PPLN based SRO, which yielded up to 3.6 Watt of cw idler radiation in the wavelength range of 3.3-3.9 μm . However, due to the linewidth of their pump source, the idler linewidth was approximately 2.2 GHz, which is too broad for many spectroscopic applications. Tuning with SROs can be achieved by (mode-hop) tuning the signal frequency [8,9], or by tuning the pump source while keeping the signal frequency fixed [10-12]. With pump-tuning, very wide tuning ranges can be achieved, because well developed tuning methods for the pump sources can be transferred to the generated idler frequency. A good example of this is a single-frequency SRO directly pumped by a tunable diode laser at 925 nm, with 56 GHz continuous pump-tuning for the idler wave [10,11]. This system had a relatively low output power of 200 mW and covered the 2.01-2.19 μm wavelength region, which is easier to operate on compared to the widely used 3 μm idler region. Recently, a single frequency SRO pumped by a Nd:YAG source yielded 24 GHz of pump-tuning at wavelengths between 3.0 and 3.8 μm with 2.2 Watts of idler output power (line width 3 MHz/s) [12,13]. Up to now, this was the highest idler output power and continuous tunability reported for a single frequency OPO in this wavelength range.

Using the same Nd:YAG source it was possible to extend the operation of cw, single-frequency PPLN based OPOs to longer wavelengths between 3.9-4.8 μm [14,15], where absorption by the PPLN crystal is significant. This was the first report of a widely tunable, single frequency laser source within this wavelength region. Due to the strong idler absorption for wavelengths longer than 3.9 μm , OPO operation beyond this point has been a problem [16]. The only other OPO operating up to 4.8 μm was shown by Myers and Bosenberg [17] in 1997, but that system used a multi-mode pump source (linewidth \sim 2.2 GHz) and was therefore not single frequency.

Here we demonstrate an SRO pumped by a high power ($>20\text{W}$) Yb:YAG pump source with wide quasi-continuous tunability (1024-1034 nm), which we have recently used in a pilot experiment for CO_2 detection [15]. Due to the high pump power, the OPO could be operated from 2.6 to $4.66\ \mu\text{m}$, far into the range where absorption of idler wave in the PPLN crystal is significant. An idler output power of 3.0 Watt was achieved at $2.954\ \mu\text{m}$ while using an intracavity etalon to hold the signal frequency constant over a range of 100-150 GHz. To our knowledge, this is the highest idler output power ever reported for an SRO operating in this wavelength region. Pump tuning was easy and even tuning the pump source by hand gave very good results. The effect of the wide pump tuning on the stability of the signal and idler frequencies was also studied.

9.2 Experimental setup

The basic OPO setup is similar to that described before [12] and is shown in Fig. 1.

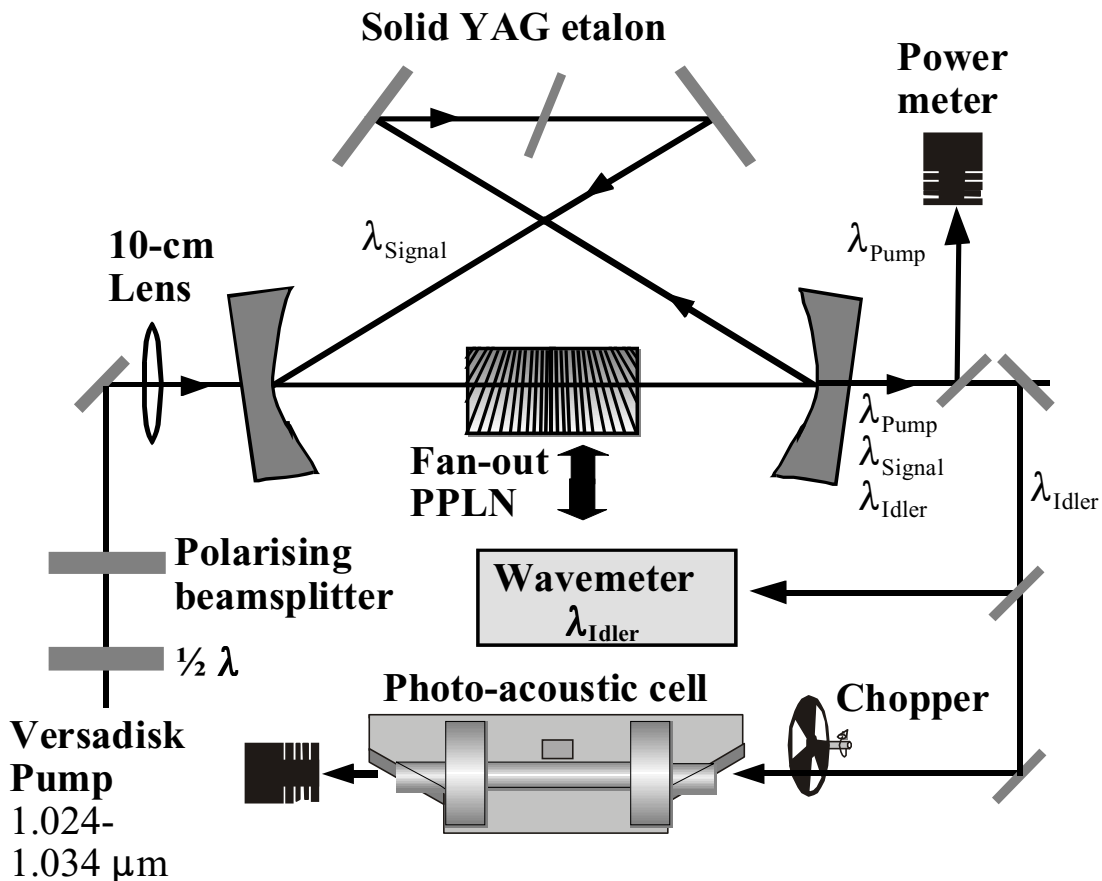


Fig. 1. Experimental setup of the OPO. The pump wavelength varies from 1024 to 1034 nm and the idler wavelength from 2.6 to $4.7\ \mu\text{m}$. A pump rejector mirror separates the pump light from the idler and signal beams, after which the idler beam is reflected towards the wavemeter and photo-acoustic cell. The signal wavelength can be measured with the same wavemeter by replacing the idler reflector with a signal reflector.

The pump source (Versadisk-1030-30-S, ELS, Gross-Zimmern, Germany) employs a diode-pumped 240 μm thick disk of Yb:YAG material inside an optical resonator, to generate up to 20 W of single-frequency output power in the range of 1024 – 1034 nm with excellent TEM₀₀ beam quality. An intracavity etalon is placed inside the optical resonator of the Yb:YAG laser to achieve single-frequency operation with a linewidth less than 5 MHz over 1 second. By combining the etalon with an intra-cavity Lyot filter the system can be tuned from 1020 to 1050 nm, but the system used here applied a different Lyot filter with tuning from 1024-1034 nm. An external chiller was used in a closed loop to cool the Yb:YAG disk with de-ionized water. Even though the output power of the pump laser could be regulated with the driving current, the pump laser was always operated at maximum output power, in order to keep a stabilized pump power. A combination with a half wave plate (New Focus, Santa Clara, CA, USA) and polarizing beam splitter (OFR, Caldwell, NJ, USA) was used to regulate the laser power delivered to the OPO.

The pump beam was focused into the PPLN crystal through the curved cavity mirror, with a 100mm focal length lens. The SRO cavity has a bowtie-ring cavity design that was resonant for the signal frequency. The cavity consisted of 2 flat and 2 curved mirrors (radius of curvature 100 mm), coated for maximum reflectivity at the signal wavelength and maximum transmission at the pump wavelength. The reflectivity at the idler wavelength was left as a free parameter and averaged around 10-20%. This configuration was used previously in our Nd:YAG pumped SRO [12,14] and hence the mirror coatings were not optimized for pump range of the Yb:YAG (1024–1034 nm). Two different sets of mirrors were used, specified in table 1, with the first set working at idler wavelengths between 3.0-3.8 μm [12] and the second set operating between 3.65-4.85 μm [14].

Table 1: Mirror specifications of both mirror sets used.

	Set 1	Set 2
Idler	T>80% at 3.0-3.8 μm	T \geq 85% at 3.65-4.85 μm
Signal	R>99.9% at 1.5-1.7 μm	R \geq 99.8% at 1.35-1.5 μm
Pump	T>90% and R<0.25% at 1064 nm	T>90% at 1064 nm

Table 2: Specifications for the anti-reflection coatings of the PPLN crystals.

AR coating	Crystal 1	Crystal 2
Idler	3.0-3.8 μm	3.0-4.85 μm
Signal	1.5-1.7 μm	1.4-1.5 μm
Pump	1.064 μm	1.064 μm

The input and output faces of the PPLN crystals were anti-reflection coated for the pump, signal and idler frequencies (see table 2). As with the cavity mirrors, the PPLN crystal AR coatings were designed for use at 1064 nm, but they should be able to have sufficient anti-reflection properties at 1024–1034 nm. To prevent photo-refractive damage, crystals were operated at 180–190°C with a commercially available oven (Super Optronics, Gardena, CA, USA), where they were temperature stabilized to 0.1 °C.

While the OPO tended to operate in a single longitudinal mode (SLM) in the resonated signal wave, SLM operation was enhanced by means of an intracavity, plane parallel (<10 arc seconds) 400- μm thick uncoated YAG etalon (reflectivity 8%, FSR 207 GHz). Combined with the single frequency pump source, this resulted in a single frequency idler beam with tuning characteristics similar to the pump laser. The intracavity etalon could be rotated to mode-hop-tune the OPO [8,9], but due to the wide tunability of the pump source this was not necessary.

9.3 Output power

Since the OPO was intended to serve as a broadly tunable, high power mid-IR source for an ultra-sensitive photo acoustic spectrometer, it was important to achieve the highest possible idler power. We investigated the OPO performance with both mirror sets throughout the tuning range of the OPO. For mirror set 1 and PPLN crystal 1 (periods ranging from 28.5 – 29.9 μm) we achieved an idler output power of 3 W with a pump power of 18 Watts (measured behind the OPO cavity with OPO operation blocked). Figure 2 shows the OPO idler output power versus pump power for a PPLN period of 29.3 μm . For a PPLN crystal temperature of 189.5 °C, this resulted in signal and idler frequencies of 1584 nm and 2954 nm, respectively. For frequency stability, the OPO was operated with the intracavity YAG etalon, which increased the oscillation threshold to 8 Watts. However, this caused almost no loss of output power at full pump power levels. More important was the loss of performance due to the non-optimized pump coatings on the input mirror and PPLN crystal. Pump reflectivity losses at the output face of the PPLN crystal and output mirror are less important as they do not effect the power reaching the PPLN crystal. For these optics, the pump power that was available at the PPLN crystal was reduced by about 15%. Since the OPO was operated substantially above threshold, we estimate that for optimized coatings the idler output power would have increased to 3.5 Watts.

With 18 W pump power reaching the exit of the OPO cavity an idler output of 3.0 Watts was achieved with a pump depletion of 67%. The high threshold and low pump depletion again can be attributed to the non-optimized coatings. Despite this, the 3.0 W idler output power of this system is the highest output power ever reported for a cw single-frequency PPLN OPO at this wavelength. Using proper coating for the optics, this can be easily improved in future.

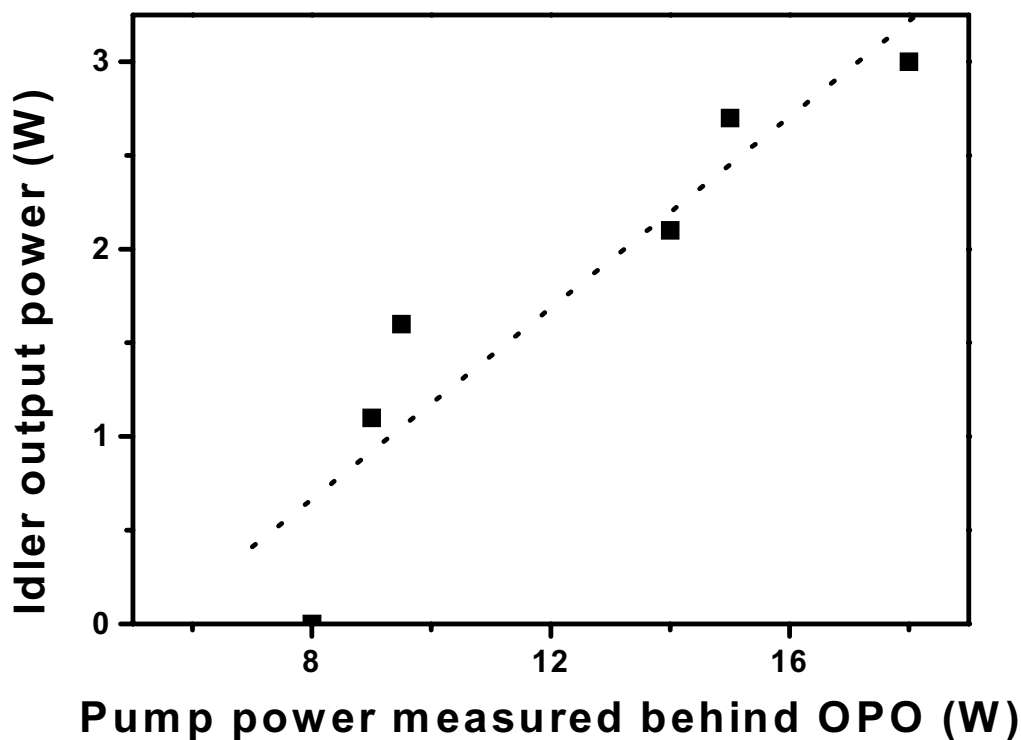


Fig. 2. The measured idler output power versus pump power at 2954 nm wavelength shows a maximum output power of 3.0 W with 18 W pump power. The pump power was measured directly behind the OPO cavity with OPO operation blocked.

9.4 Tunability

The Yb:YAG pump source can be frequency tuned with the intracavity etalon or with an intracavity Lyot filter. By tuning the intracavity etalon (FSR 25 GHz) the Yb:YAG laser showed quasi-continuous mode-hop tuning over its cavity modes (FSR 100 MHz). For scans longer than 25 GHz, the Lyot filter could be used to tune the laser over its entire range (1024-1034 nm) via 25 GHz mode hops from the intracavity etalon. The effect of Lyot filter tuning on the signal and idler frequencies was studied by monitoring these frequencies with a wavemeter (Burleigh WA1000 IR, NY, USA) while tuning the Lyot filter manually with a fine pitch adjustment screw. The effect of tuning on the signal frequency is shown in figure 3.

The figure compares the measured signal frequencies with the frequencies calculated with the Sellmeier equations of Jundt [18]. Due to the intra-cavity etalon of the OPO the signal frequency initially doesn't change when the pump wavelength is tuned up. However, after about 100-150 GHz of pump-tuning, the difference between the calculated and the measured signal frequency is greater than the free spectral range of the intra-cavity etalon (207 GHz). At that point, a mode-hop occurs in the OPO cavity, which can be observed as a 207 GHz mode-hop in the signal frequency. This effect is important for the generated idler frequencies, as is shown in figure 4.

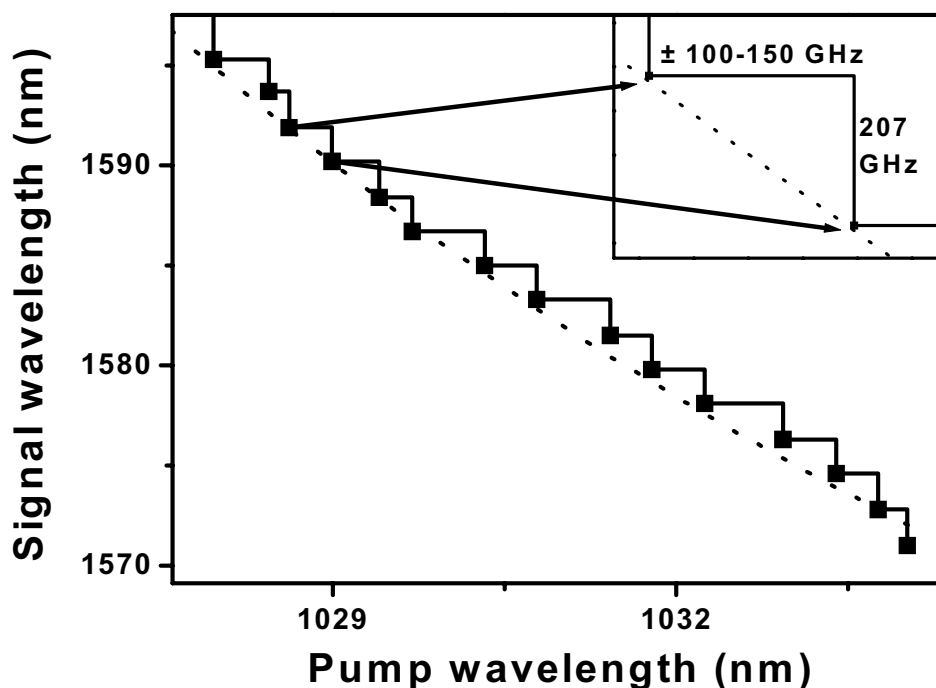


Fig. 3. Measured signal wavelengths when tuning the pump laser with the Lyot filter. The dotted line shows the signal frequencies calculated with the Sellmeier equations of Jundt [18]. The OPO cavity keeps resonating at a stable signal frequency, but makes a mode-hop when the difference between the calculated frequency and the actual frequency becomes greater than the free spectral range of the intra-cavity etalon of the OPO (207 GHz, 400 μm solid YAG). This occurs after about 100-150 GHz of pump-tuning.

When the pump frequency was tuned and the signal frequency remained fixed, the idler frequency could be mode-hop tuned with steps of 25 GHz, caused by the intracavity etalon within the pump laser. The signal frequency makes 207 GHz mode-hops after about 100-150 GHz of tuning in the pump and idler frequencies. When the signal frequency makes its mode-hop, the idler wavelength hops back over 207 GHz. This is a problem, because the direction of the idler mode-hop is in the same direction as the idler tuning, which means that not all idler frequencies are covered within the scan (see also fig. 4). To compensate for this, the etalon within the OPO cavity can be tuned. Alternatively, the temperature of the crystal can be increased or decreased in order to prevent the signal frequency from mode hopping.

By tuning the intra-cavity etalon of the pump laser, quasi-continuous mode-hop tuning can be achieved over its free spectral range of 25 GHz. Very wide scans can be made when this is combined with tuning of the Lyot filter. This was demonstrated by recording a 190 GHz wide absorption spectrum of a mixture of 20-ppm ethane in nitrogen with photo acoustic spectroscopy [19,20]. The photo acoustic cell was the same as described earlier [21] and has an open-ended cylindrical acoustic resonator (length 300 mm, radius 2 mm) excited in its first acoustical

longitudinal mode at a resonance frequency of 560 Hz. The photo acoustic signal was detected by 3 Knowles IK3024 electret microphones and amplified with a lock-in amplifier.

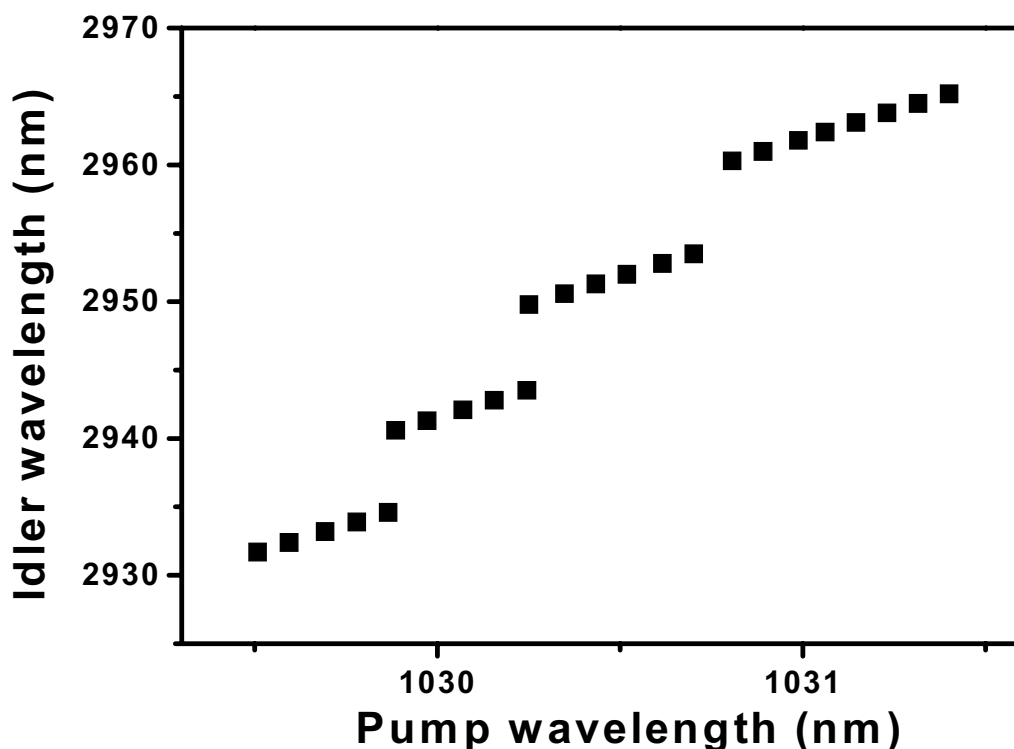


Fig. 4. Measured idler wavelength while tuning the pump laser. The pump frequency makes mode-hops over the free spectral range of the intracavity etalon within the pump source (25 GHz), which are visible as 25 GHz hops in the idler wavelength. After about 100-150 GHz of idler tuning a mode-hop occurs in the signal frequency, which is visible as a 207 GHz mode-hop to a longer idler frequency.

Tuning of the idler frequency was performed by hand, using one fine pitch adjustment screw on the Lyot filter and one on the intra-cavity etalon of the pump laser. Tuning was accomplished in two steps. First, the pump intracavity etalon was used to tune the idler frequency over 25 GHz with 100 MHz mode hops in the pump laser. Then the Lyot filter was tuned slightly in order to induce an intracavity pump-etalon mode-hop of 25 GHz, after which the pump-etalon could be tuned again. This process was repeated several times in order to cover a 190 GHz region containing several absorption lines of ethane (figure 5). This shows two strong absorption peaks in the recorded ethane spectrum, which agrees very well with an ethane spectrum measured previously with an FTIR spectrometer [22].

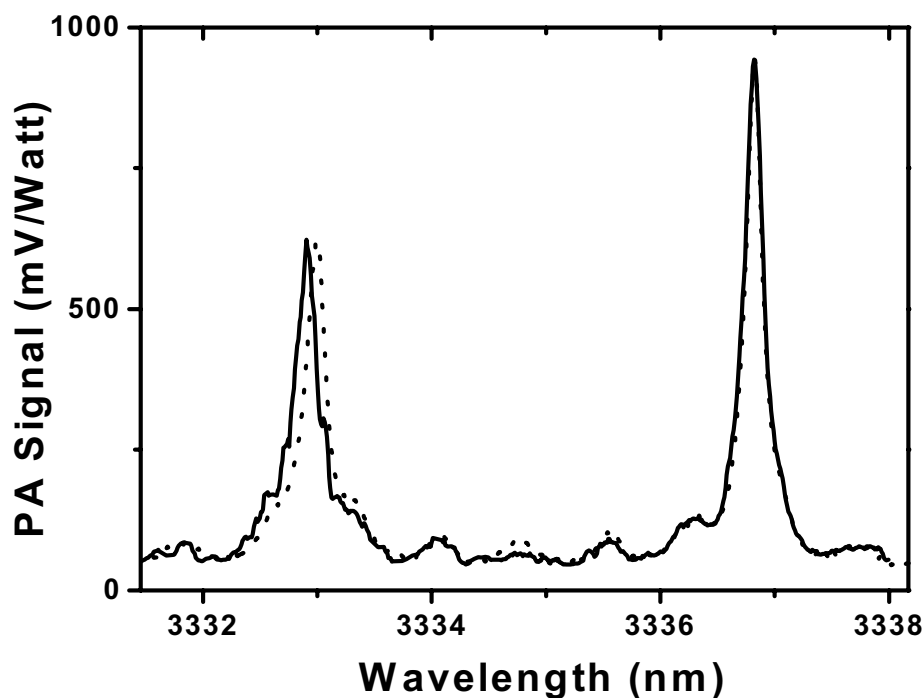


Fig. 5. A mode-hop scan could be made by manually tuning the pump laser. This is demonstrated by an absorption spectrum of a mixture of 20 parts per million of ethane in nitrogen, recorded with photoacoustic spectroscopy. The absorption peak at shorter wavelengths was recorded by quickly tuning the pump laser, whereas the other peak was recorded with more careful tuning. The dotted line shows the ethane absorption spectrum as it was measured with an FTIR spectrometer [22].

The peak to the left was recorded by relatively fast tuning of the pump laser, whereas the peak to the right was recorded when tuning the pump laser more carefully. In the future, a stepper motor could be used to make tuning easier and more controllable resulting in a much higher quality of the recorded spectrum than the current hand-tuned result. However, the manual tuning demonstrates the simplicity by which the pump laser and the OPO can be tuned. The strongest recorded ethane absorption line (fig. 5) has a maximum strength of 950 mV/Watt, which is in agreement with previously reported results using a continuously-tunable Nd:YAG pumped OPO [21]. In that report an ethane detection limit of 0.01 ppb was achieved with 1.2 W of power, whereas this system has an output power of 2.15 Watt at the same idler frequency. This means that this OPO system has the potential to improve the ethane detection limit by a factor of two, because the photo acoustic signal scales linearly with the applied laser power.

9.5 Frequency stability

For the current setup unwanted etalon and resonance effects are expected, as the coatings of the cavity mirrors and PPLN crystals are not optimized for the current combination of pump, signal and idler frequencies. In order to ensure singly resonant operation of the OPO it is important to suppress residual reflectivity of the mirrors at the pump and idler frequencies, otherwise the OPO

can become slightly doubly resonant [9,23]. Similarly, the AR coatings on the PPLN crystal must be of good quality otherwise etalon effects will be observed. In the present case this is mitigated through the use of an angled cut of 1° on the PPLN crystal face. Both of these effects (double resonance and etaloning) can have adverse effects on the frequency stability and tuning of the OPO [23]. As shown, pump tuning of the idler frequency was not affected significantly. The wavelength stability and high-resolution performance of the OPO were examined using a photo-acoustic recording of a low-pressure (77 milliBar) absorption line of the same 20-ppm ethane mixture that was used for the tuning experiments. The strongest peak of figure 5 at 2996.9 cm^{-1} was used for this experiment. The laser emission was placed at the half maximum of this absorption line in order to estimate the frequency stability of the idler wavelength by the change of the photo acoustic signal over time [13].

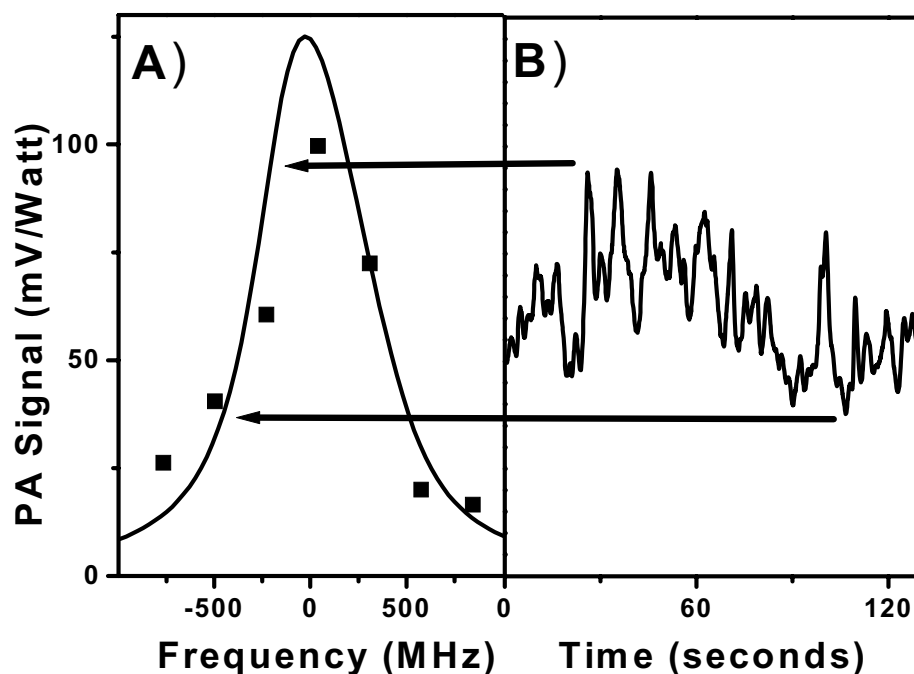


Fig. 6. The high resolution performance and the wavelength stability of the OPO are demonstrated by recording the photoacoustic signal from the half maximum of a 77 mBar pressure broadened absorption line of 20 ppm of ethane in nitrogen at 2996.9 cm^{-1} . When not tuning the pump frequency, the photoacoustic signal shows random oscillations at a rather high frequency (90 MHz/s), combined with an oscillation at a lower frequency (250 MHz in 200s).

Fig. 6a shows a fairly good overlap between the recorded photo acoustic spectrum and the calculated absorption line with 670 MHz full width at half maximum. When tuning the intra-cavity etalon of the pump laser, the output frequency was mode-hop tuning over the free spectral range of the pump laser cavity (100 MHz). Fortunately, the mode-hops were small enough to be able to record an absorption at this low pressure. However, a continuously tunable laser source

would achieve a much better resolution and would therefore be more suited to measure such an absorption.

The frequency stability of the system is shown in figure 6b, which shows the recorded photo-acoustic signal with all tuning elements stationary. The signal shows many random power oscillations at high frequencies, combined with an oscillation at a lower frequency. These oscillations are caused by detuning of the idler frequency, resulting in a different photo acoustic signal. The slow oscillations have been identified before as originating from oscillations in the temperature of the PPLN crystal [13]. In 200 seconds the slow oscillations caused an idler frequency drift of 250 MHz, which is similar to the stability of a Nd:YAG pumped OPO [13]. However, the fast frequency drift has not been observed with that OPO system, but here this can be as high as 90 MHz per second. It is likely that the not-optimized coatings of the optics used in this setup cause these oscillations through resonance and etaloning effects. In this case the mirror transmission was about 15% for the pump light. The idler frequency was well within the specified range of the anti-reflection coatings, with the signal frequency at the edge of these coatings at 1.5 μm . Another explanation for the bad short-term frequency stability could be the fact that the OPO cavity was not covered with a box, so air currents could have caused instabilities. If this is solved with properly optimized coatings and a cover around the cavity, the OPO frequency stability can be below 3 MHz/s [13], limiting the idler stability to the frequency stability of the pump source (less than 5 MHz in 1 second).

9.6 OPO operation between 4 and 5 μm

As there are many species of interest that absorb at wavelengths longer than 4.0 μm , there is considerable interest in extending OPO operation beyond 4.0 μm . Continuous wave OPO operation beyond 3.9 μm has proved difficult in lithium niobate as intrinsic absorption becomes significant at longer wavelengths [14,16,17]. However, there is considerable interest in PPLN OPOs operating above this wavelength, as there are currently no powerful, widely tunable, single-frequency laser sources available in this range. Recently, the first single-frequency OPO operating in this range was presented [14]. This was a Nd:YAG (1064 nm) pumped SRO, operating at idler wavelengths between 3.9 and 4.7 μm . Here, we extend operation of this OPO using the same optics that were used for the previous OPO demonstration but with a tunable Yb:YAG pump laser.

Using the wide pump-tuning range combined with the 8 poling periods of the PPLN crystal, an idler wavelength range between 3.3 and 4.6 μm could be achieved. This means that the OPO can be aligned with the default procedure at 3.3 μm , after which the crystal can be tuned to generate wavelengths above 3.9 μm . Figure 7 shows the output power of the system with a pump power of 11.5 W (measured behind the OPO cavity with OPO operation blocked), which is the same output power used with the Nd:YAG pumped system [14].

As expected, the output power drops quickly for idler wavelengths longer than 3.9 μm . At 3.8 μm the output power (without the intra-cavity etalon) was 1.5 W, which dropped to 90 mW at 4.66 μm . From 3.8 to 4.66 μm the oscillation threshold and pump depletion went from 3.5 W to 7.5 W and from 65% to 17%, respectively. This is similar to the previous results with the

Nd:YAG pump source, but since this system can be pumped with much more power than 11.5 W, the maximum output power can be much higher. With full pump power this system was able to produce 200 mW of output power at 4.235 μm (2361.47 cm^{-1}), where the strongest absorption line of gaseous CO_2 is located. This is an order of magnitude higher than the Nd:YAG pumped OPO system [15]. In a pilot experiment we have shown that this system can potentially be used to monitor the CO_2 release of single plant cells [15].

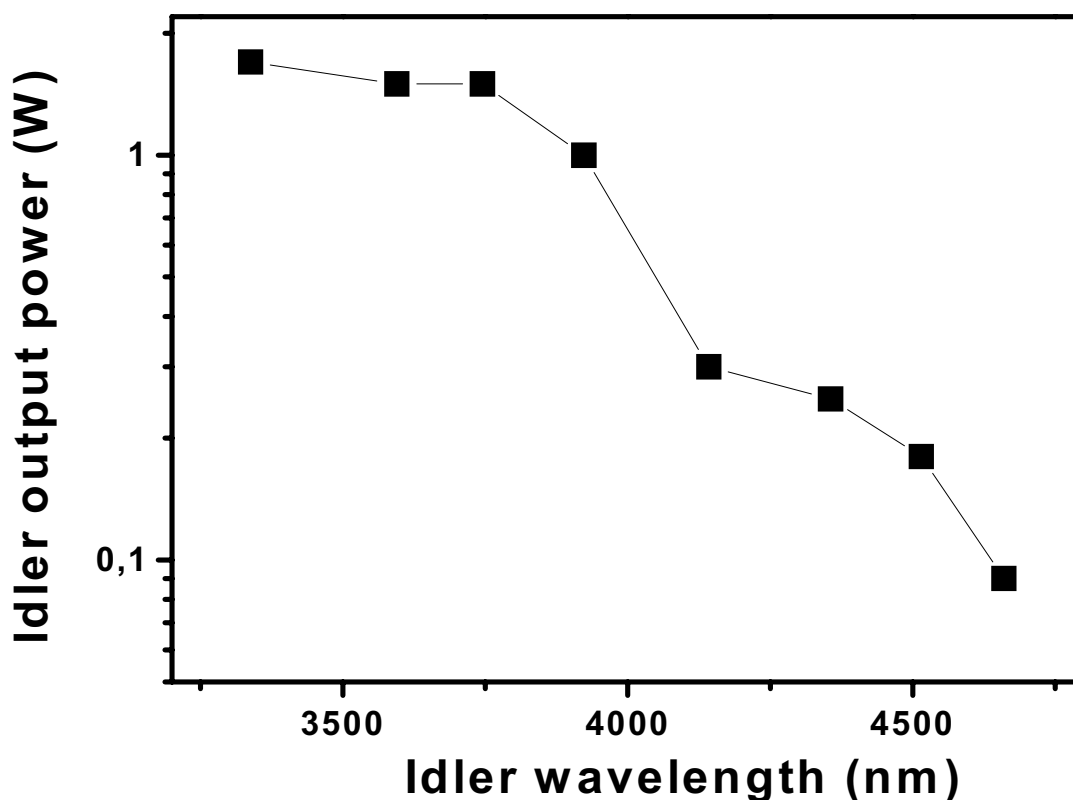


Fig. 7. OPO idler tuning with a multi-grating crystal beyond the 3.9 μm transparency edge of PPLN, using 11.5 Watt of pump power. The output power drops significantly with decreasing PPLN transparency.

9.7 Conclusion

The Yb:YAG Versadisk laser has proved to be very well suited as pump source for a widely tunable OPO at idler wavelength between 3 and 5 μm . One advantage of the Versadisk is its high output power, resulting in a high idler output power for the OPO. In addition, the wide tunability of the pump laser can be used to tune the OPO with little effort with steps of 100 MHz. Tuning of the pump source is easy, and even with manual tuning very accurate and detailed

spectra can be recorded. When tuning the pump source, the OPO intra-cavity etalon or the PPLN temperature needs to be adjusted to prevent or compensate for mode-hops in the signal frequency. A possible drawback of the system is that the ability to tune the pump source means that a wavemeter or spectrum analyzer is required in order to measure the pump or idler wavelengths. With a fixed-frequency pump source, a rough indication of the idler frequency can be derived from the PPLN period and its temperature [14]. The performance of the OPO setup was limited due to un-optimized coatings on the cavity mirrors and PPLN crystal, which were designed for use with a 1064 nm pump source. This caused instabilities in the generated idler frequency of 90 MHz/s. The stability of the idler frequency was 250 MHz over 200s, caused primarily by fluctuations in

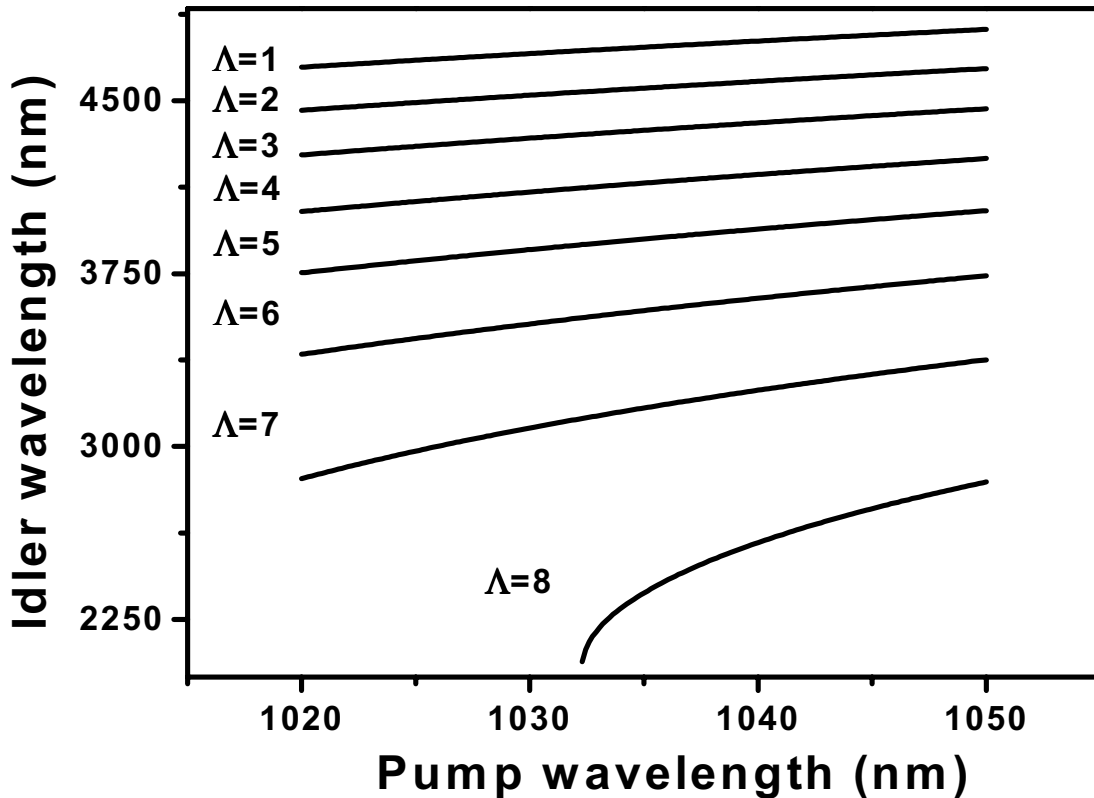


Fig. 8. By choosing the right values of the 8 PPLN poling periods it is possible to cover the total idler range from 2.5 to 5 μm with a single crystal. This is possible due to the wide pump tuning range of the pump source. The periods used in this example are: 25.5, 25.9, 26.4, 27.0, 27.6, 28.3, 29.1 and 30.0 μm .

the temperature of the PPLN crystal. Despite the use of un-optimized coatings, an output power of 3 W was achieved at 2954 nm idler wavelength. The system also operated at wavelengths between 3.9 and 4.66 μm , where crystal absorption at the idler wavelengths makes OPO operation difficult. Due to its wide tunability, the system could potentially cover the full idler wavelength region from 2.5 to 5 μm with just one single multi-period PPLN crystal, using the right choice of PPLN periods (figure 8).

References

1. F. Kühnemann, K. Scheider, A. Hecker, A.A.E. Martis, W. Urban, S. Schiller, J. Mlynek, "Photoacoustic trace-gas detection using a cw single-frequency parametric oscillator", *Appl. Phys. B* **66**, 741-745 (1998)
2. A. Popp, F. Muller, F. Kühnemann, S. Schiller, G. von Basum, H. Dahnke, P. Hering, M. Murtz, "Ultra-sensitive mid-infrared cavity leak-out spectroscopy using a cw optical parametric oscillator", *Appl. Phys. B* **75**, 751-754 (2002)
3. O.B. Jensen, T. Skettrup, O.B. Petersen, M.B. Larsen, "Diode-pumped intracavity optical parametric oscillator in pulsed and continuous-wave operation", *J. Opt. A* **4** (2): 190-193 2002
4. A.J. Henderson, P.M. Roper, L.A. Borschowa, and R.D. Mead, "Stable, continuously tunable operation of a diode-pumped doubly resonant optical parametric oscillator", *Opt. Lett.* **25**, 1264-1266 (2000).
5. K.S. Zhang, T. Coudreau, M. Martinelli, A. Maître, C. Fabre, "Generation of bright squeezed light at 1.06 μm using cascaded nonlinearities in a triply resonant cw periodically-poled lithium niobate optical parametric oscillator", *Phys. Rev. A* **64**, 033815 (2001)
6. W. R. Bosenberg, A. Drobshoff, J.I. Alexander, L.E. Myers and R.L. Byer, "Continuous-wave, singly resonant optical parametric oscillator based on periodically poled LiNbO_3 ", *Opt. Lett.* **21**, 713-715 (1996)
7. W. R. Bosenberg, A. Drobshoff, J.I. Alexander, L.E. Myers and R.L. Byer, "93% pump depletion, 3.5-W continuous-wave, singly resonant optical parametric oscillator", *Opt. Lett.* **21**, 1336-1338 (1996)
8. P.E. Powers, T.J. Kulp, and S.E. Bisson, "Continuous tuning of a continuous-wave periodically poled lithium niobate optical parametric oscillator by use of a fan-out grating design", *Opt. Lett.* **23**, 159-161 (1998).
9. S.E. Bisson, K.M. Armstrong, T.J. Kulp, M. Hartings, "Broadly tunable, mode-hop-tuned cw optical parametric oscillator based on periodically poled lithium niobate", *Appl. Opt.* **40**, 6049-6055 (2001)
10. M.E. Klein, D.-H. Lee, J.-P. Meyn, K.-J. Boller, and R. Wallenstein, "Singly resonant continuous-wave optical parametric oscillator pumped by a diode laser", *Opt. Lett.* **24**, 1142-1144 (1999).
11. M. E. Klein, C.K. Laue, D.-H. Lee, K.-J. Boller, and R. Wallenstein, "Diode-pumped singly resonant continuous-wave optical parametric oscillator with wide continuous tuning of the near-infrared idler wave", *Opt. Lett.* **25**, 490-492 (2000).
12. M.M.J.W. van Herpen, S. te Lintel Hekkert, S.E. Bisson, F.J.M. Harren, "Wide single mode tuning of a 3.0-3.8 micron, 700 mW, continuous wave Nd:YAG-pumped optical parametric oscillator based on periodically poled lithium niobate", *Opt. Lett.* **27**, issue 8, (2002)
13. M.M.J.W. van Herpen, S. Li, S.E. Bisson, S. te Lintel Hekkert, F.J.M. Harren, "Tuning and stability of a continuous-wave mid-infrared high-power single resonant optical parametric oscillator.", *Appl. Phys. B* **75**, 329 (2002)
14. M.M.J.W. van Herpen, S.E. Bisson, F.J.M. Harren, "Continuous-wave operation of single frequency optical parametric oscillator between 4-5 μm based on periodically poled LiNbO_3 ", *Opt. Lett.* **28**, 2497-2499 (2003)

15. M.M.J.W. van Herpen, A.K.Y. Ngai, S.E. Bisson, J.H.P. Hackstein, E.J. Woltering, F.J.M. Harren, "Real-time monitoring of the respiration of small insects and single cells with laser based CO₂ detection", submitted to *Appl. Phys. Lett.* (2003)
16. D.D. Lowenthal, "CW Periodically Poled LiNbO₃ Optical Parametric Oscillator Model with Strong Idler Absorption", *IEEE J. Quantum Electron.* **34**, 1356-1366 (1998)
17. L.E. Myers, W.R. Bosenberg, "Periodically Poled Lithium Niobate and Quasi-Phase-Matched Optical Parametric Oscillators", *IEEE J. Quantum Electron.* **33**, 1663-1672 (1997)
18. D.H. Jundt, "Temperature-dependent Sellmeier equation for the index of refraction, $n(e)$, in congruent lithium niobate", *Optics Lett.* **22** 1553 (1997)
19. F.J.M. Harren, G. Cotti, J. Oomens, S. te Lintel Hekkert, "Photoacoustic spectroscopy in trace gas monitoring" in *Encyclopedia of Analytical Chemistry*, (Ed.) R.A. Meyers (John Wiley Ltd, Chichester, 2000), 2203-2226.
20. M.W. Sigrist, "Trace gas monitoring by laser photoacoustic spectroscopy and related techniques (plenary)", *Rev. Sci. Instr.* **74**, 486-490 (2003)
21. M.M.J.W. van Herpen, S. Li, S.E. Bisson, F.J.M. Harren, "Photoacoustic trace gas detection of ethane using a continuously tunable, continuous-wave optical parametric oscillator based on periodically poled lithium niobate", *Appl. Phys. Lett.* **81**, 1157-1159 (2002)
22. A. Popp, H. Dahnke, F. Kühnemann, J. Orphal, G. Basum, J.P. Burrows: unpublished work report, Institut für Angewandte Physik (Bonn) and Institut für Umweltphysik (Bremen) (1999)
23. S.T. Yang, R.C. Eckardt, R.L. Byer, "Power and spectral characteristics of continuous-wave parametric oscillators – the doubly to singly resonant transition", *J. Opt. Soc. B* **10**, 1684-1695 (1993)

10

Real-time monitoring of the respiration of small insects and single cells with laser based CO₂ detection

Abstract

We have built a new laser system for detecting ultra-low concentrations of gasses. The laser is unique, because it works in an infrared spectral range where no laser existed that was suitable for ultra-sensitive experiments. CO₂ is one of many new gasses that can be detected now. We are able to detect CO₂ levels below one part in a billion and we demonstrate this by measuring the CO₂ gas exhaled by a single ant or fruit fly. The sensitivity appears to be good enough to track the respiration of single plant cells and opens up many possibilities in physics, biochemistry, life science and nano-technology.

This work has been published in:

M.M.J.W. van Herpen, A.K.Y. Ngai, S.E. Bisson, J.H.P. Hackstein, E.J. Woltering, F.J.M. Harren, "Real-time monitoring of the respiration of small insects and single cells with laser based CO₂ detection", submitted to Appl. Phys. Lett. (2003)

10.1 Introduction

In the life sciences there is considerable interest in the detection of minute quantities of trace gasses like CO₂ released by various biological sources. Trace gas detectors based on infrared (laser) spectroscopy are a good option for this, especially when fast, on-line time resolution is needed. Up to now, the technique has been limited by the availability of suitable laser sources for the wavelength range with the strongest absorptions of gasses. For CO₂ this is near 4.234 μm in the infrared wavelength region. Here, we present a new optical parametric oscillator generating high-power, continuously tunable laser radiation (between 3.9 and 4.8 μm) in continuous-wave, single mode operation. As a CO₂ detector, this system is able to detect concentrations as low as 0.7 parts per billion. This was demonstrated by monitoring the respiration of a 3.7 mg ant (*Lasius niger*) and a single *Drosophila* fly. The system can be used to monitor the metabolic pathway of a single cell, on-line. Moreover, it has the potential to detect many other gasses and has, therefore, many other potential fields of use.

To understand the metabolism of living samples, it is useful to analyze the temporal emission of CO₂. However, collecting information from small biological samples is limited by the sensitivity of CO₂ detection. Currently the most sensitive on-line CO₂ detectors use direct absorption spectroscopy, employing a broadband infrared light source with an optical filter near 4.2 μm , where the strongest CO₂ absorptions are found. The most sensitive commercial detector that uses this method (Licor LI-7000) has a CO₂ detection limit of 86 part per billion (ppb) with a 2s integration time. Here we show that the sensitivity for the detection of CO₂ can be increased by two orders of magnitude, using a laser source instead of a broadband light source. Until recently, no suitable cw laser source with the required tunability and power has been available in this spectral range.

The generation of mid-infrared radiation with Optical Parametric Oscillators (OPOs) is perhaps the most promising method, because it can generate mid-infrared radiation with wide tunability, high power, excellent stability and narrow linewidth¹⁻⁶. Using a nonlinear crystal, in this case Periodically Poled Lithium Niobate (PPLN), a pump photon can be converted into two new tunable photons of lower frequency (termed signal and idler) which sum to that of the pump. The optical transmission window of the PPLN crystal limits the operational range of the OPO to wavelengths shorter than 3.9 μm ⁶. At longer wavelengths the transparency of Lithium Niobate decreases which severely limits the generation of radiation^{3, 7}. For pulsed operation, it has been shown that OPO operation is possible at idler wavelengths up to 7.3 μm despite the absorption loss in the PPLN crystal^{8,9}. However, for highly sensitive detection, pulsed lasers are not well suited due to their pulse-to-pulse fluctuations. Furthermore, for high resolution spectroscopy cw excitation is usually preferred over pulsed excitation for two reasons: the ability to use extremely narrow band detection (<10 MHz) and the use of lower power avoids the problem of saturating the absorption.

In continuous-wave (cw) operation, OPO generation of idler wavelengths above 3.9 μm has continued to be a problem. In 1997 Myers and Bosenberg² demonstrated that cw OPO operation is possible between 3.6 and 4.7 μm with very high pump powers, but their design was not suited for highly sensitive, spectroscopic applications due to multi-mode operation. For many

spectroscopic applications, the OPO must have a narrow linewidth (<10 MHz), good stability and broad tunability. Up to now, probably due to a lack of suitable pump sources, no further successful attempt has been made to develop such an OPO operating with long idler wavelengths.

10.2 Experiment

Our experimental setup is similar to the setup described elsewhere^{5,6}, however, the mirror and PPLN coatings have been adjusted to the new wavelengths and a different PPLN crystal was used with poling periods ranging from 25.9 to 28.7 μm . The pump beam, which was generated by an 11W cw Nd:YAG source (Lightwave M6000) operating at 1064nm, was converted into a tunable signal (1370-1510 nm) and idler beam (3620-4760 nm). Because the pump beam was single mode (single frequency) and the signal wave was constrained to a single frequency by an intra-cavity etalon, the idler frequency was therefore constrained to a single frequency which was determined by energy conservation between the pump and signal frequencies. For short frequency scans, the pump frequency was tuned over 24 GHz, which correspondingly tuned the idler wave over 24GHz but in the opposite direction⁵. Pump tuning of the idler wave is an important advantage for mid-IR spectroscopic applications since the tuning is performed external to the OPO and allows the use of sources for which tuning methods are well developed. This is an important feature for high-resolution mid-IR spectroscopy and for performing highly sensitive trace gas detection in the presence of other gasses¹⁰.

For wavelengths longer than 3.9 μm , the absorption in the PPLN crystal becomes significant, causing a reduction in the idler output power. However, due to the high pump power, the OPO can be operated from 3.62 μm (1.2 W output power) to 4.76 μm (120 mW). The decrease in output power with increasing idler wavelength is a direct reflection of the increased absorption in the PPLN crystal as a function of wavelength. The strongest CO₂ absorption is located at 4.235 μm (2361.47 cm^{-1}), which is well within the operating range of our OPO. At this wavelength, the OPO generates 110 mW of power, but when the intra-cavity etalon was inserted into the OPO cavity the output was further reduced to 30mW. To minimize additional loss of power due to absorption of ambient CO₂, the setup was placed in a closed box and flushed with nitrogen gas. In this way, the loss of power at the peak of the CO₂ absorption was limited to 30%, so 20 mW remains for the detection of CO₂.

10.3 Detection limit of CO₂

In order to determine the CO₂ detection limit, the absorption signal of a mixture of 7 parts per million (ppm) CO₂ in nitrogen, was measured with photoacoustic spectroscopy¹¹ and compared to the electronic noise of the system. With a 300 ms integration time, the detection limit (signal-to-noise ratio = SNR = 1) was 88 ppb, which was an order of magnitude higher than expected. This was caused by the slow release of vibrational energy from the excited CO₂ molecules, caused by the combination of a small energy difference between CO₂ and N₂ levels, the high abundance of N₂ in air, and the slow vibrational relaxation time of N₂ (~msec)¹². This in combination with a 560 Hz modulation frequency of the light beam results in a smaller signal. This problem can be

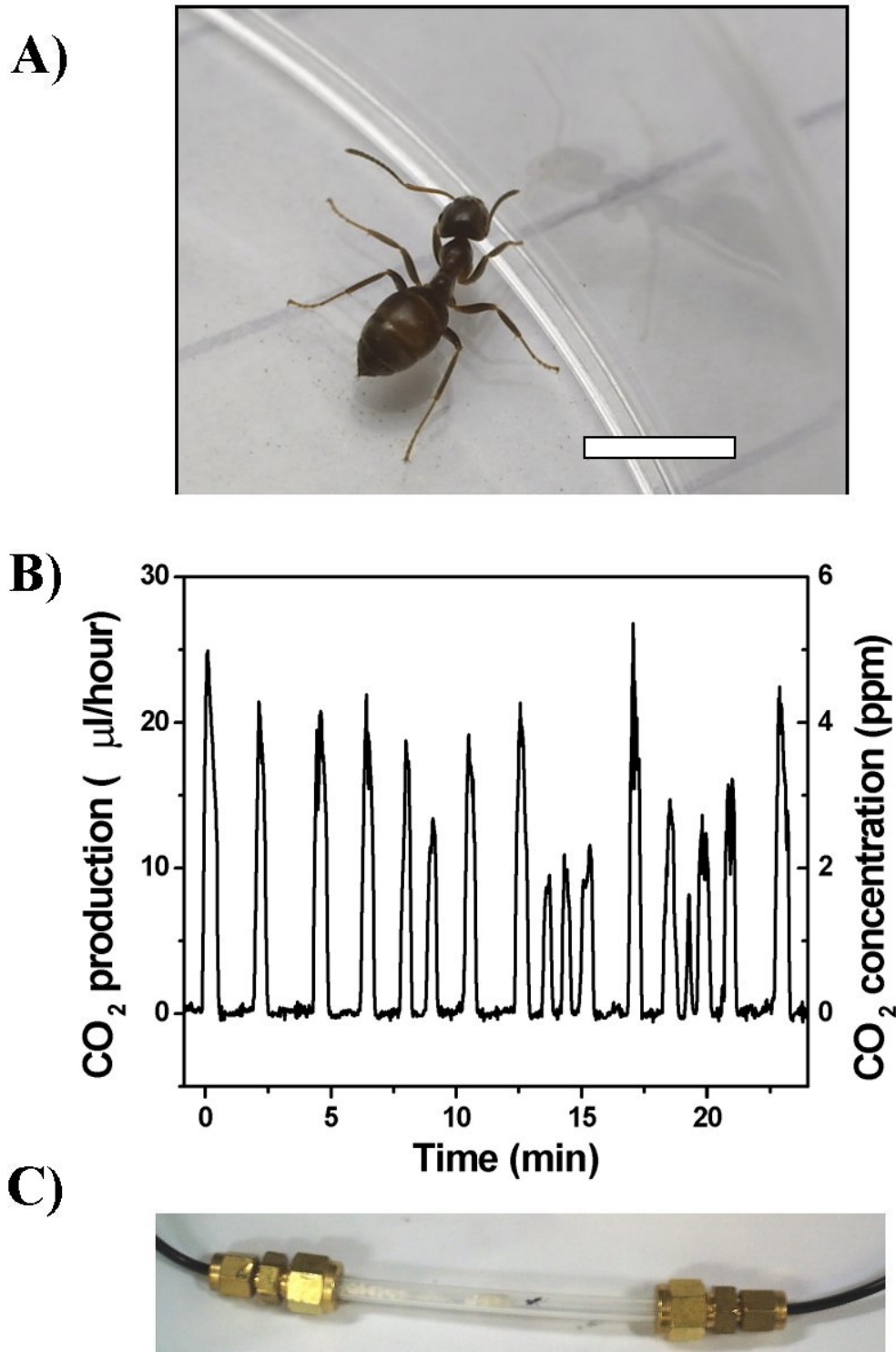


Fig. 1. Real-time CO₂ emission of a small ant (*Lasius niger*). **a**, picture of the ant used in this experiment. The white bar indicates a length of 3 mm. **b**, The respiration analysis of the ant shows periodic peaks of CO₂, which repeat on average once every 1.5 minutes. **c**, During the experiment the ant lives inside a small tube (diameter 4.5 mm) through which air is flowed.

mitigated however by adding a rapidly relaxing gas that couples through vibrational energy transfer to the excited N₂ molecules. For this purpose, 4% of SF₆ gas¹² was added to the gas, which significantly increased the signal strength, and lowered the CO₂ detection limit from 88ppb to 7 ppb with a 300 ms integration time.

10.4 Monitoring insect breath

To demonstrate the feasibility of the system for real-time detection of trace amounts of CO₂, we examined the gas released by the respiration of a small ant (*Lasius niger*) of weight 3.7 mg (Fig. 1a). The ant was placed in a 2 cm long tube with 4.5 mm internal diameter (Fig. 1c). Air was passed through two scrubbers in order to remove water vapor and CO₂, before it passed the ant and was sent through the photoacoustic cell (flow rate 5 l/h). For this experiment no SF₆ was added.

Fig. 1b shows that the ant periodically releases CO₂ over a time span of several minutes. Between the peaks, which reach maxima between 10 and 25 μ l/hour, a constant zero baseline could be measured. Similar measurements have been performed earlier with a decapitated and motionless *Camponotus vicinis* ant, which had a fresh weight of more than 100 mg¹³. These authors used a conventional Sable Systems TR-3 respirometry system (Sable Systems, Salt Lake City, USA) in order to study certain details of the discontinuous gas-exchange cycle^{14,15} (DGC), which is characteristic for certain insects, including ants. Such insects can control their gas exchange by opening and closing their spiracles, which control the connection of the insect's tracheal system with ambient air. It has been assumed that the CO₂ release is zero with closed spiracles, but the detection limit reached in the above-mentioned publication did not allow detection of a CO₂ release at the closed-spiracle phase with sufficient resolution. Our setup allows a quantitative determination of the CO₂ with a time resolution of 300 ms using a free-moving ant of a weight two orders of magnitude lower.

In a second experiment, we placed a single *Drosophila melanogaster* fruit fly (an Oregon R wild-type female of weight 1.4 mg) into the same setup. CO₂ release from single *Drosophila* flies had been measured earlier by Williams *et al.*¹⁶ with the aid of a Licor LI-6251 infrared CO₂ analyzer. However, it remained unclear as to whether *Drosophila* flies exhibit a classical DGC since the patterns of CO₂ release were rather irregular. Only *Drosophila* lines selected over more than a decade for desiccation resistance, showed a more regular pattern of CO₂ release. With our setup, we were able to obtain recordings of the CO₂ release similar to those published by Williams *et al.*¹⁶, but with a better resolution (Fig. 2a,b). In order to enhance the quality of the recordings 2% of SF₆ was added to the air flowing over the fly at a rate of 2.5 l/h.

Our recordings show, that the pattern of CO₂ release by the fly is different from the classic DGC of the ant. Here, the CO₂ release does not drop to a close to zero base line. Rather, the fly seems to enter a new CO₂ release cycle without closing its spiracles in between. Our set up will allow a more accurate analysis of the gas exchange in *Drosophila*.

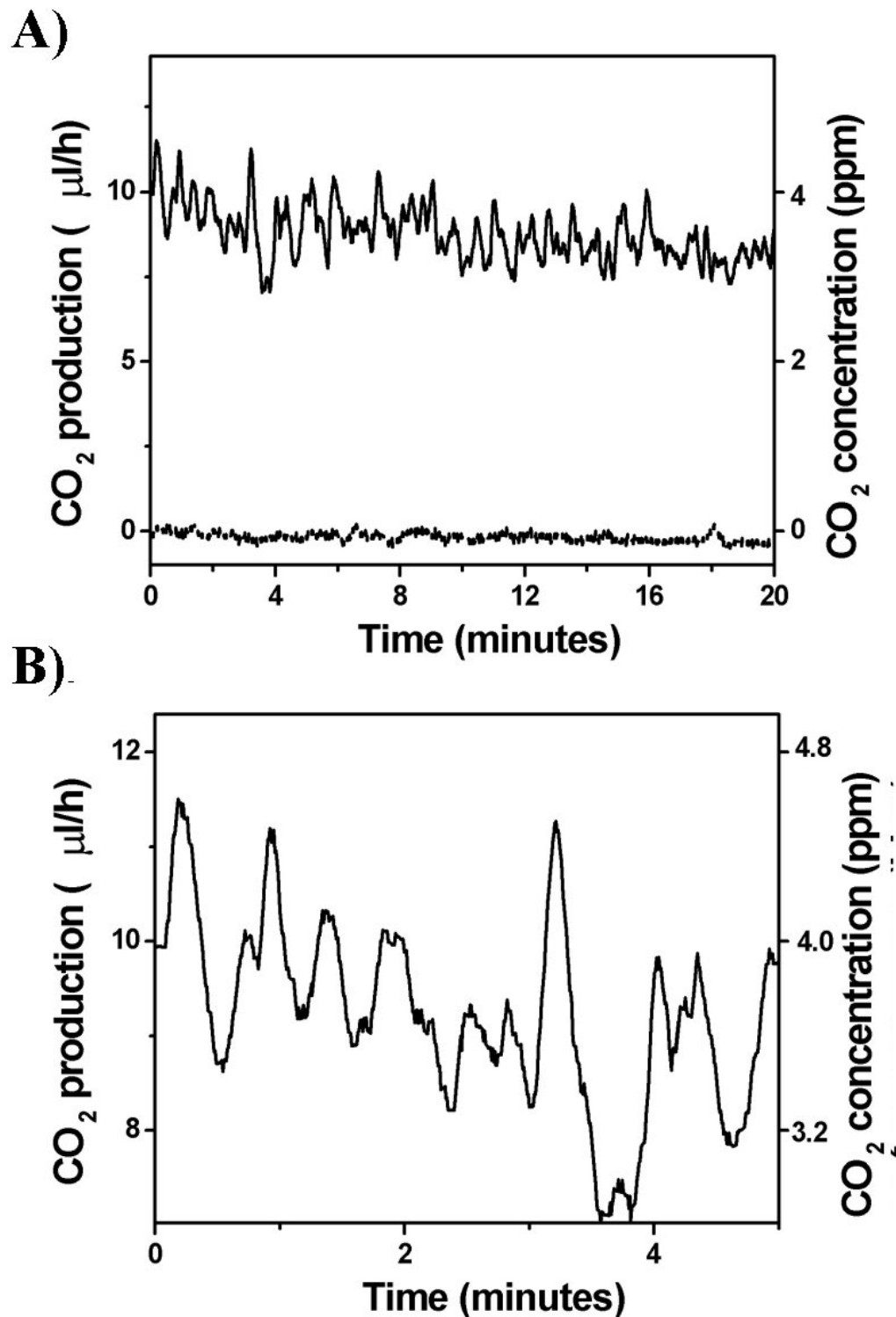


Fig. 2. On-line detection of the CO₂ release of a *Drosophila Melanogaster*. **a**, The comparison of the CO₂ signal with the background signal shows that the CO₂ release does not drop to zero. **b**, A close up image demonstrates the accuracy of the CO₂ detection. It shows peaks of CO₂ release with varying height and frequency.

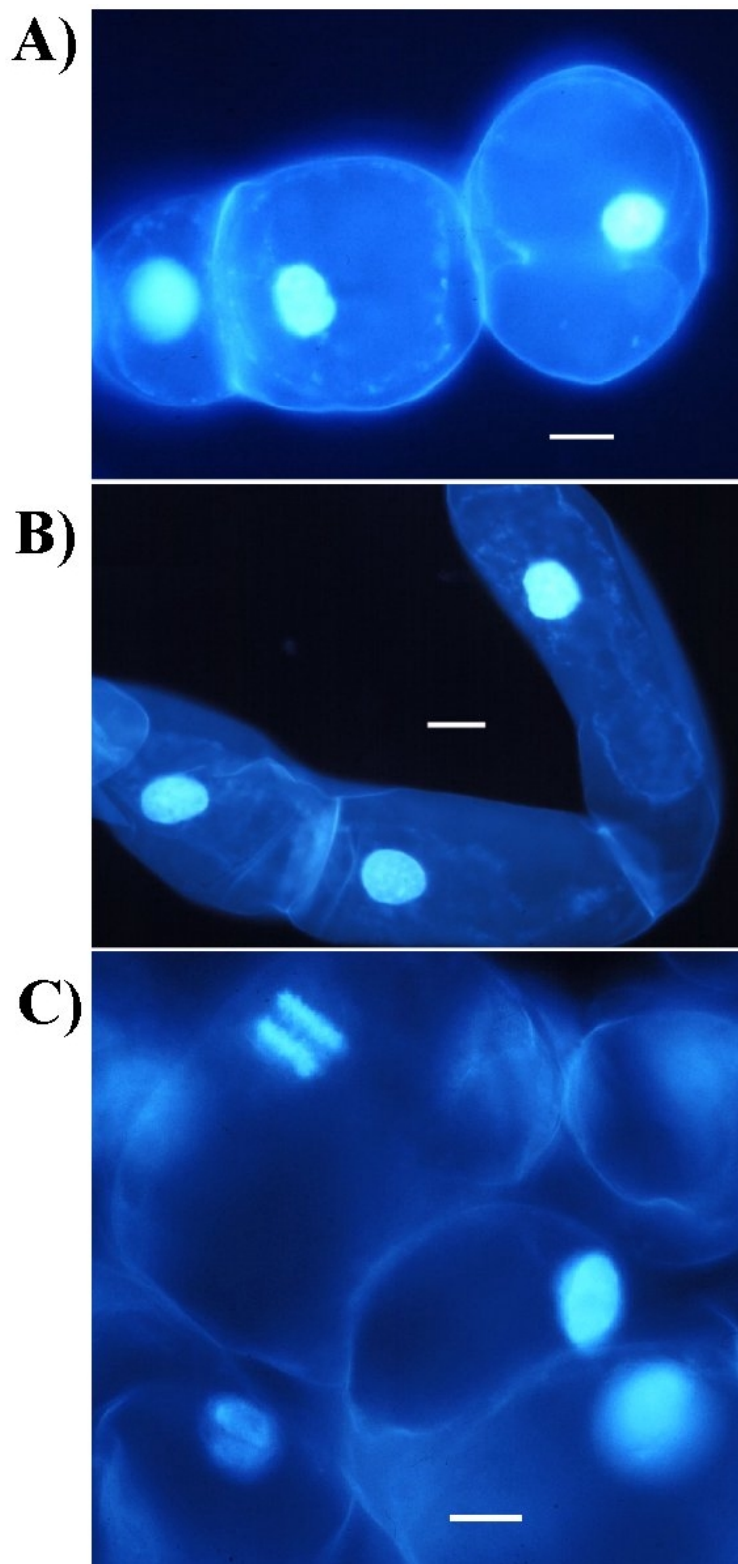


Fig. 3. Tomato suspension cells line MSK8 stained with Hoechst 33258 DNA marker. In **a**, **b** and **c** the white bar indicates a length of 25 micrometer. The size of the cells can be up to 140 μm . Panel **c** shows a dividing cell.

10.5 Improving the sensitivity

There are various possibilities to improve the sensitivity of the system, for instance by applying a different detection technique such as cavity ring-down spectroscopy¹⁷, or by using a more powerful pump laser. An example of a more powerful pump laser is the Versadisk (ELS GmbH, Germany), which has a slightly larger bandwidth than the current pump laser, but can supply more than 20W of radiation between 1020 nm and 1050 nm. In a pilot experiment we have been able to generate 10 times more power at the maximum of the CO₂ absorption (200 mW including intra-cavity etalon). This increased the sensitivity by the same factor, pushing the CO₂ detection limit down to 0.7 ppb (with 4% SF₆ addition).

10.6 Single cell respiration

Plant cell cultures are often used as model systems to study biochemical pathways involved in e.g. the production of secondary metabolites, pathogen defense responses and cell death¹⁸. In the latter case, individual cells may or may not commit suicide (apoptosis) depending on the balance of pro- and anti-apoptotic factors. Therefore, it would be interesting to monitor the metabolic changes in individual cells. Routinely, experiments are performed with cell cultures consisting of large numbers of cells or cell clusters.

In order to estimate the feasibility of measuring the metabolic changes in a single cell, the CO₂ release of a small volume of suspension cultures tomato cells¹⁸ was analyzed with a commercial infrared CO₂ analyzer (Uras 14, Hartman & Braun, Frankfurt, Germany). CO₂ production per milligram fresh weight of tomato cells ranged between 150-570 nanoliter per hour. Fig. 3 shows that such cells have up to about 100 μ m diameter. Assuming sphere shaped cells filled with water a single cell may weigh up to 0.5 mg. Given the production rate, flushing with a carrier gas flow of approximately 0.1 liter per hour, the CO₂ release of single cell is estimated to yield concentrations between 0.7 and 2.6 ppb, which can be detected by this system. This suggests that the described system may allow the detection of the CO₂ release of single plant cells and this should allow us to closely monitor cellular metabolism during e.g. division and death of individual cells.

10.7 Conclusion

The high sensitivity and temporal response of photoacoustic spectroscopy, coupled with the ability to operate on fundamental molecular vibrational modes enabled by the use of this PPLN based OPO, makes this system ideal for life science applications. Other methods such as GCMS (gas chromatography mass-spectrometry), while sensitive, do not have the required temporal resolution to observe such effects.

Table 1: Several strong absorptions in the wavelength range between 3.9 and 5.0 μm .

Molecular end-group or bond type	Spectral range (nm)	Molecule	Spectral position (nm)	3-3.9 μm range groups	Spectral range (nm)
-S-H	3846-3922	HBr	3800	C \equiv CH	3000-3040
P-H	4167-4255	SO ₂	4000	COOH	3330-4000
-N=C=O	4396-4444	CO ₂	4235	O=CH ₃	3380-3420
-N ₃	4629-4717	C ₂ H ₃ NO	4380	CH ₂ or CH ₃	3390-3510
-N=C=N-	4640-4695	N ₂ O	4470	CHO	3450-3700
>C=C=O	~4650	CO	4610	O-CH ₃	3500-3560
R-S-C \equiv N	4670-4600	OCS	4820	POOH	3700-3900
-N=C=S	4673-5025			SH	3850-3920

The use of vibrational relaxation by SF₆, coupled with operation on a fundamental vibrational mode, we derive an extrapolated CO₂ detection limit of 0.7ppb, which can be improved in future for instance by applying a different detection technique such as cavity ring-down spectroscopy¹⁷. The ability to operate in the 3-4.7- μm region with continuous tuning and high power is unprecedented. This will allow access to a broad range of species, in their fundamental vibrational modes, thus expanding the range of applicability of the instrument (see Table 1). In addition, the newly developed laser system will open many new possibilities within molecular physics and physical chemistry such as molecular dynamics and chemical kinetics.

References

1. Bosenberg, W. R., Drobshoff, A. & Alexander, J.I. 93% Pump depletion, 3.5-W continuous-wave, singly resonant optical parametric oscillator. *Opt. Lett.* **21**, 1336-1338 (1996)
2. Myers, L.E. & Bosenberg, W.R. Periodically Poled Lithium Niobate and Quasi-Phase-Matched Optical Parametric Oscillators. *IEEE J. Quantum Electron.* **33**, 1663-1672 (1997)

3. Powers, P.E., Kulp, T.J. & Bisson, S.E. Continuous tuning of a continuous wave periodically poled lithium niobate optical parametric oscillator by use of a fan-out grating design. *Opt. Lett.* **23**, 159-161 (1998)
4. Klein, M. E., Laue, C.K., Lee, D.-H., Boller, K.-J. & Wallenstein, R. Stable, continuously tunable operation of a diode-pumped doubly resonant optical parametric oscillator. *Opt. Lett.* **25**, 490-492 (2000)
5. van Herpen, M.M.J.W., te Lintel Hekkert, S., Bisson, S.E. & Harren, F.J.M. Wide single mode tuning of a 3.0-3.8 micron, 700 mW, continuous wave Nd:YAG-pumped optical parametric oscillator based on periodically poled lithium niobate. *Opt. Lett.* **27** (2002)
6. van Herpen, M.M.J.W., Li, S., Bisson, S.E., te Lintel Hekkert, S. & Harren, F.J.M. Tuning and stability of a continuous-wave mid-infrared high-power single resonant optical parametric oscillator. *Appl. Phys. B* **75**, 329 (2002)
7. Lowenthal, D.D. CW Periodically Poled LiNbO₃ Optical Parametric Oscillator Model with Strong Idler Absorption. *IEEE J. Quantum Electron.* **34**, 1356-1366 (1998)
8. Loza-Alvarez, P., Brown, C.T.A., Reid, D.T., Sibbett, W. & Missey, M. High-repetition-rate ultrashort-pulse optical parametric oscillator continuously tunable from 2.8 to 6.9 μm . *Opt. Lett.* **24**, 1523-1525 (1999)
9. Watson, M.A. *et al.* Extended operation of synchronously pumped optical parametric oscillators to longer idler wavelengths. *Opt. Lett.* **27**, 2106-2108 (2002)
10. van Herpen, M.M.J.W., Li, S., Bisson & S.E., Harren, F.J.M. Photoacoustic trace gas detection of ethane using a continuously tunable, continuous-wave optical parametric oscillator based on periodically poled lithium niobate. *Appl. Phys. Lett.* **81**, 1157-1159 (2002)
11. Harren, F. J. M., Cotti, G., Oomens, J. & te Lintel Hekkert, S. Photoacoustic Spectroscopy in Trace Gas Monitoring. *Encyclopedia of Analytical Chemistry* 2203–2226, (Ed. R. A. Meyers, Wiley, Chichester, 2000)
12. Buchwald, M.I. & Bauer, S.H. Vibrational Relaxation in CO₂ with Selected Collision Partners. *J. Phys. Chem.* **76**, 3108-3115 (1972)
13. Lighton, J.R.B. & Garrigan, D. Ant Breathing: Testing regulation and mechanism hypotheses with hypoxia. *J. Exp. Biol.* **198**, 1613-1620 (1995)
14. Kestler, A. Respiration and respiratory water loss. *Environmental Physiology and Biochemistry of Insects* 137-183 (ed. K.H. Hoffmann, Springer Verlag, Berlin, 1985)
15. Lighton, J.R. B. Discontinuous ventilation in terrestrial insects. *Physiol. Zool.* **67** 142-162 (1994)
16. Williams, A. E., Rose, M.R. & Bradley, T.J. CO₂ release patterns in *Drosophila Melanogaster*: The effect of selection for desiccation resistance. *J. Exp. Biol.* **200**, 615-624 (1997)
17. Popp, A. *et al.* Ultra-sensitive mid-infrared cavity leak-out spectroscopy using a cw optical parametric oscillator. *Appl. Phys. B* **75**, 751–754 (2002)
18. De Jong, A.J., Hoeberichts, F.A., Yakimova, E.T., Maximova, E. & Woltering, E.J. Chemical-induced apoptotic cell death in tomato cells: Involvement of Caspase-like proteases. *Planta* **211**, 656-662 (2000)

Summary

For many spectroscopic applications such as molecular beam spectroscopy and photo-acoustic spectroscopy, high power combined with continuous single frequency tuning of the laser source is essential. Photo-acoustic spectroscopy is a technique commonly used in trace-gas detection experiments, where very low detection limits can be achieved. In order to reach these detection limits very high powers are essential and therefore high-power laser sources such as CO₂ and CO lasers are used often. However, these sources are line-tunable lasers, which means that they can only generate a specific set of frequencies within their operating range. This means that a certain gas molecule can only be detected if there is a co-incident overlap between the absorptions of this molecule and the emitted laser frequency. To avoid this need for coincidence a new high-power laser source is needed. Optical Parametric Oscillators (OPOs) are very suited for this, because they can generate high-power infrared laser radiation that is widely (continuously) tunable.

This thesis reports the development of several continuous-wave, single frequency, high-power optical parametric oscillators (OPOs) for trace gas detection in life science research. An important aim was to develop a source that is widely tunable and preferably also continuously tunable and easy to use.

In chapter 4 the possibilities for continuous-wave OPO tuning with intra-cavity elements are explored. The OPO was continuously tuned over 34 GHz by tuning the cavity length, while a low-finesse air-spaced intra-cavity etalon was locked to the signal frequency with an electronic feedback loop. Tuning of the cavity length normally causes misalignment of the OPO cavity, but this could be avoided using a skewed (folded) bowtie ring cavity architecture. The OPO had an output power of 80 mW and a frequency jitter of 100 MHz in several tenths of seconds was observed. Up till now, the continuous tuning range reported in this chapter is the highest ever reported for a Nd:YAG pumped OPO system.

Chapter 5 reports the development of a new OPO for the mid infrared wavelength region of 3-3.8 μm with an idler output power of up to 700 mWatt, using an intra-cavity air-spaced etalon to enforce single mode operation. The single resonant OPO (SRO) is pumped by a single mode, 10 Watt, cw, Nd:YAG laser and consists of a bowtie ring cavity with a fan-out periodically poled lithium niobate crystal. The idler frequency can be continuously pump-tuned over 24 GHz. At the moment this is the highest continuous pump-tuning range ever reported for a Nd:YAG pumped system. Tuning was demonstrated by recording an absorption line of ethane with photo-acoustic spectroscopy.

In chapter 6 improvements are made to the OPO reported in chapter 5 and the performance of the system is analyzed. By optimizing the pump beamwaist and the length of the OPO cavity the output power of the system could be improved to 2.2 Watt, but introducing the intra-cavity etalon typically reduced this to 1.6 Watts. Both an air-spaced and solid etalon were tested to frequency stabilize and tune the OPO, from which the solid etalon gave the best performance. The frequency stability of the OPO was analyzed by recording the photo-acoustic signal from a

low-pressure ethane absorption, without tuning the OPO. The idler frequency stability appears to be less than 200 MHz over 300 seconds and less than 3 MHz over 1 second, caused by temperature oscillations in the PPLN crystal.

In chapter 7 the OPO reported in the previous two chapters is used for trace-gas detection of ethane. The detection limit of ethane was found to be 10 parts per trillion. This could be achieved by making a 24 GHz wide pump laser scan over the ethane absorption line at 2996.9 cm^{-1} , after which a Lorentzian fit determined the total area of the absorption signal. In this way it was also possible to measure the ethane signal on a varying background signal, which is not possible with a line-tunable source. Both area value and peak value proved to be linearly dependent on the ethane concentration. The results of this chapter show that the developed OPO system is very useful for trace gas detection experiments.

Further improvements are made to the OPOs by extending the operation range of single-frequency continuous-wave OPOs beyond the $3.9\text{ }\mu\text{m}$ absorption edge of lithium niobate in chapter 8. In this spectral range, absorption of the idler wave in the LiNbO_3 crystal is significant, causing the oscillation threshold to increase with a subsequent decrease in output power from 1.2 Watts at $3.9\text{ }\mu\text{m}$ to 120 milliWatts at $4.7\text{ }\mu\text{m}$. Introducing an intra-cavity solid etalon further reduced this power by 50%. This is the first time that a cw, single frequency PPLN OPO is operated in this wavelength range and it allows detection of a wide range of new gasses, such as CO_2 . The usefulness for spectroscopy was demonstrated by recording a photo-acoustic spectrum of a strong CO_2 absorption using a 24 GHz continuous idler scan.

In chapter 9 a new type of pump laser (Versadisk) is used for an OPO. This Yb:YAG source is very suited as pump source for an OPO, because it has very wide tunability (1024-1034 nm) and very high power ($>20\text{ W}$). At an idler frequency of 2954 nm an output power of 3.0 W is achieved, which was frequency stabilized with an intra-cavity etalon. The high pump power also allowed the OPO to be operated beyond $3.9\text{ }\mu\text{m}$, resulting in a total idler tuning range of $2.6 - 4.7\text{ }\mu\text{m}$. Tuning of the idler frequency is achieved by longitudinal mode-hop tuning of the pump source (FSR 100 MHz). In this way a frequency scan of 100-150 GHz is obtained, after which the signal frequency hops over the FSR of the intracavity etalon of the OPO (207 GHz). Due to un-optimized mirror coatings for the OPO cavity and PPLN crystal the frequency stability was limited to 90 MHz over 1s, with an unaffected long-term frequency stability of 250 MHz over 200 seconds. The use for spectroscopy is demonstrated by recording a 190 GHz wide scan containing several absorption lines of ethane.

After the previous two reports of new $4\text{-}5\text{ }\mu\text{m}$ sources, chapter 10 focuses on the application of these lasers for trace-gas detection in life science research. A CO_2 detection limit of below one part in a billion is achieved with 4% of SF_6 gas added to the gas mixture in order to avoid relaxation problems. The use of the system is demonstrated by measuring the CO_2 gas exhaled by a single ant (*Lasius Niger*) and fruit fly (*Drosophila melanogaster*) in real-time. It is also expected that it will be possible to monitor the respiration of single plant cells on-line.

Populair wetenschappelijke samenvatting

Dit proefschrift beschrijft de ontwikkeling van een nieuw type laser. Met behulp van deze laser kunnen concentraties gemeten worden van allerlei gassen. Dit kan in de toekomst gebruikt worden om een blaastest voor de gezondheid te ontwikkelen. Om te laten zien hoe gevoelig het systeem is, is zelfs een blaastest afgenomen bij een mier!

Met behulp van een blaastest kun je veel te weten komen over de gezondheid van een persoon. Vergelijk het maar met de blaastest die de politie gebruikt om het gehalte van alcohol in je bloed te bepalen. In Nijmegen wordt gewerkt aan de ontwikkeling van een blaastest die niet alleen alcohol, maar honderden verschillende stoffen kan meten in de ademhaling van mensen. In principe moet deze blaastest in veel gevallen het gebruik van bloed kunnen vervangen. Dit proefschrift draagt bij aan deze ontwikkeling.

Om de gassen te detecteren wordt gebruik gemaakt van het gegeven dat alle stoffen bepaalde kleuren licht absorberen. Iedere stof neemt slechts bepaalde kleuren op, en daardoor heeft ieder gas ook zijn eigen ‘vingerafdruk’ van absorpties. Door naar deze absorpties te kijken kunnen de onderzoekers bepalen hoeveel van een bepaalde stof er aanwezig is.

Om dat te doen wordt de ademhaling van de proefpersoon naar een buisje gestuurd waar een laserbundel met een bepaalde kleur licht doorheen schijnt. In dit buisje kan een stof het licht absorberen, waardoor de lucht opwarmt (zoals het licht van de zon ook je huid kan verwarmen). Door deze opwarming zal het gas uitzetten, waardoor de druk een beetje toeneemt. Door de laser nu telkens aan en uit te schakelen kunnen de onderzoekers drukgolftjes produceren in het buisje. Het leuke is dat geluid een drukgolf is, en dus ontstaat er geluid in het buisje, wat opgevangen wordt door een microfoon. Het geluid wordt ook versterkt, omdat het buisje een soort orgelpijpje is. Deze methode wordt *Foto-akoestiek* genoemd.

Op de afdeling molecuul -en laserfysica van de Katholieke Universiteit Nijmegen wordt veel onderzoek gedaan naar gassen die uitgedemd worden door planten, dieren en mensen. Zij meten deze gassen met behulp van lasers. Op het moment worden zogenaamde CO₂ en CO lasers gebruikt. Dit zijn lijn-afstembare lasers, wat betekent dat ze slechts specifieke lichtkleuren binnen hun bereik kunnen produceren. Daarom is er een nieuw lasertype ontwikkeld dat alle lichtkleuren kan maken binnen zijn bereik.

Dit proefschrift beschrijft de ontwikkeling van deze nieuwe laser, die *OPO* genoemd wordt. Dit is een afkorting voor *Optical Parametric Oscillator*. De OPO laser heeft veel voordelen. Om te beginnen kan hij, zoals gezegd, veel meer kleuren produceren dan de meeste andere lasers, waardoor er meer verschillende stoffen gemeten kunnen worden. Daarnaast heeft het laserlicht ook een hoge intensiteit, waardoor lagere concentraties van die stoffen gemeten kunnen worden. Verder is een OPO ook veel compacter dan de CO en CO₂ lasers, waardoor het gemakkelijker wordt om de laser mee te nemen om ergens ter plekke metingen te doen.

Het principe van deze OPO laser is gebaseerd op de omzetting van de ene lichtkleur in de andere lichtkleur. Dit wordt gedaan door middel van een speciaal *niet-lineair* kristal. In dit kristal treden

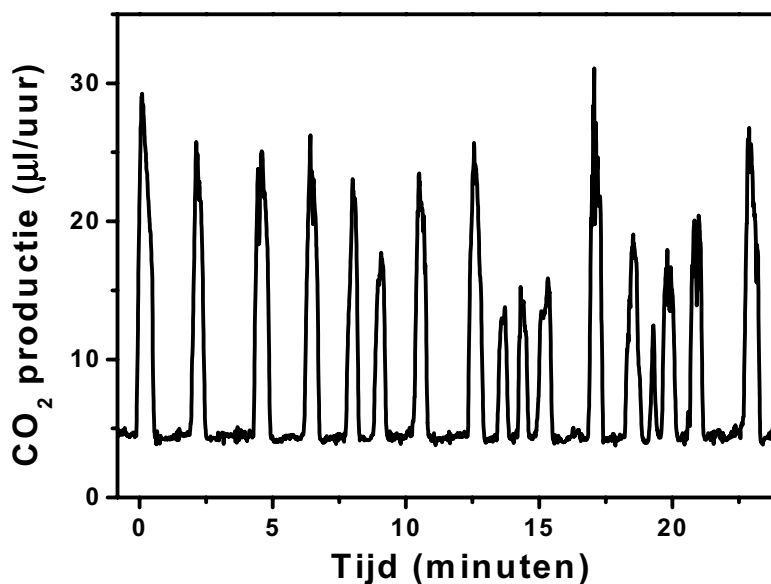
effecten op die niet in ieder kristal voorkomen. In dit geval wordt er een infrarood lichtdeeltje van 1064 nm opgesplitst in twee nieuwe deeltjes, en wel zodanig dat de som van de energieën gelijk is aan de oorspronkelijke energie. Omgerekend van energie naar golflengte krijg het ene nieuwe deeltje dan bijvoorbeeld een golflengte van ongeveer 1550 nm en het andere ongeveer 3300 nm.

Toen deze OPO operationeel was, werd al snel duidelijk dat het systeem zeer gevoelige metingen kon doen. Zo kon het systeem van het gas ethaan (C_2H_6) zelfs een verdunning meten van één deel ethaan in honderd miljard delen lucht. Dit was een nieuw wereldrecord voor de detectie van dit gas. Meer hierover is te lezen in hoofdstuk 7.

Recent is de laser gebruikt om een blaastest af te nemen bij een mier. Dit was een duidelijke demonstratie van de gevoeligheid van dit nieuwe apparaat. Hiervoor was in de tuin van de universiteit een mier gevangen en de koolstof-dioxide (CO_2) in de uitgeademde lucht van die mier is met behulp van de OPO geanalyseerd (zie hoofdstuk 10).

Bij mensen kan een mondkapje gebruikt worden om de uitgeademde lucht op te vangen, maar bij een mier gaat dat natuurlijk niet. Daarom werd de mier in een dun buisje gestopt, dat dichtgemaakt was met watten. Door een stroompje lucht langs de mier te sturen kon de uitgeademde lucht van de mier opgevangen worden. De mier bleek slechts eens per 1 à 2 minuten adem te halen, wat overigens normaal is voor deze insecten (zie figuur 1).

Voor de ontwikkeling van een blaastest voor de gezondheid van mensen is het werk nog lang niet klaar. Er moet nu gewerkt worden aan de volgende stap en dat is een apparaat dat zonder moeite in ziekenhuizen door artsen gebruikt kan worden. Ook moet gezocht worden naar gassen in de ademhaling van mensen die belangrijk zijn voor de geneeskunde. Dit is nog een flink karwei, omdat er honderden verschillende stoffen voorkomen in de ademhaling van de mens.



Figuur 1: In dit figuur is te zien dat de mier iedere 1 à 2 minuten uitademt. Dit is te zien aan die piekjes koolstof-dioxide (CO_2) die gemeten worden met de laser.

Publications

Related to this thesis:

1. *Real-time monitoring of the respiration of small insects and single cells with laser based CO₂ detection.*
M.M.J.W. van Herpen, A.K.Y. Ngai, S.E. Bisson, J.H.P. Hackstein, E.J. Woltering and F.J.M. Harren, Appl. Phys. Lett., submitted (2003)
2. *Wide pump tuning and high power of a continuous-wave single resonant optical parametric oscillator.*
M.M.J.W. van Herpen, S.E. Bisson, A.K.Y. Ngai and F.J.M. Harren, Appl. Phys. B., accepted (2003)
3. *Continuous-wave operation of a single frequency optical parametric oscillator at 4-5 μm based on periodically poled LiNbO₃*
M.M.J.W. van Herpen, S.E. Bisson and F.J.M. Harren, Opt. Lett. **28**, 2497-2499 (2003)
4. *Wide single-mode tuning of a 3.0-3.8- μm , 700-mW, continuous-wave Nd:YAG-pumped optical parametric oscillator based on periodically poled lithium niobate*
M.M.J.W. van Herpen, S. te Lintel Hekkert, S.E. Bisson, F.J.M. Harren, Opt. Lett. **27**, 640-642 (2002)
5. *Tuning and stability of a continuous-wave mid-infrared high-power single resonant optical parametric oscillator*
M.M.J.W. van Herpen, S. Li, S.E. Bisson, S. te Lintel Hekkert, F.J.M. Harren, Appl. Phys. B **75**, 329 (2002)
6. *Photo acoustic trace gas detection of ethane using a continuously tunable, continuous-wave optical parametric oscillator based on periodically poled lithium niobate.*
M.M.J.W. van Herpen, S. Li, S.E. Bisson & F.J.M. Harren, Appl. Phys. Lett. **81**, 1157-1159 (2002)
7. *The development of a powerful continuous tunable, mid infrared, cw PPLN OPO for trace gas detection*
M. van Herpen, S. te Lintel Hekkert, S.E. Bisson, F.J.M. Harren **Proceedings SPIE** Vol. xxx (Bellingham, USA, 2001) pp Conference proceedings ALT'01 Advanced Laser Technologies 2001, Constanta, Romania, September 2001

8. *A high power cw, continuous tunable mid infrared OPO for detection of trace gases*
F. Harren, Sacco te Lintel Hekkert, M. van Herpen **Proceedings SPIE** Vol. xxx
(Bellingham, USA, 2002) pp Conference proceedings: BIOS 2002, January 2002, San
Jose, California

Other publications

9. *Influence of nitrogen addition on oxyacetylene flame chemical vapor deposition of diamond as studied by solid state techniques and gas phase diagnostics*
R.L.Stolk, M.M.J.W.van Herpen, J.J.Schermer and J.J.ter Meulen, *J. of Appl. Phys.*
93(8), 4909-4921, 2003
10. *The effects of nitrogen addition on flame deposition of diamond*
R.L. Stolk, M.M.J.W. van Herpen, J.J. Schermer and J.J. ter Meulen, *Proc. of the
Combustion Institute* **28**, 1447-1454, 2000
11. *Relation between gas phase CN radical distributions, nitrogen incorporation, and growth rate in flame deposition of diamond*
R.L.Stolk, M.M.J.W. van Herpen, J.J. ter Meulen and J.J Schermer, *J. Appl. Phys.* **88**(6),
3708-3716, 2000

Curriculum Vitae

Maarten van Herpen is op 12 december 1976 geboren te Oss. In 1995 heeft hij zijn diploma VWO behaald op het Maaslandcollege te Oss. Aansluitend is hij begonnen met een studie natuurkunde aan de Katholieke Universiteit Nijmegen. Als afstudeer-stage heeft hij gewerkt bij de afdeling molecuul –en laserfysica onder begeleiding van dr. Robert Stolk en prof. dr. J.J. ter Meulen. Hier heeft hij onderzoek verricht naar naar het effect van stikstof op de groei van diamant bij chemische damp depositie. Zijn studie heeft hij na 4 jaar afgerond met het behalen van zijn doctoraal diploma in 1999.

Direct hierna is hij begonnen aan een promotie-onderzoek. Dit was ook bij de afdeling molecuul –en laserfysica, maar in een andere groep die onder leiding stond van prof. dr. Dave Parker en dr. Frans Harren. In het eerste jaar van het promotie-onderzoek heeft Maarten onder begeleiding van dr. Scott Bisson gedurende 1 maand gewerkt bij Sandia National Laboratories aan de bouw van een Optical Parametric Oscillator met een gestrekte bowtie ring cavity. De kennis die hij hier heeft heeft opgedaan was zeer nuttig, omdat hij hierna in Nijmegen een soortgelijk, maar vernieuwd systeem heeft ontwikkeld. Na vier jaar is hij op dit onderzoek gepromoveerd. De resultaten van zijn promotie onderzoek zijn weergegeven in dit proefschrift.

Tijdens zijn studie natuurkunde en promotie heeft Maarten verschillende studenten begeleid en was hij assistent bij colleges ‘groepentheorie’ en ‘inleiding in de statistische fysica’. In zijn vrije tijd is hij actief als freelance computer programmeur.

Op het moment zet hij zijn werkzaamheden voort als post-doc in dezelfde groep. Hij werkt hier mee aan de ontwikkeling van een ‘rapid trace gas detector and analyzer’.

